To the Graduate Council:

I am submitting herewith a thesis written by Chris C. Dobson entitled "Laser Irradiation and Heating of Spherical Particles". I have examined the final copy of this thesis for form and content and recommend that it be accepted in partial fulfillment of the requirements for the degree of Master of Science, with a major in Physics.

J. W. L. Lewis, Major Professor

We have read this thesis
and recommend its acceptance:

Dennis Keefer

Horace Crater

Accepted for the council:

Vice Provost
and Dean of The Graduate School

LASER IRRADIATION
AND HEATING OF
SPHERICAL PARTICLES

Thesis

Presented for the

Master of Science

Degree

The University of Tennessee, Knoxville

Chris C. Dobson

March 1987

ABSTRACT

The internal and scattered fields of the Mie problem are determined with the vector multipole method of classical electrodynamics, giving a complete treatment of the derivation. Both popular phase conventions for the complex representation of the fields are treated in detail, clarifying distinctions necessary for valid results. The expressions for the internal electric field are used to study the behavior of the source function for a wide range of size parameters and complex refractive indices.

The source function is inserted in the differential equation of heat conduction and solutions are obtained from orthogonal function expansion for the approximation of constant thermal and optical properties and from finite difference differential approximation for the general case. Using these solutions, several specific cases of photoabsorptional heating and thermal diffusion in laser irradiated water drops are examined.

A number of source function and temperature plots are given for illustration, and a brief discussion of non-monochromatic laser pulses and indications of other elaboration are included.

TABLE OF CONTENTS

LIST OF FIGURES

FIGURE PAGE

INTRODUCTION

This work is a theoretical study of two related physical phenomena: the electromagnetic field patterns involved in laser irradiation of spherical media and the energy transfer effects resulting from such interaction. The approach will be to isolate mechanisms of interest and develop mathematical models of their behavior from basic physical principles. The central theory exercised is the classical electrodynamics of the Maxwell equations, from which expressions for the fields within the sphere arise. These internal fields heat the material of the sphere, generating a thermal gradient and, thereby, heat transport phenomena.

The application of the classical physics of electricity and magnetism to the scattering and absorption of light by homogeneous spheres was first begun in the mid-nineteenth century. Since that time, the phenomenon has been treated extensively by workers such as Clebsch, Lorentz, Mie, and Debye [29]. The general theory, which, oddly, has come to be nominally identified with Gustav Mie, is valid for arbitrary interface shapes, but this work, as is typical, will be confined to spheres. The pivotal circumstance here is the characteristic configuration of the fields at the medium boundary, information embedded in the Maxwell equations. It is just those expressions for the internal and external fields which simultaneously satisfy the governing equations throughout, and the boundary conditions at the interface, that describe the patterns which are observed in practice. This is prototypical physical theory and, as will be seen, is essentially the same approach as that taken in solution of the heat conduction problem.

One particular warrants mention here; there are two different phase conventions in popular use for the complex representation of the electromagnetic fields. Neither seems to offer a clear advantage: both carry the same physical content, and the two forms, which are complex conjugates, give rise to complementary derivations. Unfortunately, the existence of such a delicate distinction in a mathematical construction of this complexity provides large opportunity for confusion. Mixing expressions from opposing conventions in a calculation produces results which are generally invalid, and which, according to the specifics, will vary widely in manner and extent of invalidity (p.23) [8]. This circumstance has motivated an expansion of the scope of this work to include both popular phase conventions.

The basic interaction between the light field and the spherical medium is the conversion of electromagnetic field energy into thermal energy of the atoms or molecules comprising the material*. Since the internal fields are generally inhomogeneous, this heating establishes a thermal gradient, producing heat flow within the sphere. Groups of atoms or molecules given greater than average vibrational or collisional energy impart some of their surplus motion to adjacent, or nearby, less agitated particles, and the macroscopic result is heat

* This conversion is discussed briefly in Chapter 3.

flux proportional the temperature gradient, that is, thermal conduction (J. B. J. Fourier, 1822 [21]). Further, if the medium is in a fluid phase, conduction is complicated by the presence of an external force field such as gravity, and convective action may be generated.

Free convection is a collaboration of density heterogeneity and heat conduction with gravitation. An increase of thermal activity in a group of constituent particles in a fluid will place greater demand on the volume required to contain them, thereby reducing local density. Other volume elements within the medium, populated by more sluggish, closely packed particles, sink toward the force center, displacing and raising the lighter, more lively pockets. Concomitantly, the individual molecules transfer energy by conduction and migrate into adjacent regions, so that the pockets tend to dissolve into one another [16]. However, since the buoyant force is the operative agent, convection is a comparatively slow process; for the microsecond observation times common in laser phenomena, mass transport by convection, even in the total absence of viscosity ($d = \frac{1}{2}gt^2$), is negligible. For the study to be done here, heat transport within the sphere will be via thermal conduction exclusively.

The intended application of the computer programs assembled for these calculations is the modeling of the detailed behavior of the constituent spheres (or approximate spheres) in mists, such as water fog or fuel spray, or particulate collections common in smoke and flames [9]. The attenuation of laser light by water drops suspended in the air can be a critical parameter of intensity ceilings for propagation through the atmosphere. The fragmentation of hydrocarbon fuel drops possible with laser radiation enhances the amenability of the fuel/air mixture to the chemistry necessary for the energy release sought, that is, the combustion process [7]. Of particular interest is the determination of heating times and spatial regions involved in the explosive vaporization of such spherical media.

The computer models can provide the field and/or temperature data in numerical form, but the greatest utility lies perhaps in the graphic display of the calculational results. Two formats, in particular, have been developed: a simulated three-dimensional rendition of the source function or a temperature distribution in a cross-sectional plane of the sphere, and a two-dimensional altitude map in the same plane which is essentially overlapping cross-sections of the three-dimensional version. As described in Chapter 2, a heating pattern common to a variety of situations is determined by the simple specification of size parameter and refractive index. Any particular frame in this sequence may be correlated with a time and temperature, but only by consideration of a specific laser pulse and set of thermal properties [as per (2.1.6)].

Chiefly because of its importance, liquid water is chosen in Chapter 3 to illustrate the effects of mechanisms governed by the heat equation. The two basic approximations examined are those of negligible diffusion, and of constant thermal and optical properties. The mathematics involved are completely general, and analogous calculations for arbitrary media are straightforward, given knowledge of the temperature-dependence of the relevant properties. The ready availability of these data for water has also been influential in its exemplary selection here.

CHAPTER 1

THE MIE PROBLEM

Of critical importance to this thesis is the determination of the electromagnetic fields within the spherical medium. This problem is formally defined as follows: a plane, monochromatic wave of unit amplitude propagating in the positive z direction is incident on a sphere of radius a centered at the origin; all media are assumed to be uncharged and isotropic with constant permittivity, permeability, and conductivity (and Ohm's Law behavior). The sphere is characterized by permittivity $\epsilon_\circ = \varepsilon_\circ + i\frac{4\pi\sigma_\circ}{\omega}$ and permeability $\mu_\circ$, and the ambient medium by $\epsilon = \varepsilon + i\frac{4\pi\sigma}{\omega}$ and μ.

1.1 The Maxwell Equations

The central theme of the electrodynamic theory used to model this phenomenon is the specification that all the fields in both media are described everywhere by Maxwell's equations (for source-free regions):

$$\nabla \cdot \mathbf{D} = \nabla \cdot \mathbf{B} = \nabla \times \mathbf{E} + \frac{1}{c}\frac{\partial \mathbf{B}}{\partial t} = \nabla \times \mathbf{H} - \frac{1}{c}\frac{\partial \mathbf{D}}{\partial t} = 0, \tag{1.1.1}$$

the Coulomb, "absent monopole", Faraday, and Ampere/Maxwell Laws, respectively.

Two conventions are possible for the sinusoidal variation of the fields: $\mathrm{e}^{+i(\kappa z-\omega t)}$ [15], [23], and $\mathrm{e}^{-i(\kappa z-\omega t)}$ [19], [29], where $\kappa = \frac{\omega}{c}\mathrm{n}$, n the complex refractive index. Both describe waves moving in the direction of increasing refractive index. Both describe waves moving in the direction of increasing coordinate, and both are physically acceptable and in common use. It will be noted that the optical and electrical quantities are related by

$$\mathrm{n_{Re}} = \left[\mu\varepsilon\frac{\sqrt{1+\left(\frac{4\pi\sigma}{\omega\varepsilon}\right)^2}+1}{2}\right]^{\frac{1}{2}} \quad \text{and} \quad \mathrm{n_{Im}} = \left[\mu\varepsilon\frac{\sqrt{1+\left(\frac{4\pi\sigma}{\omega\varepsilon}\right)^2}-1}{2}\right]^{\frac{1}{2}} \tag{1.1.2}$$

[15, p.269], and that to preserve the absorptive nature of $\mathrm{n_{Im}}$ in either convention, opposing signs are required for it:

$$\mathrm{e}^{+i\kappa z} = \mathrm{e}^{+i\frac{\omega}{c}[\mathrm{n_{Re}}+i\mathrm{n_{Im}}]z} = \mathrm{e}^{+i\frac{\omega}{c}\mathrm{n_{Re}}z}\mathrm{e}^{-\frac{\omega}{c}\mathrm{n_{Im}}z} \,, \tag{1.1.3a}$$

$$\text{whereas} \quad \mathrm{e}^{-i\kappa z} = \mathrm{e}^{-i\frac{\omega}{c}[\mathrm{n_{Re}}-i\mathrm{n_{Im}}]z} = \mathrm{e}^{-i\frac{\omega}{c}\mathrm{n_{Re}}z}\mathrm{e}^{-\frac{\omega}{c}\mathrm{n_{Im}}z} \,. \tag{1.1.3b}$$

With the constitutive relations,

$$\mathbf{D} = \epsilon\mathbf{E} \quad \text{and} \quad \mathbf{B} = \mu\mathbf{H} \,, \tag{1.1.4a, b}$$

and the definition $k \equiv \frac{\omega}{c}$, the Maxwell equations become :

$$\nabla\cdot\mathbf{E} = \nabla\cdot\mathbf{B} = 0 \tag{1.1.5a, b}$$

$$\nabla\times\mathbf{E} = \pm ik\mathbf{B} \,,\ \nabla\times\mathbf{B} = \mp ik\epsilon\mu\mathbf{E} \,, \tag{1.1.5c, d}$$

where the upper sign is for the "plus" convention and the lower for the "minus". Representing **B** as a curl in Ampere's law, in light of the the vector identity (true for arbitrary vector **F**),

$$\nabla\times(\nabla\times\mathbf{F}) = \nabla(\nabla\cdot\mathbf{F}) - \nabla\cdot\nabla\mathbf{F} \,, \tag{1.1.6}$$

and the Coulomb law indicates that

$$(\nabla^2 + \epsilon\mu k^2)\mathbf{E} = 0 \ , \tag{1.1.6a}$$

and, similarly, beginning with the Faraday law leads to

$$(\nabla^2 + \epsilon\mu k^2)\mathbf{B} = 0 \ . \tag{1.1.6c}$$

(1.1.6a,c) are vector wave equations, each the equivalent of three homogeneous scalar equations for the cartesian components of the fields. Moreover, owing again to the solenoidal nature of these fields, the vector identity,

$$\nabla^2(\mathbf{r}\cdot\mathbf{F}) = \mathbf{r}\cdot(\nabla^2\mathbf{F}) + 2\nabla\cdot\mathbf{F} \ , \tag{1.1.7}$$

implies that the radial components in a spherical polar coordinate resolution of the fields satisfy the homogeneous scalar Helmholtz equation as well. These wave equations, along with the original curl relations, completely specify the Maxwell requirements:

$$(\nabla^2 + \epsilon\mu k^2)\mathbf{E} = (\nabla^2 + \epsilon\mu k^2)\mathbf{r}\cdot\mathbf{E} = 0 \tag{1.1.6a,b}$$

$$(\nabla^2 + \epsilon\mu k^2)\mathbf{B} = (\nabla^2 + \epsilon\mu k^2)\mathbf{r}\cdot\mathbf{B} = 0 \tag{1.1.6c,d}$$

$$\mathbf{E} = \pm\frac{i}{\epsilon\mu k}\nabla\times\mathbf{B} \quad , \quad \mathbf{B} = \mp\frac{i}{k}\nabla\times\mathbf{E} \ . \tag{1.1.6e,f}$$

GENERAL SOLUTION OF THE MAXWELL EQUATIONS

The Helmholtz form of the Maxwell equations, (1.1.6), serves as the starting point in the construction of a general solution to the original, equivalent, formulation, (1.1.5). It is, in fact, the eigenfunctions of the Helmholtz operator which will be used in Chapter 2 to generate a solution to the diffusion equation (Appendix A). These eigenfunctions form a complete basis set of orthogonal functions; that is, $(\nabla^2+\lambda^2)\psi(\mathbf{r})=0$ implies $\psi(\mathbf{r})=\sum_{n,m} C_{nm} f_n(\lambda r) Y_{nm}(\theta,\phi)$, where $f_n(\lambda r)$ are combinations of the spherical Bessel and Neumann functions and $Y_{nm}(\theta,\phi)$ is the (scalar) spherical harmonic [15,p.742]. For the present purpose, it is the radial electric and magnetic fields which are expanded in terms this basis:

$$\mathbf{r}\cdot\mathbf{E}=\pm\sum_{n,m}\alpha_E(n,m)f_n(\kappa r)Y_{nm}(\Omega) \tag{1.1.8a}$$

$$\mathbf{r}\cdot\mathbf{B}=\pm\sum_{n,m}\alpha_B(n,m)f_n(\kappa r)Y_{nm}(\Omega)\ , \tag{1.1.8b}$$

where $\kappa\equiv\sqrt{\epsilon\mu}k$, and $\Omega\sim\theta,\phi$. The definition of explicitly negative expansion coefficients in the minus convention is, of course, not necessary; it is done to enhance the symmetry of the results [(1.2.18),(1.4.5,7)].

Representing $\mathbf{E}$ and $\mathbf{B}$ in (1.1.8), again, as curls, and exchanging the scalar and vector product operators give

$$\mathbf{L}\cdot\mathbf{B}=-\epsilon\mu k\sum_{n,m}\alpha_E(n,m)f_n(\kappa r)Y_{nm}(\Omega) \tag{1.1.9a}$$

$$\mathbf{L}\cdot\mathbf{E}=k\sum_{n,m}\alpha_B(n,m)f_n(\kappa r)Y_{nm}(\Omega)\ , \tag{1.1.9b}$$

where $\mathbf{L}$ is the ordinary angular momentum operator, $i^\star\mathbf{r}\times\nabla$ [15,p.743]. The well-known property $\mathbf{L}\cdot\mathbf{L}Y_{nm}(\Omega)=n(n+1)Y_{nm}(\Omega)$[5,p.84] then suggests that expressions of the form

$$\lambda \sum_{n,m} \alpha(n,m) f_n(\kappa r) \mathbf{L} Y_{nm}(\Omega)[n(n+1)]^{-1} \tag{1.1.10}$$

satisfy (1.1.9); however, the vectors in the summation are purely tangential (Appendix C) and $\mathbf{E}$ and $\mathbf{B}$, generally, are not. In response, the so-called multipole fields are defined by the conditions:

$$\nabla \times \mathbf{E}^{\mathrm{E}} = \pm ik\mathbf{B}^{\mathrm{E}} \qquad \nabla \times \mathbf{B}^{\mathrm{E}} = \mp i\epsilon\mu k\mathbf{E}^{\mathrm{E}} \tag{1.1.11a,b}$$

$$\nabla \times \mathbf{E}^{\mathrm{B}} = \pm ik\mathbf{B}^{\mathrm{B}} \qquad \nabla \times \mathbf{B}^{\mathrm{B}} = \mp i\epsilon\mu k\mathbf{E}^{\mathrm{B}} \tag{1.1.11c,d}$$

$$\mathbf{r}\cdot\mathbf{E}^{\mathrm{B}} \quad = \quad \mathbf{r}\cdot\mathbf{B}^{\mathrm{E}} \quad = \quad 0\,. \tag{1.1.11e,f}$$

The total fields will then be expressed as $\mathbf{E} = \mathbf{E}^{\mathrm{E}} + \mathbf{E}^{\mathrm{B}}$ and $\mathbf{B} = \mathbf{B}^{\mathrm{B}} + \mathbf{B}^{\mathrm{E}}$ so that they have essentially been divided into tangential ($\mathbf{E}^{\mathrm{B}}$, $\mathbf{B}^{\mathrm{E}}$) and general ($\mathbf{E}^{\mathrm{E}}$, $\mathbf{B}^{\mathrm{B}}$) parts.

(1.1.11e) implies that $\mathbf{r}\cdot\mathbf{E}^{\mathrm{E}} = \mathbf{r}\cdot\mathbf{E}$, and if the former is inserted in the radial expansion, (1.1.8a), and subsequent manipulation above, there follows $\mathbf{L}\cdot\mathbf{B}^{\mathrm{E}} = -\epsilon\mu k \sum_{n,m} \alpha_E(n,m) f_n(\kappa r) Y_{nm}(\Omega)$, which, since $\mathbf{B}^{\mathrm{E}}$ is purely tangential, does have, as an acceptable solution,

$$\mathbf{B}^{\mathrm{E}} = -\epsilon\mu k \sum_{n,m} \alpha_E(n,m) f_n(\kappa r) \mathbf{L} Y_{nm}(\Omega)[n(n+1)]^{-1}\,, \tag{1.1.12a}$$

and, by the same token,

$$\mathbf{E}^{\mathrm{B}} = k \sum_{n,m} \alpha_B(n,m) f_n(\kappa r) \mathbf{L} Y_{nm}(\Omega)[n(n+1)]^{-1}\,. \tag{1.1.12b}$$

Then the curl equations provide radial components as well as a second (orthogonal to the first) transverse pair (Appendix C):

$$\mathbf{E}^{\mathrm{E}} = \pm\frac{i}{\epsilon\mu k}(-\epsilon\mu k)\sum_{n,m}\alpha_E(n,m)\nabla\times f_n(\kappa r)\mathbf{L}Y_{nm}(\Omega)[n(n+1)]^{-1} \quad (1.1.12c)$$

$$\mathbf{B}^{\mathrm{B}} = \mp\frac{i}{k}(+k)\sum_{n,m}\alpha_B(n,m)\nabla\times f_n(\kappa r)\mathbf{L}Y_{nm}(\Omega)[n(n+1)]^{-1} \ . \quad (1.1.12d)$$

Finally, since all the multipole fields are curls, they are divergenceless and it is straightforward to show that they satisfy the Maxwell equation set (1.1.5).

Therefore, these expressions constitute a general solution to the same:

$$\mathbf{E}(\mathbf{r}) = \mathbf{E}^{\mathrm{B}}(\mathbf{r}) + \mathbf{E}^{\mathrm{E}}(\mathbf{r}) \quad (1.1.13a)$$

$$\mathbf{B}(\mathbf{r}) = \mathbf{B}^{\mathrm{E}}(\mathbf{r}) + \mathbf{B}^{\mathrm{B}}(\mathbf{r}) \ . \quad (1.1.13b)$$

Introducing the vector spherical harmonic, $\mathbf{X}_{nm}(\Omega) \equiv [n(n+1)]^{-\frac{1}{2}}\mathbf{L}Y_{nm}(\Omega)$, into (1.1.12) and substituting the results into (1.1.13) give, after rearrangement:

$$\mathbf{E}(\mathbf{r}) = \sum_{n=1}^{\infty}\sum_{m=-n}^{n}\left[a_B(n,m)f_n(\kappa r)\mathbf{X}_{nm}(\theta,\phi) \pm \frac{i}{\kappa}a_E(n,m)\nabla\times f_n(\kappa r)\mathbf{X}_{nm}(\theta,\phi)\right] \quad (1.1.14a)$$

$$\mathbf{B}(\mathbf{r}) = \mathrm{n}\sum_{n=1}^{\infty}\sum_{m=-n}^{n}\left[a_E(n,m)f_n(\kappa r)\mathbf{X}_{nm}(\theta,\phi) \pm \frac{1}{i\kappa}a_B(n,m)\nabla\times f_n(\kappa r)\mathbf{X}_{nm}(\theta,\phi)\right] \quad (1.1.14b)$$

where $a_E(n,m) \equiv \frac{-\alpha_E(n,m)\kappa}{\sqrt{n(n+1)}}$, $a_B(n,m) \equiv \frac{\alpha_B(n,m)k}{\sqrt{n(n+1)}}$, $\mathrm{n} \equiv \sqrt{\epsilon\mu}$, and the $n = 0$ term is excluded since $\mathbf{X}_{00} \equiv 0$. Comparison will show that this is just the generalized version of Jackson Eq. 16.46 [15,p.746], to which it reduces for $\epsilon = \mu = 1,\ \ \kappa = k$.

COEFFICIENT EVALUATION

The coefficients may be specified by a variety of methods according to the circumstances (for example, Jackson Eq. 16.47 [15,p.747]). Of interest here is, firstly, coefficient specification from knowledge of the entire fields, and secondly, from interface field matching. That is, working from general multipole expansions of incident, internal, and scattered fields, (1.1.14), the unknown coefficients are determined for the incident wave from knowledge of its closed form and for the remaining fields, from the boundary conditions inherent in Maxwell's equations. Since, in all cases, the orthonormality of the spherical harmonics plays the central role, the following relations [15, pp.99,746,768] are cited for reference in what follows:

$$\int \mathbf{X}^{\star}_{n'm'}(\Omega)\cdot[\nabla\times f_n(r)\mathbf{X}_{nm}(\Omega)]d\Omega = \int \mathbf{X}^{\star}_{n'm'}(\Omega)\cdot[\mathbf{r}\times\mathbf{X}_{nm}(\Omega)]d\Omega = 0\ , \tag{1.1.15a,b}$$

$$\int Y^{\star}_{n'm'}(\Omega)Y_{nm}(\Omega)d\Omega = \int \mathbf{X}^{\star}_{n'm'}(\Omega)\cdot\mathbf{X}_{nm}(\Omega)d\Omega =$$
$$\int[\hat{\mathbf{r}}\times\mathbf{X}^{\star}_{n'm'}(\Omega)]\cdot[\hat{\mathbf{r}}\times\mathbf{X}_{nm}(\Omega)]d\Omega = \delta_{n'n}\delta_{m'm}\ . \tag{1.1.15c,d,e}$$

1.2 Incident Wave Coefficients

Jackson describes the evaluation of the incident field coefficients in the spherical wave expansion of a vector plane wave with circular polarizations of either helix sense (in the plus phase convention) [15,pp.767–9]. This series form is necessary for the specification of the scattered and internal coefficients from boundary condition imposition, and, since the planar polarization case to be addressed may, as well, be handled in terms of circular waves, it is sufficient here to consider this evaluation procedure, which will be generalized to both phase conventions, only for this circular pair(s):

$$\mathbf{E}^{(\pm)} = \frac{1}{\sqrt{2}}(\hat{\epsilon}_1 \pm i\hat{\epsilon}_2)\mathrm{e}^{i\kappa z} \qquad (+convention: \ 1.2.1a)$$

$$\mathbf{E}^{(\pm)} = \frac{1}{\sqrt{2}}(\hat{\epsilon}_1 \mp i\hat{\epsilon}_2)\mathrm{e}^{-i\kappa z}\ , \qquad (-convention: \ 1.2.1b)$$

where $\hat{\epsilon}_1$ and $\hat{\epsilon}_2$ are real unit vectors in the x and y directions, and the $\pm$'s refer to positive and negative helicity. These field relations for the two sign conventions differ physically in that the imaginary components are $\frac{\pi}{2}$ ahead of the phase of the real components for the plus convention and $\frac{\pi}{2}$ behind in the minus; this feature is demonstrated in the derivation of (1.2.1), which, along with that of

$$\mathbf{B}^{(\pm)} = \mp in\mathbf{E}^{(\pm)} \qquad (+convention: \ 1.2.2a)$$

$$\mathbf{B}^{(\pm)} = \pm in\mathbf{E}^{(\pm)}\ , \qquad (-convention: \ 1.2.2b)$$

is given in Appendix B. It is of moment that the retarded phase versions of these expressions differ from their counterparts exclusively in that $\sqrt{-1}$ is replaced by its negative. This is a reflection of the trend begun in (1.1.3) and carried through (1.1.14), and will prove to be true of the situation generally.

Necessary to the coefficient determination is an open form of the exponential, $e^{\pm i\kappa z}$, which, appropriately enough, arises as a limiting case of the Helmholtz Green function:

$$(\nabla^2 + \lambda^2)\frac{e^{i\lambda|\mathbf{r}-\mathbf{r}'|}}{|\mathbf{r}-\mathbf{r}'|} = -4\pi\delta(\mathbf{r}-\mathbf{r}') \qquad (+convention: \ 1.2.3)$$

[15,pp.223−6]. Jackson gives the expansion of this Green function as

$$\frac{e^{i\lambda|\mathbf{r}-\mathbf{r}'|}}{|\mathbf{r}-\mathbf{r}'|} = 4\pi\sum_{n=0}^{\infty} A j_n(\lambda r_<)h_n^{(1)}(\lambda r_>) \sum_{m=-n}^{n} Y_{nm}^{\star}(\Omega')Y_{nm}(\Omega) \ , \qquad (1.2.4)$$

and identifies A as $i\lambda$, a result of slope discontinuity which follows from (the first of) the Wronskian relations,

$$W\{j_n(z) \ , \ h_n^{(1,2)}(z)\} = \pm\frac{i}{z^2} \qquad (1.2.5a,b)$$

[15, pp.111−113,742], [13,p.437], and since, for the minus convention, it is $h_n^{(2)}(\lambda r_>)$ that describes outgoing waves, it follows that

$$\frac{e^{\pm i\lambda|\mathbf{r}-\mathbf{r}'|}}{|\mathbf{r}-\mathbf{r}'|} = \pm 4\pi i\lambda\sum_{n=0}^{\infty} j_n(\lambda r_<)h_n^{(1,2)}(\lambda r_>) \sum_{m=-n}^{n} Y_{nm}^{\star}(\theta',\phi')Y_{nm}(\theta,\phi) \ .$$

$$(1.2.6a,b)$$

Then, as $|\mathbf{r}'| \longrightarrow \infty$, introduction of the asymptotic Hankel functions $h_n^{(1,2)}(\lambda r') = (\mp i)^{n+1}\frac{e^{\pm i\lambda r'}}{r'}$ [1,p.524], the exponential approximation, $e^{\pm i\lambda|\mathbf{r}-\mathbf{r}'|} \cong e^{\pm i\lambda(r'-\hat{\mathbf{r}}'\cdot\mathbf{r})}$ [15,p.393], and abbreviated denominator: $|\mathbf{r}-\mathbf{r}'|^{-1} \longrightarrow \frac{1}{r'}$ gives, upon specification to $\lambda \longrightarrow \kappa$, and $\hat{\mathbf{r}}' \longrightarrow \hat{\mathbf{k}}$, the unit wave vector (taken to be in the positive z direction; that is, $\theta' \longrightarrow 0$):

$$e^{\mp i\kappa z}\frac{e^{\pm i\kappa r'}}{\kappa r'} = \pm i4\pi\kappa\sum_{n=0}^{\infty} j_n(\kappa r)(\mp i)^{n+1}\frac{e^{\pm i\kappa r'}}{\kappa r'} \sum_{m=-n}^{n} Y_{nm}^{\star}(0,\phi')Y_{nm}(\theta,\phi) \ ,$$

$$(1.2.7a,b)$$

where $r_<$ is r and $r_>$ is r', naturally, and $\hat{\mathbf{r}}'$ denotes $\frac{\mathbf{r}'}{r'}$. Dividing out the terms common to both sides of (1.2.7) and substituting from Jackson Eqs. 3.57 and 3.62 [15,pp.100,1],

$$Y_{n0}(\theta,\phi) = \frac{2n+1}{4\pi}P_n(\cos\theta) = \sqrt{\frac{4\pi}{2n+1}}\sum_{m=-1}^{n} Y^{\star}_{nm}(0,\phi')Y_{nm}(\theta,\phi) \ , \quad (1.2.8a,b)$$

in the resulting expressions give:

$$e^{\pm i\kappa z} = \sum_{n=0}^{\infty}(\pm i)^n[4\pi(2n+1)]^{\frac{1}{2}}j_n(\kappa r)Y_{n0}(\theta,\phi) \ . \quad (1.2.9a,b)$$

It is this single-order harmonic permutation of the series form which facilitates the isolation of the multipole expansion coefficients. This procedure is carried out here incipiently for the plus sign convention, but it will be noted that, just as in the derivation of (1.2.9)−and (1.1.14)−, the alternate convention is easily recovered by the simple replacement of the explicit imaginary unit with its conjugate, which circumstance is indicated below by the use of square brackets.

From (1.1.14), the expansions are:

$$\mathbf{E}^{(\pm)} = \sum_{n',m'}\left\{a_B^{(\pm)}(n',m')j_{n'}(\kappa r)\mathbf{X}_{n'm'}(\Omega) + \frac{[i]}{\kappa}a_E^{(\pm)}(n',m')\nabla\times j_{n'}(\kappa r)\mathbf{X}_{n'm'}(\Omega)\right\} \quad (1.2.10a)$$

$$\mathbf{B}^{(\pm)} = \mathrm{n}\sum_{n',m'}\left\{a_E^{(\pm)}(n',m')j_{n'}(\kappa r)\mathbf{X}_{n'm'}(\Omega) + \frac{1}{[i]\kappa}a_B^{(\pm)}(n',m')\nabla\times j_{n'}(\kappa r)\mathbf{X}_{n'm'}(\Omega)\right\} \quad (1.2.10b)$$

Operation with $\int d\Omega \mathbf{X}^{\star}_{nm}\cdot$ on (1.2.10a) gives, upon appeal to (1.1.15a) and (1.1.15d),

$$a_B^{(\pm)}(n,m)j_n(\kappa r) = \int \mathbf{X}^{\star}_{nm}(\Omega)\cdot\mathbf{E}^{(\pm)}(\mathbf{r})d\Omega \ , \quad (1.2.11)$$

and, in the same way, (1.2.10b) gives, after substitution from (1.2.2a[b]) and comparison with (1.2.11),

$$a_E^{(\pm)}(n,m) = \pm[i]a_B^{(\pm)}(n,m)\ . \tag{1.2.12}$$

Reinstating the scalar harmonic and inserting (1.2.1a[b]) in (1.2.11) give

$$a_B^{(\pm)}(n,m)j_n(\kappa r) = \{2n(n+1)\}^{-\frac{1}{2}} \int (\mathbf{L}Y_{nm})^\star \cdot (\hat{\epsilon}_1 \pm [i]\hat{\epsilon}_2)\mathrm{e}^{[i]\kappa z} d\Omega\ , \tag{1.2.13}$$

the integrand of which is just

$$\{\mathbf{L}\cdot(\hat{\epsilon}_1 \mp [i]\hat{\epsilon}_2)Y_{nm}\}^\star \mathrm{e}^{[i]\kappa z} = \{(L_x \mp [i]L_y)Y_{nm}\}^\star \mathrm{e}^{[i]\kappa z}\ . \tag{1.2.14}$$

The effect of the operation of the components of $\mathbf{L}$ on Y_{nm} is seen from Jackson Eqs. 16.26 and 16.28 [15,p.743] to be

$$(L_x \mp iL_y)Y_{nm} = \sqrt{(n\pm m)(n\mp m+1)}\,Y_{n,m\mp 1}\ , \tag{1.2.15}$$

so that

$$a_B^{(\pm)}(n,m)j_n(\kappa r) = \begin{bmatrix} \sqrt{\frac{(n\pm m)(n\mp m+1)}{2n(n+1)}} \int Y^\star_{n,m\mp 1}(\Omega)\mathrm{e}^{i\kappa z} d\Omega \\ \sqrt{\frac{(n\mp m)(n\pm m+1)}{2n(n+1)}} \int Y^\star_{n,m\pm 1}(\Omega)\mathrm{e}^{-i\kappa z} d\Omega \end{bmatrix}, \tag{1.2.16a, b}$$

where, to avoid confusion, both phase convention expressions have been given explicitly. Finally, insertion of (1.2.9a[b]) in (1.2.16a[b]) eliminates, via $Y_{n'm'}$ orthonormality, the n' summation in the former, leaving, after dividing out j_n, a Kronecker delta in m:

$$a_B^{(\pm)}(n,m) = \begin{bmatrix} \sqrt{\frac{2\pi(n\pm m)(n\mp m+1)(2n+1)}{n(n+1)}}\, i^n \delta_{0,m\mp 1} \\ \sqrt{\frac{2\pi(n\mp m)(n\pm m+1)(2n+1)}{n(n+1)}}\,(-i)^n \delta_{0,m\pm 1} \end{bmatrix}. \tag{1.2.16a, b}$$

Therefore, $a_B^{(\pm)}(n,m)$ is zero except for $m = \pm 1$ in the plus convention and $m = \mp 1$ in the minus, and for these cases, the radicals in (1.2.16) both reduce to $[2\pi(2n+1)]^{\frac{1}{2}}$, so that, with reference also to (1.2.10) and (1.2.12), and the definitions $\mathbf{X}_n^{(\pm)} \equiv \mathbf{X}_{n,m=\pm 1}$ and $a^{(\pm)} \equiv a(n, m = \pm 1)$, the series representations of the incident fields are seen to be

$$\mathbf{E}^{(\pm)}(\mathbf{r}) = \sum_{n=1}^{\infty} \left[a_B^{(\pm)} j_n(\kappa r) \mathbf{X}_n^{(\pm)}(\Omega) + \frac{i}{\kappa} a_E^{(\pm)} \nabla \times j_n(\kappa r) \mathbf{X}_n^{(\pm)}(\Omega) \right]$$

$$\mathbf{B}^{(\pm)}(\mathbf{r}) = \mathrm{n} \sum_{n=1}^{\infty} \left[a_E^{(\pm)} j_n(\kappa r) \mathbf{X}_n^{(\pm)}(\Omega) + \frac{1}{i\kappa} a_B^{(\pm)} \nabla \times j_n(\kappa r) \mathbf{X}_n^{(\pm)}(\Omega) \right]$$

$$a_B^{(\pm)} = i^n [2\pi(2n+1)]^{\frac{1}{2}} = \pm i a_E^{(\pm)} , \qquad (+convention: \; 1.2.18a)$$

and

$$\mathbf{E}^{(\pm)}(\mathbf{r}) = \sum_{n=1}^{\infty} \left[a_B^{(\pm)} j_n(\kappa r) \mathbf{X}_n^{(\mp)}(\Omega) - \frac{i}{\kappa} a_E^{(\pm)} \nabla \times j_n(\kappa r) \mathbf{X}_n^{(\mp)}(\Omega) \right]$$

$$\mathbf{B}^{(\pm)}(\mathbf{r}) = \mathrm{n} \sum_{n=1}^{\infty} \left[a_E^{(\pm)} j_n(\kappa r) \mathbf{X}_n^{(\mp)}(\Omega) - \frac{1}{i\kappa} a_B^{(\pm)} \nabla \times j_n(\kappa r) \mathbf{X}_n^{(\mp)}(\Omega) \right]$$

$$a_B^{(\pm)} = (-i)^n [2\pi(2n+1)]^{\frac{1}{2}} = \mp i a_E^{(\pm)} . \qquad (-convention: \; 1.2.18b)$$

The complex nature of the vector harmonics lies entirely with the parameter m (Appendix C), so it is not surprising that, in contrast with the situation in the plus phase convention, the *positive*-helical fields of the minus convention are described by the *negative*-order harmonics, and vice versa. Also noteworthy is that the minus convention coefficients are the complex conjugates of their counterparts. Exclusion of the gratuitous $\pm$ in the original radial field expansion (1.1.8) would have generated a *negative* conjugate relationship here.

1.3 Boundary Condition Coefficients

For clarity in the evaluation of the internal and scattered coefficients, the $\pm$ superscripts on the fields and coefficients are temporarily dismissed, with the understanding that they are implied throughout; also the sign appendages on the vector harmonics will be dropped, remembering here that the wave-helicity/harmonic-order affiliations are opposites for the two cases. With these stipulations, the $\pm$'s appearing explicitly in the development will refer to the different phase conventions.

To begin, the general expressions for all three field sets are given below, recalling that the spherical medium parameters are identified with the subscript "$_\circ$", and noting that, for the scattered fields, it is the Hankel function (well-behaved at ∞) which is appropriate, rather than the ordinary spherical Bessel function used for the localized (incident and internal) fields. Also, the scattered fields and their coefficients will be distinguished by the subscript "$_s$".

The Mie fields are:

$$\mathbf{E} = \sum_{n=1}^{\infty} \left[a^B j_n(\kappa r)\mathbf{X}_n(\Omega) \pm \frac{i}{\kappa} a^E \nabla \times j_n(\kappa r)\mathbf{X}_n(\Omega) \right] \tag{1.3.1a}$$

$$\mathbf{B} = \mathrm{n} \sum_{n=1}^{\infty} \left[a^E j_n(\kappa r)\mathbf{X}_n(\Omega) \pm \frac{1}{i\kappa} a^B \nabla \times j_n(\kappa r)\mathbf{X}_n(\Omega) \right] \tag{1.3.1b}$$

$$\mathbf{E}_s = \sum_{n=1}^{\infty} \left[a_s^B h_n^{(1,2)}(\kappa r)\mathbf{X}_n(\Omega) \pm \frac{i}{\kappa} a_s^E \nabla \times h_n^{(1,2)}(\kappa r)\mathbf{X}_n(\Omega) \right] \tag{1.3.1c}$$

$$\mathbf{B}_s = \mathrm{n} \sum_{n=1}^{\infty} \left[a_s^E h_n^{(1,2)}(\kappa r)\mathbf{X}_n(\Omega) \pm \frac{1}{i\kappa} a_s^B \nabla \times h_n^{(1,2)}(\kappa r)\mathbf{X}_n(\Omega) \right] \tag{1.3.1d}$$

$$\mathbf{E}_\circ = \sum_{n=1}^{\infty} \left[a_\circ^B j_n(\kappa_\circ r)\mathbf{X}_n(\Omega) \pm \frac{i}{\kappa_\circ} a_\circ^E \nabla \times j_n(\kappa_\circ r)\mathbf{X}_n(\Omega) \right] \tag{1.3.1e}$$

$$\mathbf{B}_\circ = \mathrm{n}_\circ \sum_{n=1}^{\infty} \left[a_\circ^E j_n(\kappa_\circ r)\mathbf{X}_n(\Omega) \pm \frac{1}{i\kappa_\circ} a_\circ^B \nabla \times j_n(\kappa_\circ r)\mathbf{X}_n(\Omega) \right] . \tag{1.3.1f}$$

The curls in these equations may be separated into radial and transverse components in such a way as to render the fields at a point cast onto a mutually orthogonal triad compatible with the boundary condition process. This is accomplished with the curl decomposition,

$$\nabla \times f_n(\lambda r)\mathbf{X}_n(\Omega) = i[n(n+1)]^{\frac{1}{2}} \frac{\hat{\mathbf{r}}}{r} f_n(\lambda r) Y_n(\Omega) + \frac{1}{r} \frac{d[r f_n(\lambda r)]}{dr} \hat{\mathbf{r}} \times \mathbf{X}_n(\Omega) , \tag{1.3.2}$$

from Appendix C.

THE MAXWELL BOUNDARY CONDITIONS

The integral forms of $(1.1.5a, b)$, converted with the divergence theorem into surface integrals applied to a shallow Gaussian pillbox straddling the medium interface, indicate a necessary continuity of the normal, in this case radial, **D** and **B** fields there. Similarly, the use of Stokes' theorem with $(1.1.5c, d)$ in an analogous procedure implies continuity of the tangential **E** and **H** fields at the boundary. These are the ordinary Maxwell boundary conditions and their derivation is detailed in Jackson [15,pp.17–20]. It should be noted that the **D** and **H** continuities rely on the absence of surface charge and current.

Thus, equating the radial component of the total ambient **D** field at the interface, $\hat{\mathbf{r}} \cdot [\mathbf{D} + \mathbf{D}_s]|_{r=a}$, with that inside, $\hat{\mathbf{r}} \cdot \mathbf{D}_\circ|_{r=a}$, gives

$$\mp \sum_{n=1}^{\infty} \sqrt{n(n+1)} \left\{ \frac{\epsilon}{\kappa a} a^E j_n(\kappa r) Y_n(\Omega) + \frac{\epsilon}{\kappa a} a_s^E h_n^{(1,2)}(\kappa r) Y_n(\Omega) \right\}$$

$$\pm \quad \sum_{n=1}^{\infty} \sqrt{n(n+1)} \left\{ \frac{\epsilon_\circ}{\kappa_\circ a} a_\circ^E j_n(\kappa_\circ r) Y_n(\Omega) \right\} = 0 \; , \qquad (1.3.3)$$

where (1.3.2) has been used to isolate the radial components in (1.3.1a, c, e), after the constitutive adaptation of the latter by (1.1.4a). Application of the operator $\int d\Omega Y^\star_{n',\pm 1}(\Omega)$ to (1.3.3), in conjunction with the use of (1.1.15c) then shows that, since $\frac{\epsilon}{\kappa}\frac{\kappa_\circ}{\epsilon_\circ} = \frac{\mathrm{n}_\circ \epsilon}{\mathrm{n}\epsilon_\circ}$,

$$\mp \frac{\mathrm{n}_\circ \epsilon}{\mathrm{n} \epsilon_\circ} \left[a^E j_n(\kappa a) + a_s^E h_n^{(1,2)}(\kappa a) \right] \pm a_\circ^E j_n(\kappa_\circ a) = 0 \; , \qquad (1.3.4a)$$

so that the same equation (different h_n, κ) develops with either sign convention. Repeating this procedure for the continuity of the radial magnetic induction leads, after simplification, to

$$[a^B j_n(\kappa a) + a_s^B h_n^{(1,2)}(\kappa a)] - a_\circ^B j_n(\kappa_\circ a) = 0 \; . \qquad (1.3.4b)$$

Turning to the tangential continuities, it should first be noted that, as it happens, the equations for the $\mathbf{X}_n$ directed components of the tangential fields furnish the same information as the normal boundary condition equations; that is, (1.3.4a) and (1.3.4b) may, alternatively, be derived from the application of (1.1.15d) to the continuity equations of tangential $\mathbf{H}$ and $\mathbf{E}$, respectively, arising from the left-hand terms in (1.3.1), as inspection will demonstrate. It is, then, the

$\mathbf{r} \times \mathbf{X}_n$ directed field components which afford the completion of the coefficient determination:

$\int d\Omega \hat{\mathbf{r}} \times \mathbf{X}^{\star}_{n'}(\Omega) \cdot$ operation on $\mathbf{E}_{\mathrm{TAN}}$ $(at\ r = a)$ gives, via (1.1.15e),

$$\frac{\kappa_\circ}{\kappa}\left\{a^E\left[\frac{d[rj_n(\kappa r)]}{dr}\right]_{r=a} + a_s^E\left[\frac{d[rh_n^{(1,2)}(\kappa r)]}{dr}\right]_{r=a}\right\} = a_\circ^E\left[\frac{d[rj_n(\kappa_\circ r)]}{dr}\right]_{r=a}, \tag{1.3.4c}$$

and $\int d\Omega \hat{\mathbf{r}} \times \mathbf{X}^{\star}_{n'}(\Omega) \cdot$ operation on $\mathbf{H}_{\mathrm{TAN}}$ $(at\ r = a)$ gives, in the same way,

$$\frac{\mu_\circ}{\mu}\left\{a^B\left[\frac{d[rj_n(\kappa r)]}{dr}\right]_{r=a} + a_s^B\left[\frac{d[rh_n^{(1,2)}(\kappa r)]}{dr}\right]_{r=a}\right\} = a_\circ^B\left[\frac{d[rj_n(\kappa_\circ r)]}{dr}\right]_{r=a}. \tag{1.3.4d}$$

Thus the coefficients for the scattered and internal fields are entirely specified by (1.3.4). In solving explicitly for these coefficients, it is convenient to introduce the Ricatti-Bessel functions:

$$\psi_n(z) = zj_n(z)\ , \quad \varsigma_n^{(1,2)}(z) = zh_n^{(1,2)}(z)\ , \tag{1.3.5}$$

in regard to which, it will be noted that, if $\eta_n(\lambda r) \equiv \lambda r f_n(\lambda r)$, then $\frac{d[rf_n(\lambda r)]}{dr} = \frac{d[\eta_n(\lambda r)]}{d(\lambda r)} \equiv \eta_n'(\lambda r)$. With these in place of the Bessel and Hankel functions, the coefficient equations become, after simplification:

$$\left\{\begin{array}{l} \frac{\mathrm{n}_\circ}{\mathrm{n}}[a^B\psi_n(\kappa a) + a_s^B\varsigma_n^{(1,2)}(\kappa a)] = a_\circ^B\psi_n(\kappa_\circ a) \\ \frac{\mu_\circ}{\mu}[a^E\psi_n(\kappa a) + a_s^E\varsigma_n^{(1,2)}(\kappa a)] = a_\circ^E\psi_n(\kappa_\circ a) \\ \frac{\mathrm{n}_\circ}{\mathrm{n}}[a^E\psi_n'(\kappa a) + a_s^E\varsigma_n'^{(1,2)}(\kappa a)] = a_\circ^E\psi_n'(\kappa_\circ a) \\ \frac{\mu_\circ}{\mu}[a^B\psi_n'(\kappa a) + a_s^B\varsigma_n'^{(1,2)}(\kappa a)] = a_\circ^B\psi_n'(\kappa_\circ a)\ . \end{array}\right. \tag{1.3.6a - d}$$

The solution of this simultaneous set of equations is straightforward and the results are:

$$a_s^E(n,\pm1) \quad = \quad a^E(n,\pm1)\ \left\{\frac{\frac{\mu_\circ}{\mu}\psi_n(\kappa a)\psi_n'(\kappa_\circ a) - \frac{\mathrm{n}_\circ}{\mathrm{n}}\psi_n'(\kappa a)\psi_n(\kappa_\circ a)}{\frac{\mathrm{n}_\circ}{\mathrm{n}}\psi_n(\kappa_\circ a)\varsigma_n'(\kappa a) - \frac{\mu_\circ}{\mu}\psi_n'(\kappa_\circ a)\varsigma_n(\kappa a)}\right\} \tag{1.3.7a}$$

$$a_s^B(n,\pm1) \quad = \quad a^B(n,\pm1)\ \left\{\frac{\frac{\mathrm{n}_\circ}{\mathrm{n}}\psi_n(\kappa a)\psi_n'(\kappa_\circ a) - \frac{\mu_\circ}{\mu}\psi_n'(\kappa a)\psi_n(\kappa_\circ a)}{\frac{\mu_\circ}{\mu}\psi_n(\kappa_\circ a)\varsigma_n'(\kappa a) - \frac{\mathrm{n}_\circ}{\mathrm{n}}\psi_n'(\kappa_\circ a)\varsigma_n(\kappa a)}\right\} \tag{1.3.7b}$$

$$a_\circ^E(n,\pm1) \quad = \quad a^E(n,\pm1)\ \left\{\frac{\frac{\mathrm{n}_\circ}{\mathrm{n}}\frac{\mu_\circ}{\mu}\left[\psi_n(\kappa a)\varsigma_n'(\kappa a) - \psi_n'(\kappa a)\varsigma_n(\kappa a)\right]}{\frac{\mathrm{n}_\circ}{\mathrm{n}}\psi_n(\kappa_\circ a)\varsigma_n'(\kappa a) - \frac{\mu_\circ}{\mu}\psi_n'(\kappa_\circ a)\varsigma_n(\kappa a)}\right\} \tag{1.3.7c}$$

$$a_\circ^B(n,\pm1) \quad = \quad a^B(n,\pm1)\ \left\{\frac{\frac{\mathrm{n}_\circ}{\mathrm{n}}\frac{\mu_\circ}{\mu}\left[\psi_n(\kappa a)\varsigma_n'(\kappa a) - \psi_n'(\kappa a)\varsigma_n(\kappa a)\right]}{\frac{\mu_\circ}{\mu}\psi_n(\kappa_\circ a)\varsigma_n'(\kappa a) - \frac{\mathrm{n}_\circ}{\mathrm{n}}\psi_n'(\kappa_\circ a)\varsigma_n(\kappa a)}\right\}\ , \tag{1.3.7d}$$

where once again, the $\pm$'s now refer to helicity.

For the plus convention, $\mathrm{n} = \mathrm{n_{Re}} + i\mathrm{n_{Im}}$, $\varsigma_n = \varsigma_n^{(1)}(\mathrm{n}ka)$, and $a^B(n,\pm1) = i^n\sqrt{2\pi(2n+1)} \;=\; \pm i a^E(n,\pm1)$.

For the minus convention, $\mathrm{n} = \mathrm{n_{Re}} - i\mathrm{n_{Im}}$, $\varsigma_n = \varsigma_n^{(2)}(\mathrm{n}ka)$, and $a^B(n,\pm1) = (-i)^n\sqrt{2\pi(2n+1)} \;=\; \mp i a^E(n,\pm1)$.

It will prove useful to isolate these Ricatti-Bessel product-difference ratios. Using "$\oslash$" to denote relative quantities (i.e., sphere/medium), and letting $\xi \equiv \kappa a$, these "Mie coefficients" take the following form:

$$\begin{cases} \mathcal{E}_n = \mathcal{M}_n = 1 \\ \mathcal{E}_n^s = \left\{\frac{\mu_\oslash\psi_n(\xi)\mathrm{A}_n(\mathrm{n}_\oslash\xi) - \mathrm{n}_\oslash\psi_n'(\xi)}{\mathrm{n}_\oslash\varsigma_n'(\xi) - \mu_\oslash\varsigma_n(\xi)\mathrm{A}_n(\mathrm{n}_\oslash\xi)}\right\} \\ \mathcal{M}_n^s = \left\{\frac{\mathrm{n}_\oslash\psi_n(\xi)\mathrm{A}_n(\mathrm{n}_\oslash\xi) - \mu_\oslash\psi_n'(\xi)}{\mu_\oslash\varsigma_n'(\xi) - \mathrm{n}_\oslash\varsigma_n(\xi)\mathrm{A}_n(\mathrm{n}_\oslash\xi)}\right\} \\ \mathcal{E}_n^\circ = \left\{\frac{\mathrm{n}_\oslash\mu_\oslash\varsigma_0(\pi)/\psi_n(\mathrm{n}_\oslash\xi)}{\mathrm{n}_\oslash\varsigma_n'(\xi) - \mu_\oslash\varsigma_n(\xi)\mathrm{A}_n(\mathrm{n}_\oslash\xi)}\right\} \\ \mathcal{M}_n^\circ = \left\{\frac{\mathrm{n}_\oslash\mu_\oslash\varsigma_0(\pi)/\psi_n(\mathrm{n}_\oslash\xi)}{\mu_\oslash\varsigma_n'(\xi) - \mathrm{n}_\oslash\varsigma_n(\xi)\mathrm{A}_n(\mathrm{n}_\oslash\xi)}\right\}\ , \end{cases} \tag{1.3.8a - f}$$

wherein $A_n(n_{\oslash}\xi) \equiv \psi_n'(n_{\oslash}\xi)/\psi_n(n_{\oslash}\xi)$ (a computationally more tractable form), and $\varsigma_0^{(1,2)}(\pi) \;=\; \pm\, i$.

This allows the expression of the fields for both phase conventions in the more convenient form :

$$\mathbf{E}^{(\pm)}_{\text{PLUS}} \;=\; \sum_{n=1}^{\infty} \; i^n \; [2\pi(2n{+}1)]^{\frac{1}{2}} \left\{ \mathcal{M}_n f_n(\kappa r)\mathbf{X}_n^{(\pm)}(\Omega) \pm \mathcal{E}_n \frac{1}{\kappa}\nabla \times f_n(\kappa r)\mathbf{X}_n^{(\pm)}(\Omega) \right\} \tag{1.3.9a}$$

$$\mathbf{E}^{(\pm)}_{\text{MINUS}} = \sum_{n=1}^{\infty}(-i)^n[2\pi(2n{+}1)]^{\frac{1}{2}} \left\{ \mathcal{M}_n f_n(\kappa r)\mathbf{X}_n^{(\mp)}(\Omega) \pm \mathcal{E}_n \frac{1}{\kappa}\nabla \times f_n(\kappa r)\mathbf{X}_n^{(\mp)}(\Omega) \right\} . \tag{1.3.9b}$$

For scattered fields, $\mathcal{E}_n^s$ and $\mathcal{M}_n^s$ are used for the coefficients and the spherical Hankel functions for the radial dependence.

For internal fields, $\mathcal{E}_n^\circ$ and $\mathcal{M}_n^\circ$ are the coefficients and the spherical Bessel functions give the radial dependence (and κ, n $\longrightarrow$ $\kappa_\circ$, $n_\circ$, of course).

Also, for the switch from plus phase convention to minus, there is a change of Hankel functions ($h_n^{(1)} \longrightarrow h_n^{(2)}$), and a refractive index conjugation which transforms all the Ricatti-Bessel functions and their arguments(save ς_0's) in both the coefficients and the radial dependence ($\psi_n(\mathrm{n}kr) = \mathrm{n}krj_n(\mathrm{n}kr) \longrightarrow \mathrm{n}^\star krj_n(\mathrm{n}^\star kr)$, etc.). If the radial functions and the refractive indices($\mathrm{n}_{\mathrm{Im}} \neq 0$) are not correlated, the resulting field expressions are physically nonsensical, albeit only subtly so when $\mathrm{Im}\{\kappa_\circ a\}$ is small, and if correctly matched h_n and n are inserted in the wrong field equation, the result is, as discussed in the next section, a rotation through π, about the x-axis, of the y-z plane.

1.4 The Electric Field in Component Form

(1.3.9) gives the electric field for the Mie problem. The use of this result for practical calculation is customarily facilitated by the resolution of (1.3.9) into its spherical coordinate components. For this, the component forms of the vector harmonic and its curl are extracted in Appendix C, and given here as

$$\mathbf{X}_{n,\pm 1}(\theta,\phi) = i\sqrt{\frac{2n+1}{4\pi}}\frac{1}{n(n+1)}\left(\hat{\theta}\frac{i}{\sin\theta} \mp \hat{\phi}\frac{d}{d\theta}\right)P_n^1(\cos\theta)\mathrm{e}^{\pm i\phi} \tag{1.4.1}$$

and $\nabla \times f_n(\kappa r)\mathbf{X}_{n,\pm 1} =$

$$i\sqrt{\frac{2n+1}{4\pi}}\frac{\mathrm{e}^{\pm i\phi}}{rn(n+1)}\left[\pm\hat{\mathrm{r}}\frac{n(n+1)}{r} + (\hat{\phi}\frac{i}{\sin\theta} \pm \hat{\theta}\frac{d}{d\theta})\frac{d}{dr}\right] rf_n(\kappa r)P_n^1(\cos\theta)\ . \tag{1.4.2}$$

Substituting these expressions in (1.3.9a) gives $\mathbf{E}$ as

$$\sum_{n=1}^{\infty} i^n\sqrt{2\pi(2n+1)}\left\{\mathcal{M}_n f_n(\kappa r) i\sqrt{\frac{2n+1}{4\pi}}\frac{\mathrm{e}^{\pm i\phi}}{n(n+1)}\left[\hat{\theta}\frac{i}{\sin\theta} \mp \hat{\phi}\frac{d}{d\theta}\right]P_n^1(\cos\theta)\right.$$

$$\left.\pm\mathcal{E}_n\frac{i}{\kappa}\sqrt{\frac{2n+1}{4\pi}}\frac{\mathrm{e}^{\pm i\phi}}{rn(n+1)}\left[\pm\hat{\mathrm{r}}\frac{n(n+1)}{r} + (\hat{\phi}\frac{i}{\sin\theta} \pm \hat{\theta}\frac{d}{d\theta})\frac{d}{dr}\right] rf_n(\kappa r)P_n^1(\cos\theta)\right\}\ , \tag{$+convention:$ 1.4.3a}$$

and $\mathbf{E}$ from (1.3.9b) is

$$\sum_{n=1}^{\infty} (-i)^n\sqrt{2\pi(2n+1)}\left\{\mathcal{M}_n f_n(\kappa r) i\sqrt{\frac{2n+1}{4\pi}}\frac{\mathrm{e}^{\mp i\phi}}{n(n+1)}\left[\hat{\theta}\frac{i}{\sin\theta} \pm \hat{\phi}\frac{d}{d\theta}\right]P_n^1(\cos\theta)\right.$$

$$\left.\pm\mathcal{E}_n\frac{i}{\kappa}\sqrt{\frac{2n+1}{4\pi}}\frac{\mathrm{e}^{\mp i\phi}}{rn(n+1)}\left[\mp\hat{\mathrm{r}}\frac{n(n+1)}{r} + (\hat{\phi}\frac{i}{\sin\theta} \mp \hat{\theta}\frac{d}{d\theta})\frac{d}{dr}\right] rf_n(\kappa r)P_n^1(\cos\theta)\right\}\ . \tag{$-convention:$ 1.4.3b}$$

Collecting the contributions to the individual vector components, enlisting the generic Ricatti-Bessel function, $\eta_n(\kappa r)$, and defining

$$\pi_n(\cos\theta) \equiv \frac{P_n^1(\cos\theta)}{\sin\theta} \quad , \quad \tau_n(\cos\theta) \equiv \frac{d}{d\theta}P_n^1(\cos\theta) \quad , \tag{1.4.4}$$

lead to

$$\mathrm{E}_r^{(\pm)} = \frac{\mathrm{e}^{\pm i\phi}}{\sqrt{2}\kappa^2 r^2}\sum_{n=1}^{\infty} i^{n+1}(2n+1)\mathcal{E}_n\eta_n(\kappa r)\pi_n(\cos\theta)\sin\theta$$

$$\mathrm{E}_\theta^{(\pm)} = \frac{\mathrm{e}^{\pm i\phi}}{\sqrt{2}\kappa r}\sum_{n=1}^{\infty} i^{n+1}\frac{2n+1}{n(n+1)}\left[\mathcal{E}_n\eta_n'(\kappa r)\tau_n(\cos\theta) + i\mathcal{M}_n\eta_n(\kappa r)\pi_n(\cos\theta)\right]$$

$$\mathrm{E}_\phi^{(\pm)} = \pm i\frac{\mathrm{e}^{\pm i\phi}}{\sqrt{2}\kappa r}\sum_{n=1}^{\infty} i^{n+1}\frac{2n+1}{n(n+1)}\left[\mathcal{E}_n\eta_n'(\kappa r)\pi_n(\cos\theta) + i\mathcal{M}_n\eta_n(\kappa r)\tau_n(\cos\theta)\right] \ ,$$

$$(+convention: \ 1.4.5a)$$

and

$$\mathrm{E}_r^{(\pm)} = \frac{\mathrm{e}^{\mp i\phi}}{\sqrt{2}\kappa^2 r^2}\sum_{n=1}^{\infty}(-i)^{n+1}(2n+1)\mathcal{E}_n\eta_n(\kappa r)\pi_n(\cos\theta)\sin\theta$$

$$\mathrm{E}_\theta^{(\pm)} = \frac{\mathrm{e}^{\mp i\phi}}{\sqrt{2}\kappa r}\sum_{n=1}^{\infty}(-i)^{n+1}\frac{2n+1}{n(n+1)}\left[\mathcal{E}_n\eta_n'(\kappa r)\tau_n(\cos\theta) - i\mathcal{M}_n\eta_n(\kappa r)\pi_n(\cos\theta)\right]$$

$$\mathrm{E}_\phi^{(\pm)} = \mp i\frac{\mathrm{e}^{\mp i\phi}}{\sqrt{2}\kappa r}\sum_{n=1}^{\infty}(-i)^{n+1}\frac{2n+1}{n(n+1)}\left[\mathcal{E}_n\eta_n'(\kappa r)\pi_n(\cos\theta) - i\mathcal{M}_n\eta_n(\kappa r)\tau_n(\cos\theta)\right] \ .$$

$$(-convention: \ 1.4.5b)$$

Then, for the incident *plane* polarization cases, the E fields are just $\mathbf{E}^{(\mathrm{x})} = \frac{1}{\sqrt{2}}\left[\mathbf{E}^{(+)} + \mathbf{E}^{(-)}\right] =$ (*plus convention*) $\frac{1}{2}\left[(\hat{\epsilon}_1 + i\hat{\epsilon}_2)\mathrm{e}^{i\kappa z} + (\hat{\epsilon}_1 - i\hat{\epsilon}_2)\mathrm{e}^{i\kappa z}\right] = \hat{\epsilon}_1\mathrm{e}^{i\kappa z}$, and $\mathbf{E}^{(\mathrm{y})} = \frac{1}{i\sqrt{2}}\left[\mathbf{E}^{(+)} - \mathbf{E}^{(-)}\right] = \frac{1}{2i}\left[(\hat{\epsilon}_1 + i\hat{\epsilon}_2)\mathrm{e}^{i\kappa z} - (\hat{\epsilon}_1 - i\hat{\epsilon}_2)\mathrm{e}^{i\kappa z}\right] = \hat{\epsilon}_2\mathrm{e}^{i\kappa z}$, so that, since $\frac{1}{2}(\mathrm{e}^{i\phi} + \mathrm{e}^{-i\phi}) = \cos\phi = \sin(\frac{\pi}{2} - \phi)$, and $\frac{1}{2i}(\mathrm{e}^{i\phi} - \mathrm{e}^{-i\phi}) = \sin\phi = \cos(\phi - \frac{\pi}{2})$, these may, with the definition

$$\delta = \begin{cases} 0 \ , \ \mathbf{E} = \mathbf{E}^{(\mathrm{x})} \\ \frac{\pi}{2} \ , \ \mathbf{E} = \mathbf{E}^{(\mathrm{y})} \ , \end{cases} \tag{1.4.6}$$

be written as

$$E_r^{(x,y)} = \frac{\cos(\delta-\phi)}{\kappa^2 r^2} \sum_{n=1}^{\infty} i^{n+1}(2n+1)\mathcal{E}_n \eta_n(\kappa r)\pi_n(\cos\theta)\sin\theta$$

$$E_\theta^{(x,y)} = \frac{\cos(\delta-\phi)}{\kappa r} \sum_{n=1}^{\infty} i^{n+1}\frac{2n+1}{n(n+1)}\left[\mathcal{E}_n \eta_n'(\kappa r)\tau_n(\cos\theta) + i\mathcal{M}_n \eta_n(\kappa r)\pi_n(\cos\theta)\right]$$

$$E_\phi^{(x,y)} = \frac{\sin(\delta-\phi)}{\kappa r} \sum_{n=1}^{\infty} i^{n+1}\frac{2n+1}{n(n+1)}\left[\mathcal{E}_n \eta_n'(\kappa r)\pi_n(\cos\theta) + i\mathcal{M}_n \eta_n(\kappa r)\tau_n(\cos\theta)\right] ,$$

$$(+convention: \ 1.4.7a)$$

and

$$E_r^{(x,y)} = \frac{\cos(\delta-\phi)}{\kappa^2 r^2} \sum_{n=1}^{\infty} (-i)^{n+1}(2n+1)\mathcal{E}_n \eta_n(\kappa r)\pi_n(\cos\theta)\sin\theta$$

$$E_\theta^{(x,y)} = \frac{\cos(\delta-\phi)}{\kappa r} \sum_{n=1}^{\infty} (-i)^{n+1}\frac{2n+1}{n(n+1)}\left[\mathcal{E}_n \eta_n'(\kappa r)\tau_n(\cos\theta) - i\mathcal{M}_n \eta_n(\kappa r)\pi_n(\cos\theta)\right]$$

$$E_\phi^{(x,y)} = \frac{\sin(\delta-\phi)}{\kappa r} \sum_{n=1}^{\infty} (-i)^{n+1}\frac{2n+1}{n(n+1)}\left[\mathcal{E}_n \eta_n'(\kappa r)\pi_n(\cos\theta) - i\mathcal{M}_n \eta_n(\kappa r)\tau_n(\cos\theta)\right] .$$

$$(-convention: \ 1.4.7b)$$

It bears mention that, in this form, the minus convention equations may be obtained from the plus merely by replacing the explicit imaginary unit with its conjugate, just as in the earlier work.

AXES REVERSAL

One point to be made here concerns the effective axes-reversal which can result from mixing phase conventions. This is an effect of the Legendre functions which could undoubtedly be derived from the case of incident light in the *negative* z direction. To see this, it is only necessary to consider the case $\mathbf{E}^{(x)}$, for which it is evident that a sign reversal of ϕ has no effect except to reverse the direction of the ϕ component [from (1.4.7)]; this, in tandem with the behavior of the π and τ functions for $\theta' = 180° - \theta$,

$$\pi_n(\cos\theta') = \frac{i^{n+1}}{(-i)^{n+1}}\pi_n(\cos\theta) \ , \tag{1.4.8a}$$

$$\tau_n(\cos\theta') = -\frac{i^{n+1}}{(-i)^{n+1}}\tau_n(\cos\theta) \ , \tag{1.4.8b}$$

[19,p.73] indicates that using the plus(minus) convention indices and Hankel functions in the minus(plus) convention equations simply converts $\mathbf{E}(r,\theta,\phi)$ to

$$\hat{\mathbf{r}}E_r(r,\theta',-\phi) - \hat{\theta}E_\theta(r,\theta',-\phi) - \hat{\phi}E_\phi(r,\theta',-\phi) \ . \tag{1.4.9}$$

But this is precisely the change required of the directions and angles in a reversal of the z and y axes; that is, $\hat{\theta}, \hat{\phi}$, and ϕ go to their negatives, and θ to its supplement.

As it happens, then, a sign reversal of the i's reverses the direction (relative to axes) and exchanging indices (and Hankel functions), the phase convention, of the light:

$$\begin{cases} +\textit{convention equations} \ : \ \mathrm{n_{Re}} \pm i\mathrm{n_{Im}}, h_n^{(1,2)} & \sim \quad \exp[\pm i(\mathrm{n}kz \mp \omega t)] \\ -\textit{convention equations} \ : \ \mathrm{n_{Re}} \pm i\mathrm{n_{Im}}, h_n^{(1,2)} & \sim \quad \exp[\pm i(\mathrm{n}kz \pm \omega t)] \ . \end{cases}$$

SOURCE TERM

The major application of (1.4.5) and (1.4.7) has been in the determination of the rate of laser energy deposition in the sphere, which is measured in units of power density. Since the fields defined in (1.2.1) are dimensionless, so too are those of (1.4.5,7), and to express the actual physical fields, units must be appended. Thus the electric field within the sphere is

$$\mathbf{E}_{\mathrm{INT}} = \mathbf{E}_\circ \left[\frac{\mathrm{erg}}{\mathrm{cm}^3}\right]^{\frac{1}{2}} \; . \tag{1.4.10}$$

Also, since the coefficients of the derived fields are proportional to those of the incident field [from (1.3.7)], the internal field for arbitrary incident amplitude, $|\mathbf{E}| \neq 1$, may be expressed simply as

$$\mathbf{E}_\circ = |\mathbf{E}|\mathbf{E}_\circ \; , \tag{1.4.11}$$

where it is understood that $\mathbf{E}_\circ$ retains its unit case definition, (1.4.5,7).

Therefore, the source function, given by the divergence of the Poynting vector within the sphere as

$$\mathrm{S}(\mathbf{r}) = \frac{\omega}{4\pi}\frac{1}{\mu_\circ}\mathrm{n}^\circ_{\mathrm{Re}}\mathrm{n}^\circ_{\mathrm{Im}}\mathbf{E}^\star_{\mathrm{INT}} \cdot \mathbf{E}_{\mathrm{INT}} \; , \tag{1.4.12}$$

may, from (1.4.10) and (1.4.11), be written for arbitrary incident amplitude as

$$\mathrm{S}(\mathbf{r}) = \frac{\omega}{4\pi}\mathcal{N}|\mathbf{E}|^2\hat{S}(\mathbf{r})\frac{\mathrm{erg}}{\mathrm{cm}^3} \; , \tag{1.4.13a}$$

where

$$\mathcal{N} \equiv \frac{1}{\mu_\circ}\mathrm{n}^\circ_{\mathrm{Re}}\mathrm{n}^\circ_{\mathrm{Im}} \; , \tag{1.4.13b}$$

$$\text{and} \quad \hat{S}(\mathbf{r}) \equiv \mathbf{E}^\star_\circ(\mathbf{r}) \cdot \mathbf{E}_\circ(\mathbf{r}) \; . \tag{1.4.13c}$$

In practice, it will be convenient to express (1.4.13) in terms of the incident laser flux, which is related by

$$I = \frac{c\mathrm{n}_{\mathrm{Re}}}{8\pi\mu}|\mathbf{E}|^2\frac{\mathrm{erg}}{\mathrm{cm}^3} \; , \tag{1.4.14}$$

so that the source function for the Mie problem is given by

$$\mathrm{S}(\mathbf{r}) = \frac{4\pi\mu I}{\lambda_0 \mathrm{n_{Re}}} \mathcal{N} \hat{S}(\mathbf{r}) \ , \tag{1.4.15}$$

in which I is the incident laser flux in power per area, λ_0 is the free-space wavelength, and μ and $\mathrm{n_{Re}}$ refer to the ambient medium. The derivations of (1.4.12) and (1.4.14) are given in Appendix D.

The normalized source function, $\hat{S}(\mathbf{r})$, deserves some attention [24]. Because of the azimuthal behavior of the fields, (1.4.7), it will prove expeditious here, as well as in what is to follow, to decompose this relative energy density in relation to the z axis; that is, $\hat{S}(\mathbf{r})$ will be described in terms of contributions arising from the fields coplanar with, and solenoidal about, the z axis:

$$S_{\otimes}(r,\theta) \equiv \left| \sum_{n=1}^{\infty} \frac{i^{n+1}(2n+1)}{\kappa_\circ^2 r^2} \mathcal{E}_n^\circ \psi_n(\kappa_\circ r)\pi_n(\cos\theta)\sin\theta \right|^2 +$$

$$\left| \sum_{n=1}^{\infty} \frac{i^{n+1}(2n+1)}{\kappa_\circ r n(n+1)} \left[\mathcal{E}_n^\circ \psi_n'(\kappa_\circ r)\tau_n(\cos\theta) + i\mathcal{M}_n^\circ \psi_n(\kappa_\circ r)\pi_n(\cos\theta)\right] \right|^2 \tag{1.4.16a}$$

$$S_{\odot}(r,\theta) \equiv \left| \sum_{n=1}^{\infty} \frac{i^{n+1}(2n+1)}{\kappa_\circ r n(n+1)} \left[\mathcal{E}_n^\circ \psi_n'(\kappa_\circ r)\pi_n(\cos\theta) + i\mathcal{M}_n^\circ \psi_n(\kappa_\circ r)\tau_n(\cos\theta)\right] \right|^2 . \tag{1.4.16b}$$

For the circular polarizations, then, the source is the same for either helicity; that is, $\mathrm{e}^{\pm i\phi}[\mathrm{e}^{\pm i\phi}]^\star = \mathrm{e}^{\pm i\phi}\mathrm{e}^{\mp i\phi} = 1$:

$$\hat{S}^{(\pm)}(\mathbf{r}) = \frac{1}{2}\left[S_{\otimes}(r,\theta) + S_{\odot}(r,\theta)\right] \ , \tag{1.4.17}$$

and for plane polarizations, the appropriate form is, exploiting the diminished (and non-negative) ranges of the trigonometric squares (their insensitivity to the direction of right angle phase shifts, and to argument quadrant):

$$\hat{S}^{(x,y)}(\mathbf{r}) = \cos^2(\phi+\delta)\,S_{\otimes}(r,\theta) + \sin^2(\phi+\delta)\,S_{\odot}(r,\theta) \ , \tag{1.4.18}$$

where δ is as defined in (1.4.6). For incident light that is randomly polarized, the source term may be given in terms of those for these plane cases:

$$\hat{S}(\mathbf{r}) = \frac{1}{2}\left[\hat{S}^{(x)}(\mathbf{r}) + \hat{S}^{(y)}(\mathbf{r})\right] =$$

$$\frac{1}{2}\left[\cos^2\phi S_{\otimes}(r,\theta) + \sin^2\phi S_{\odot}(r,\theta) + \sin^2\phi S_{\otimes}(r,\theta) + \cos^2\phi S_{\odot}(r,\theta)\right] =$$

$$\frac{1}{2}\left[S_{\otimes}(r,\theta) + S_{\odot}(r,\theta)\right] \ , \tag{1.4.19}$$

which, interestingly, is the same as the circular cases. Also of note is that the plane source exhibits twofold bilateral symmetry, and that, for $\phi = \frac{\pi}{4}$, it reduces to that of the non-planar cases (at any angle).

Since S($\mathbf{r}$) represents the rate of energy deposition per unit volume, it may be integrated over the entire sphere to give the total power removed from the beam, that is, a measure of the absorption cross-section. This has provided a vital corroboration of the overall accuracy of the calculational codes in their final form as well as of the soundness of the reasoning that underlies them. The NCAR Miev0 [29] routine was used as reference; it is well documented and thoroughly tested and, for that matter, has, reciprocally, received additional testament to its reliability from these very source integrations.

For the development in Chapter 2 and the examples of Chapter 3, the incident field amplitude, and thereby, energy flux, are assumed to be functions of time, in contrast to the assumption underlying the derivation given here. If the time variation is comparatively slow, however, as discussed in section 3.3, the present results are sufficiently valid. Therefore, the time-dependent source function is taken, for use in what follows, to be

$$\mathrm{S}(\mathbf{r},t) = \frac{4\pi\mu}{\lambda_0 \mathrm{n}_{\mathrm{Re}}} I(t) \mathcal{N} \hat{S}(\mathbf{r}) \ . \tag{1.4.20}$$

CHAPTER 2

TEMPERATURE EVOLUTION

The response of the spherical medium to the radiation bath is, in general, elaborate. In tandem with the heating of the material, a number of allied processes manifest themselves. The French workers, Autric, et al [2], for example, have identified four specific mechanisms of interest (in liquid spheres): vaporization, deformation, shattering, and propulsion. Although there are not always clear distinctions separating these effects from one another, it can prove useful to provisionally isolate them for the purpose of analysis. The focus here will be on the evolution of temperature distributions produced by electromagnetic heating and thermal diffusion, with attention to the onset of shattering, or explosive vaporization.

2.1 The Heat Equation

When all or part of the sphere reaches a threshold temperature, known as the "superheat limit"[24], the critical region disrupts rapidly in what is essentially mid-air boiling, initiated by spontaneous nucleation. While this shattering does, in and of itself, represent a diffusion of thermal energy, the heat diffusion of concern here is the homogenization of the temperature distribution within the intact sphere prior to disruption through the agency of heat conduction. Of interest, then, is the activity described by:

$$\nabla \cdot \{\mathcal{K}[T(\mathbf{r},t)]\nabla T(\mathbf{r},t)\} + \mathrm{S}[\mathbf{r},t,T(\mathbf{r},t)] = \rho[T(\mathbf{r},t)]C_p[T(\mathbf{r},t)]\frac{\partial T(\mathbf{r},t)}{\partial t} \; . \quad (2.1.1)$$

The terms in this equation arise as integrands in an energy conservation statement. The middle and the first (from a converted surface integral) give the rates at which photoabsorptional heating and thermal gradient driven conduction, respectively, vary the local heat density, and the right side specifies the rate of corresponding temperature change.

One important simplification which is possible is the dismissal of the temperature dependence of the source term. This is typical strategy [24,pp.1633,7], [28,p.1139], since it precludes the computational obstacle of source evaluation for inhomogeneous index distributions and does not, in many cases, seriously compromise the fidelity of the model. The procedure in all that follows will be to allow the source values for the initial (ambient temperature) refractive index distribution (homogeneous) to represent those for all subsequent (nonhomogeneous) distributions. Thus the diffusion equation is:

$$\nabla \cdot \{\mathcal{K}[T(\mathbf{r},t)]\nabla T(\mathbf{r},t)\} + \mathrm{S}(\mathbf{r},t) = \rho[T(\mathbf{r},t)]C_p[T(\mathbf{r},t)]\frac{\partial T(\mathbf{r},t)}{\partial t} \; . \quad (2.1.2)$$

STRONG PULSE APPROXIMATION

One special case of interest is the comparatively simple situation afforded by the intense heating possible with the use of high-powered lasers. For strong pulses the superheat limit of the material may be quickly reached, and heat and mass transfer, inertially stymied, become unimportant to the process [24]. In such rapid heating, the laser energy remains at the deposit site and the temperature history of a given point is independent of the rest of the sphere (except, of course, in the sense that the fields at a point are functions of the entire light/sphere interaction).

For such an impotent gradient, the heat equation is:

$$\mathrm{S}(\mathbf{r},t) = \rho[T(\mathbf{r},t)]C_p[T(\mathbf{r},t)]\frac{\partial T(\mathbf{r},t)}{\partial t} \ , \tag{2.1.3}$$

and from (1.4.20) above, the source term is given by:

$$\mathrm{S}(\mathbf{r},t) = L(t)\mathcal{N}[T(\mathbf{r},t)]\hat{S}(\mathbf{r}) \ , \tag{2.1.4}$$

where $\hat{S}(\mathbf{r})$ is the internal field energy density relative to that of the incident field, $L(t) \equiv \frac{4\pi\mu}{\lambda_0 \mathrm{n_{Re}}} I(t)$, and $\mathcal{N}$ is defined in (1.4.13b). This allows the arrangement

$$\hat{S}(\mathbf{r}) = \frac{\rho[T(\mathbf{r},t)]C_p[T(\mathbf{r},t)]}{\mathcal{N}[T(\mathbf{r},t)]L(t)}\frac{\partial T(\mathbf{r},t)}{\partial t} \ , \tag{2.1.5}$$

which implies that all points, $\mathbf{x}$, with a given value, f, of $\hat{S}$ share a common temperature, T, at the time t. That is, the selection of a particular time and temperature identifies a set of vectors, $\mathbf{x}$ (subset of $\mathbf{r}$), for which $\hat{S}(\mathbf{r})$ has the value $f(T,t)$:

$$\hat{S}[\mathbf{r} = \mathbf{x}(T,t)] = f(T,t) = \int_{T_o}^{T} \frac{\rho(T')C_p(T')}{\mathcal{N}(T')}dT' \left[\int_0^t L(t')dt'\right]^{-1} \ . \tag{2.1.6}$$

The right hand side of (2.1.6) is a pure number whose value depends on the temperature of interest, the temperature dependences of the thermal/optical properties, the time of interest, and the laser pulse (size and shape).

The point is that, in this approximation, the history of temperature growth is the same for all thermal/optical property scenarios and laser pulses, the only variable being which observation time and temperature are correlated with a given value of $\hat{S}(\mathbf{r})$.

That is, if $\hat{S}(\mathbf{r})$ is plotted in a z-axis-containing plane, a sequence of cross-sections from the top down gives the heating pattern of any drop with that size parameter and index, for arbitrary pulses [24]. If the 3-D $\hat{S}$ plot is cut near the top, the intersection of the inserted plane with $\hat{S}$ gives the 2-D contour of a region whose temperature lies at or above a particular T at some time t, and if it is then cut again, this time near the bottom, the new contour is that for a lower cut-off temperature and/or a later time (or, for example, the same T and t for a smaller thermal/optical integrand, and/or stronger pulse, and so on). This provides a very direct practical application of the Mie theory developed in Chapter 1.

GENERAL CASE

If the sphere remains intact for longer periods conduction becomes important. The formal statement of this problem entails the specification of initial and boundary conditions in addition to the differential equation itself. That is, for a given initial distribution $T_o(\mathbf{r})$, the subsequent thermal behavior is governed by the diffusion equation within the sphere and by a second mechanism at the interface; in this case, Newton's law of cooling, heat transfer proportional to temperature difference, is assumed to be the operative process at the boundary. In particular, vaporizational mass loss and thermal radiation, both potentially relevant, are neglected.

Thus the problem is:

$$T(\mathbf{r},0) = T_o(\mathbf{r}) \quad (\text{at} \ \ t=0) \tag{2.1.7a}$$

$$\nabla\cdot\{\mathcal{K}[T(\mathbf{r},t)]\nabla T(\mathbf{r},t)\}+\mathrm{S}(\mathbf{r},t) = \rho[T(\mathbf{r},t)]C_p[T(\mathbf{r},t)]\frac{\partial T(\mathbf{r},t)}{\partial t} \ , \ |\mathbf{r}| < a \ , \ \ t>0 \tag{2.1.7b}$$

$$\mathcal{K}\frac{\partial T(\mathbf{r},t)}{\partial r} = \mathcal{H}[T_{\mathrm{a}}(\mathbf{r},t) - T(\mathbf{r},t)] \ \ \text{at} \ \ |\mathbf{r}| = a \ , \ \ t>0 \ , \tag{2.1.7c}$$

where $T_{\mathrm{a}}(\mathbf{r},t)$ is the temperature field in the ambient medium, relevant here only at the interface.

2.2 Analytic Solution

When the approximation of constant thermal and optical properties is admissible, the problem may be treated analytically, without resort to finite difference differential approximation. This proceeds as follows:

PROBLEM

$$T(\mathbf{r},0) = T_o(\mathbf{r}) \tag{2.2.1a}$$

$$\nabla^2 T(\mathbf{r},t) + \frac{1}{\mathcal{K}}\mathrm{S}(\mathbf{r},t) = \frac{1}{\beta}\frac{\partial T(\mathbf{r},t)}{\partial t} \ , \ \ r<a \ , \ \ t>0 \tag{2.2.1b}$$

$$\mathcal{K}\frac{\partial T(\mathbf{r},t)}{\partial r} = \mathcal{H}[T_{\mathrm{a}}(\mathbf{r},t) - T(\mathbf{r},t)] \ \ \text{at} \ \ r=a \ , \ \ t>0 \tag{2.2.1c}$$

SOLUTION

$$T(\mathbf{r},t) = \int_V \mathrm{G}(\mathbf{r},t|\mathbf{r}',t')|_{t'=0} T_o(\mathbf{r}')dv' +$$

$$\frac{\beta}{K}\int_{t'=0}^{t} dt' \oint_S \mathrm{G}(\mathbf{r},t|\mathbf{r}',t')|_{r'=a} \mathcal{H} T_{\mathrm{a}}(\mathbf{r}',t')ds' +$$

$$\frac{\beta}{K}\int_{t'=0}^{t} dt' \int_V \mathrm{G}(\mathbf{r},t|\mathbf{r}',t')\mathrm{S}(\mathbf{r}',t')dv', \qquad (2.2.2)$$

where G satisfies

$$\mathrm{G}(\mathbf{r},t|\mathbf{r}',t') = 0\ , \quad t < t' \qquad (2.2.3a)$$

$$\nabla^2 \mathrm{G}(\mathbf{r},t|\mathbf{r}',t') + \frac{1}{K}\delta(t-t')\delta(\mathbf{r}-\mathbf{r}') = \frac{1}{\beta}\frac{\partial \mathrm{G}(\mathbf{r},t|\mathbf{r}',t')}{\partial t}\ , \quad t > t' \qquad (2.2.3b)$$

$$K\frac{\partial \mathrm{G}}{\partial r} + \mathcal{H}\mathrm{G} = 0\ , \quad t > t' \quad . \qquad (2.2.3c)$$

This solution is taken from Özişik [22,p.213].

For the case $\mathrm{S}(\mathbf{r},t) = T_{\mathrm{a}}(\mathbf{r},t) = 0$, a solution of the form [i.e., (2.2.6,7)],

$$T(\mathbf{r},t) \ = \int_V K(\mathbf{r},\mathbf{r}',t)T_o(\mathbf{r}')dv'\ , \qquad (2.2.4a)$$

indicates that

$$\mathrm{G}(\mathbf{r},t|\mathbf{r}',t')|_{t'=0} \equiv \mathrm{G}(\mathbf{r},t|\mathbf{r}',0) = K(\mathbf{r},\mathbf{r}',t)\ , \qquad (2.2.4b)$$

and appeal to a result from Özişik [22,p.217] gives

$$\mathrm{G}(\mathbf{r},t|\mathbf{r}',t') = \mathrm{G}(\mathbf{r},t|\mathbf{r}',0)|_{t\longrightarrow t-t'} \equiv \mathrm{G}(\mathbf{r},t-t'|\mathbf{r}',0)\ . \qquad (2.2.5)$$

(The derivations of (2.2.2) and (2.2.5), which are key to this solution, are given in Chapters 5 and 6 of Özişik[22].)

Therefore, a solution to the general problem can be furnished by that to the auxiliary problem:

$$T(\mathbf{r},0) = T_o(\mathbf{r}) \quad \text{at} \quad t = 0 \tag{2.2.6a}$$

$$\nabla^2 T(\mathbf{r},t) = \frac{1}{\beta}\frac{\partial T(\mathbf{r},t)}{\partial t} \ , \quad r < a \ , \quad t > 0 \tag{2.2.6b}$$

$$\frac{\partial T(\mathbf{r},t)}{\partial r} = -\frac{\mathcal{H}}{K} T(\mathbf{r},t) \quad \text{at} \quad r = a \ , \quad t > 0 \ . \tag{2.2.6c}$$

For this situation, the separation of variables in the spherical coordinate system (Appendix A) leads directly to the expression

$$T(r,\mu,\phi,t) = \sum_{n=0}^{\infty}\sum_{\ell=1}^{\infty}\sum_{m=0}^{n} \frac{e^{-\beta\lambda_{n\ell}^2 t}}{N(m)N(n,m)N(\lambda_{n\ell})} j_n(\lambda_{n\ell}r)P_n^m(\mu) *$$

$$\int_0^a dr' \int_{-1}^{1} d\mu' \int_0^{2\pi} d\phi' r'^2 j_n(\lambda_{n\ell}r')P_n^m(\mu')\cos[m(\phi-\phi')]T_o(r',\mu',\phi') \ , \tag{2.2.7a}$$

where
$$N(m) = \frac{1}{\pi(1+\delta_{m0})} \ , \tag{2.2.7b}$$

$$N(n,m) = \int_{-1}^{1}[P_n^m(\mu)]^2 d\mu \quad (\mu = \cos\theta) \ , \quad N(\lambda_{n\ell}) = \int_0^a r^2 j_n^2(\lambda_{n\ell}r)dr \ , \tag{2.2.7c, d}$$

and $\lambda_{n\ell}$ are from the positive roots of

$$j_n'(\lambda_{n\ell}a) + \frac{\mathcal{H}}{K\lambda_{n\ell}} j_n(\lambda_{n\ell}a) = 0 \quad . \tag{2.2.7e}$$

The Legendre normalization is well-known to be simply $\frac{2}{2n+1}\frac{(n+m)!}{(n-m)!}$, and the Bessel integral is given by Özişik Eq. 3-28b [22,p.90] as

$$N(\lambda_{n\ell}) = \frac{a^3}{2}\left[\frac{j_n(\lambda_{n\ell}a)}{\lambda_{n\ell}a}\right]^2 \left[(\lambda_{n\ell}a)^2 + \left(\frac{\mathcal{H}}{K}a - \frac{1}{2}\right)^2 - \left(n+\frac{1}{2}\right)^2\right] \ . \tag{2.2.8}$$

From the prescription above, the solution to the general problem is

$$T(\mathbf{r},t) = \sum_{n,\ell,m} f_{n\ell m}(r,\mu,t) \int_V dv' T_o(\mathbf{r}') j_n(\lambda_{n\ell} r') P_n^m(\mu') \cos[m(\phi-\phi')] +$$

$$\frac{\beta}{K} \sum_{n,\ell,m} f_{n\ell m}(r,\mu,t) \int dt' \oint_S ds' e^{\beta\lambda_{n\ell}^2 t'} j_n(\lambda_{n\ell} a) P_n^m(\mu') \cos[m(\phi-\phi')] \mathcal{H} T_a(\mathbf{r}',t') +$$

$$\frac{\beta}{K} \sum_{n,\ell,m} f_{n\ell m}(r,\mu,t) \int dt' \int_V dv' e^{\beta\lambda_{n\ell}^2 t'} j_n(\lambda_{n\ell} r') P_n^m(\mu') \cos[m(\phi-\phi')] \mathrm{S}(\mathbf{r}',t') \ , \tag{2.2.9a}$$

$$\text{where } f_{n\ell m}(r,\mu,t) \equiv \frac{e^{-\beta\lambda_{n\ell}^2 t} j_n(\lambda_{n\ell} r) P_n^m(\mu)}{N(m)N(n,m)N(\lambda_{n\ell})} \ . \tag{2.2.9b}$$

For a homogeneous initial temperature distribution and a constant temperature for the ambient medium at the surface, the radial integral in the first sum of (2.2.9) and the time integral in the second are reducible analytically, and both summations have integrals in ϕ that vanish except for $m = 0$, which, in turn, confines their θ-dependence to

$$\int d\mu P_n(\mu) = \delta_{n0} \frac{2}{2n+1} \ . \tag{2.2.10}$$

Also, the third summation has vanishing azimuthal integrations except for $m = 0, 2$ [from (1.4.13)]. Therefore, $T(\mathbf{r},t)$ of (2.2.2) is given by

$$\sum_{n,\ell=0,1}^{\infty} f_{n\ell}(r,\mu,t) \left\{ \delta_{n0} \left[\frac{T_o a}{\lambda_{0\ell}^2} \left(\frac{\sin\lambda_{0\ell} a}{\lambda_{0\ell} a} - \cos\lambda_{0\ell} a \right) + \frac{T_a a}{\lambda_{0\ell}^3} \frac{\mathcal{H}}{K} (e^{\beta\lambda_{0\ell}^2 t} - 1) \sin\lambda_{0\ell} a \right] \right.$$

$$+ \quad \frac{\mathcal{N}\beta}{4K} \int_0^t L(t') e^{\beta\lambda_{n\ell}^2 t'} dt' \int_0^a dr' \int_{-1}^{1} d\mu' r'^2 j_n(\lambda_{n\ell} r') P_n(\mu') *$$

$$\left. \left[S_\otimes(r',\mu') + S_\odot(r',\mu') + [S_\otimes(r',\mu') - S_\odot(r',\mu')] \frac{(n-2)!}{(n+2)!} \frac{P_n^2(\mu) P_n^2(\mu')}{P_n(\mu) P_n(\mu')} \cos\ 2\phi \right] \right\} , \tag{2.2.11}$$

in which

$$f_{n\ell}(r,\mu,t) \equiv \frac{2n+1}{N(\lambda_{n\ell})} j_n(\lambda_{n\ell} r) P_n(\mu) \mathrm{e}^{-\beta\lambda_{n\ell}^2 t} \quad (= 4\pi f_{n\ell 0}) \quad . \tag{2.2.12}$$

It is evident from the ϕ dependence of (2.2.11) that the problem of heating by linearly polarized light is reduced to that of a quarter sphere, just as with (1.4.13). Moreover, it is clear from (2.2.9) that this is so even in the general case providing that the initial and ambient temperature distributions, if inhomogeneous, are azimuthally symmetric. Also of note is that to recover the solution for circular polarization in (2.2.11), again, just as in converting $\hat{S}^{(\mathrm{x,y})}(r,\mu,\phi,t)$ to $\hat{S}^{(\pm)}(r,\mu,t)$, it is necessary only to set $\phi = \frac{\pi}{4}$. That is to say, $T(r,\mu,t) = T(r,\mu,\frac{\pi}{4},t)$.

2.3 Numerical Solution

The derivatives of (2.1.2) may be closely approximated at a point from truncated Taylor series expansions about that point of the functions themselves evaluated at neighboring points. This finite-difference methodology is a common tactic in the solution of non-trivial differential equations. Two general avenues of application exist: explicit and implicit solution. The implicit method has the advantage of greater temporal freedom but at the cost of computational bulkiness, and the explicit approach sacrifices the temporal flexibility for computational simplicity. Explicit solution is employed in this work, primarily because of this simplicity, but it may be noted that, since heat conduction can be important on long time-scales, there may be reason to consider the algebraic format in the future.

Expanding an exemplary function, $f(\xi)$, about the point x gives, letting $\xi =$, first $x + \Delta x$, and then $x - \Delta x$,

$$f(x+\Delta x) = f(x) + \Delta x f'(x) + \frac{\Delta x^2}{2!} f''(x) + \frac{\Delta x^3}{3!} f'''(x) + \ldots \qquad (2.3.1a)$$

$$f(x-\Delta x) = f(x) - \Delta x f'(x) + \frac{\Delta x^2}{2!} f''(x) - \frac{\Delta x^3}{3!} f'''(x) + \ldots . \qquad (2.3.1b)$$

Each of these may be solved for $f'(x)$, and moreover, their difference may as well:

$$f'(x) = \frac{f(x+\Delta x) - f(x)}{\Delta x} - \frac{\Delta x}{2} f''(x) - \frac{\Delta x^2}{6} f'''(x) - \frac{\Delta x^3}{24} f''''(x) - \ldots \qquad (2.3.2a)$$

$$f'(x) = \frac{f(x) - f(x-\Delta x)}{\Delta x} + \frac{\Delta x}{2} f''(x) - \frac{\Delta x^2}{6} f'''(x) + \frac{\Delta x^3}{24} f''''(x) - \ldots \qquad (2.3.2b)$$

$$f'(x) = \frac{f(x+\Delta x) - f(x-\Delta x)}{2\Delta x} - \frac{\Delta x^2}{6} f'''(x) - \ldots . \qquad (2.3.2c)$$

In accordance with common practice, the finite difference notation,

$$x = i\Delta x \ , \quad f(x) = f_i \quad , \qquad (2.3.3)$$

is employed here to give, from $(2.3.2a, c)$,

$$f_i' = \frac{f_{i+1} - f_i}{\Delta x} + O(\Delta x) \qquad (2.3.4a)$$

$$f_i' = \frac{f_{i+1} - f_{i-1}}{2\Delta x} + O(\Delta x^2) \ , \qquad (2.3.4b)$$

and from the elimination of $f'(x)$ between $(2.3.2a)$ and $(2.3.2b)$:

$$f_i'' = \frac{f_{i+1} - 2f_i + f_{i-1}}{\Delta x^2} + O(\Delta x^2) \ . \qquad (2.3.4c)$$

These equations, (2.3.4), suffice to approximate the heat conduction equation. The notation $O(\Delta x)$ indicates the order of magnitude of the departure from exactness incurred in truncating the series. It is, of course, preferable to choose, as the lesser of the evils, the square error involved in the three-point formulas, and this indeed will be done in general. However, as will be seen below, (2.3.4a) is indicated for the initial time derivative and will therefore subsequently be used in this capacity for the entire calculation; with this exception, the heat equation derivative approximations will be accurate to within $O(\Delta x^2)$. (In practice, accuracy is limited by the relation between Δx and Δt necessary for stable solution [22,p.491].)

The relevant vector operation here is the divergence of the product of a scalar, the thermal conductivity K, and the temperature gradient:

$$\nabla \cdot K \nabla T = \left[\frac{1}{r^2}\partial_r(K r^2 \partial_r) + \frac{1}{r^2 \sin\theta}\partial_\theta(K \sin\theta \partial_\theta) + \frac{1}{r^2 \sin^2\theta}\partial_\phi(K\partial_\phi)\right] T =$$

$$\left\{ K\partial_r^2 + \left(\frac{2}{r}K + \frac{\partial K}{\partial r}\right)\partial_r + \frac{1}{r^2}\left[K\partial_\theta^2 + \left(K\cot\theta + \frac{\partial K}{\partial \theta}\right)\partial_\theta + \right.\right.$$

$$\left.\left. K\csc^2\theta\,\partial_\phi^2 + \csc^2\theta \frac{\partial K}{\partial \phi}\partial_\phi\right]\right\} T \, . \qquad (2.3.5a, b)$$

For the finite difference representation, i, j, and k will be used to index the r, θ, and ϕ grid points, respectively, and subscripted lower-case deltas will give the coordinate increments themselves; to make the notation bearable, only the ± 1 index values will be written out, with the absence of explicit indices being understood to imply ijk. Substituting from (2.3.4b, c), with these conventions, in (2.3.5b) is to say

$$\nabla\cdot\mathcal{K}\nabla T=\mathcal{K}\frac{T_{i+1}-2T+T_{i-1}}{{\delta_r}^2}+\left[\frac{2\mathcal{K}}{i\delta_r}+\frac{\mathcal{K}_{i+1}-\mathcal{K}_{i-1}}{2\delta_r}\right]\frac{T_{i+1}-T_{i-1}}{2\delta_r}+$$

$$\frac{1}{(i\delta_r)^2}\left\{\mathcal{K}\frac{T_{j+1}-2T+T_{j-1}}{{\delta_\theta}^2}+\left[\mathcal{K}\cot(j\delta_\theta)+\frac{\mathcal{K}_{j+1}-\mathcal{K}_{j-1}}{2\delta_\theta}\right]\frac{T_{j+1}-T_{j-1}}{2\delta_\theta}+\right.$$

$$\left.\csc^2(j\delta_\theta)\left[\frac{\mathcal{K}_{k+1}-\mathcal{K}_{k-1}}{2\delta_\phi}\frac{T_{k+1}-T_{k-1}}{2\delta_\phi}+\mathcal{K}\frac{T_{k+1}-2T+T_{k-1}}{{\delta_\phi}^2}\right]\right\}\ . \qquad (2.3.6)$$

Grouping the terms in this equation as coefficients of the various temperature points leads to a symmetric form which, with the definitions

$$f_i^{\pm}(\mathcal{K})\equiv\mathcal{K}\pm\frac{\mathcal{K}}{i}\pm\frac{\mathcal{K}_{i+1}-\mathcal{K}_{i-1}}{4}\ ,$$

$$f_{ij}^{\pm}(\mathcal{K})\equiv\left(\mathcal{K}\pm\frac{\mathcal{K}\delta_\theta\cot(j\delta_\theta)}{2}\pm\frac{\mathcal{K}_{j+1}-\mathcal{K}_{j-1}}{4}\right)\frac{1}{(i\delta_\theta)^2}\ ,$$

$$f_{ijk}^{\pm}(\mathcal{K})\equiv\left(\mathcal{K}\pm\frac{\mathcal{K}_{k+1}-\mathcal{K}_{k-1}}{4}\right)\frac{\csc^2(j\delta_\theta)}{(i\delta_\phi)^2}\ ,$$

$$\text{and}\quad f_{ij}(\mathcal{K})\equiv-2\mathcal{K}\left[1+\frac{1}{(i\delta_\theta)^2}+\frac{\csc^2(j\delta_\theta)}{(i\delta_\phi)^2}\right]\ , \qquad (2.3.7a-d)$$

allows the diffusion equation to be written as

$$\nabla\cdot\mathcal{K}\nabla T+\mathrm{S}=\gamma\frac{\partial T}{\partial t}=\left(f_i^+T_{i+1}+f_i^-T_{i-1}+f_{ij}^+T_{j+1}+\right.$$

$$\left.f_{ij}^-T_{j-1}+f_{ijk}^+T_{k+1}+f_{ijk}^-T_{k-1}+f_{ij}T\right)\frac{1}{{\delta_r}^2}+L\mathcal{N}\hat{S}=\gamma\frac{T_{n+1}-T}{\delta_t}\ , \qquad (2.3.8a)$$

where γ is the volumetric heat capacity, ρC_p, (2.1.4) has been used for the source term, and the index n has been introduced for the time derivative from (2.3.4a). This is solved for T_{n+1} and thereby permits specification of T for all points at the end of the first time step from knowledge of the initial distribution, and then, sequentially, all later times in like manner. It is readily specialized to the case of constant conductivity (and thermal properties generally) and to the azimuthally symmetric situation of incident circular light, and thus serves as the basis for all the numerical heat calculations done in this work.

The difficulty in using (2.3.8a) lies with the singularities at the origin and along the polar axis, both evident from (2.3.7). The remedy applied here is to evaluate the derivatives at these points with a Cartesian version of (2.3.5) (This gives a simpler equation and, but for the boundary conditions, might as well be used for the entire volume.):

$$\nabla \cdot \mathcal{K} \nabla T = \left[\mathcal{K}\left(\partial_x^2 + \partial_y^2 + \partial_z^2\right) + \left(\partial_x \mathcal{K} \partial_x + \partial_y \mathcal{K} \partial_y + \partial_z \mathcal{K} \partial_z\right)\right] T \; . \qquad (2.3.9)$$

The symmetry discussed below (2.2.12) serves to simplify this expression; since the source distribution in any quadrant of the sphere is a mirror image of that in an adjoining quadrant, so too is the temperature distribution (given azimuthal symmetry in the initial–and ambient–distributions). This means that the temperature at any point on the x or y axes is the same as that at the corresponding point on the negative axes, so that the single derivatives in (2.3.9) vanish, alá (2.3.4b), except for ∂_z, and the double derivatives with respect to x and y are simplified:

$$\nabla \cdot \mathcal{K} \nabla T =$$

$$\left\{ \mathcal{K}\left[T_{\nu+1} + T_{\nu-1} + 2(T_{\mu+1} + T_{\lambda+1}) - 6T\right] + \frac{1}{4}(T_{\nu+1} - T_{\nu-1})(\mathcal{K}_{\nu+1} - \mathcal{K}_{\nu-1}) \right\} \delta_r^{-2} \, , \qquad (2.3.8b)$$

in which λ, μ, and ν correspond to x, y, and z, and δ_r has been used for the general cartesian increment. This is completed with the source term and time derivative and used, in the same manner as (2.3.8a), to give the new temperatures on the polar axis. The situation at the origin is somewhat different from that on the axis generally, but (2.3.8b) is the operative relation in either case.

The procedure for calculating the temporally sequential temperature distributions is this: Beginning at the origin and sweeping through the full range of the polar angle (and azimuth if applicable) at each radial step, the new temperatures are calculated for all interior grid points from substitution of $T_o(\mathbf{r})$ in (2.3.8). At the boundary, the new temperatures are given in terms of the freshly updated values just below the surface by the condition (2.1.7c). Actually, in practice, the temperature on the interface is calculated from the heat equation, and then the boundary condition is imposed to update the temperature at a ficticious node just above the surface. This vagary may be avoided by direct calculation of T on the surface from the freshly computed values at *two* grid points below by means of backward-difference approximations [22,p.476], but this procedure is a little more cumbersome to implement and leads to no significant change in the outcome.

CHAPTER 3

CASE STUDIES AND CONCLUSIONS

The solutions to the Mie problem and the diffusion equation developed above provide a model of convection-free thermal evolution in constant-sized spheres heated by monochromatic light. This simulation yields useful results in several physically realistic situations and two categories of application are treated here. The first is a study of generic spheres under the action of high energy pulses, which, as indicated in section 2.1, requires a minimum of input data and gives very general results. The treatment then will be extended, by inclusion of the heat equation, to specific cases in a medium of known thermal properties. Since the source function for incident plane polarization does not often differ markedly from its circular counterpart, the latter case, which is the simpler, will be examined primarily. The graphics routines will be exercised here to illustrate the results of the calculations. Also, in reviewing the structure and scope of this model, a brief discussion of future elaboration is included.

3.1 Variation of the Source Function

The propagation velocity of an electromagnetic field in any medium is proportional to its wavelength in that medium and the constant of proportionality is the frequency of oscillation, common to all media. The ordinary index of refraction, n_{Re}, is a ratio of two such velocities, and is, therefore, the corresponding wavelength ratio as well. Since the Mie size parameter, $\alpha = \frac{2\pi a}{\lambda}$, is defined in terms of free space conditions, an enhancement of refraction (itself defined in terms of free space velocity) in the sphere carries with it a size parameter enlargement effect. For this reason it should be born in mind, especially for the low absorption cases, that it is the product of the Mie size parameter with n_{Re} which gives a measure of the relative wavelength *within* the sphere.

With this caveat, the roster of cases may be productively divided into two regimes on the basis of relative dimensions: those in which the size parameter is less than, and greater than, respectively, the value π, for which, of course, the wavelength of the laser is equal to the diameter of the sphere. The region of transition from one regime to the other will be of particular interest.

For the smallest spheres, the situation reduces to that of a static, uniform external field, for which the internal electric field is homogeneous, aligned with the incident wave, and of magnitude given by Jackson Eq. 4.55 [15, p. 151]. This has provided a limiting case corroboration of the calculations based on (1.4.7), lending additional support to the verification by volume integration described in section 1.4 .

When the size parameter is above or near the transition, the source function shows pronounced structure, and it is prudent to distinguish between media of differing absorptivities. When n_{Im} is small, the spheres are transparent and the internal fields are wavelike throughout; in the limit of large size parameters, this tends toward the approximation of geometric optics. For strong absorption, the fields are excluded from the central regions, and the effect of refraction is diminished. For the study here, wherein $\alpha \leq 100$, small n_{Im} will be nominally defined as in the range of from 10^{-6} to 10^{-2}, and strong absorption will be examined for n_{Im} as large as 5.

TRANSPARENT SPHERES

For the low absorption cases, a convex feature begins to develop in the back* portion of the sphere as the relative size approaches the parameter transition. Increasing n_{Re}, in the range of from 1.3 to 4.7, steadily reduces the size of $\hat{S}(r, \mu)$, and does so preferentially away from the optical axis, so that the maximum narrows (eventually dividing itself front and back) as it collapses. The reduction of the fields by refraction is categorical at a constant diameter of half an internal wavelength, and is an effect which, to a lesser extent, is engendered by increasing absorption as well. This behavior is illustrated in Figure 3.1.1, throughout which, it will be noted, $\alpha n_{\mathrm{Re}} = \frac{\pi}{2}$. Of particular interest is Figure 3.1.1(a), in which the complex refractive index corresponds to that of liquid water in the near infrared (1.06 microns) [11]. As in all the 2-D plots given here, the positive z direction is

---

* "Forward" and "back" will refer here to the surfaces facing toward, and away from, respectively, the incoming light, and should not be confused with the conventional (contrary) definitions of the adjectives in discussions of scattered light.

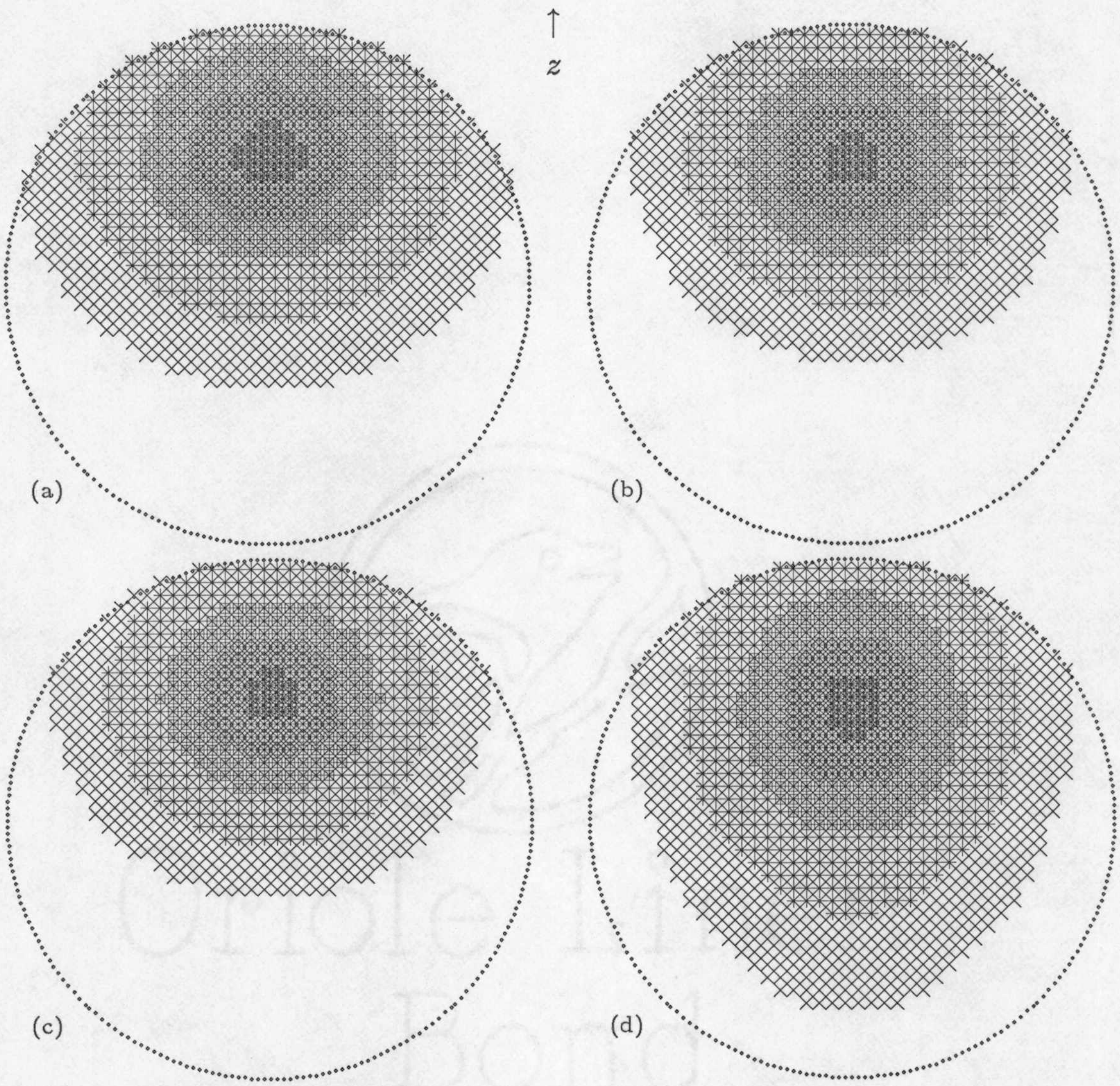

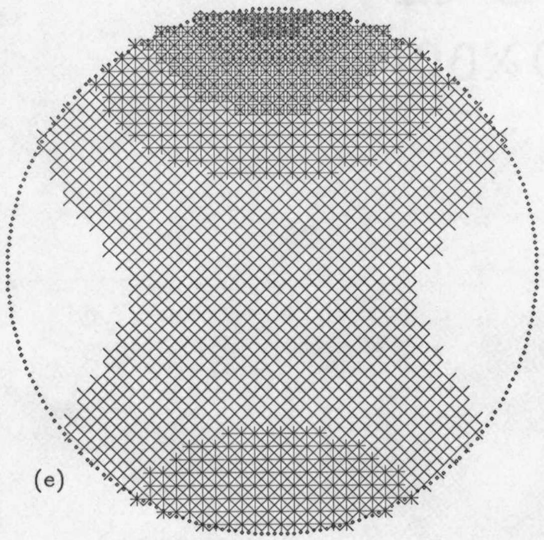

Figure 3.1.1 Low Absorption in Small Spheres: $\alpha n_{\mathrm{Re}} = \frac{\pi}{2}$

(a) $\alpha = 1.13$, $\mathrm{n} = 1.327 + i4 \times 10^{-6}$
$\hat{S}_{\mathrm{MAX}} = 1.1$

(b) $\alpha = 1.05$, $\mathrm{n} = 1.5 + i4 \times 10^{-6}$
$\hat{S}_{\mathrm{MAX}} = 1.0$

(c) $\alpha = 1.05$, $\mathrm{n} = 1.5 + i0.01$
$\hat{S}_{\mathrm{MAX}} = 0.99$

(d) $\alpha = 0.628$, $\mathrm{n} = 2.5 + i0.01$
$\hat{S}_{\mathrm{MAX}} = 0.31$

(e) $\alpha = 0.436$, $\mathrm{n} = 3.6 + i0.01$
$\hat{S}_{\mathrm{MAX}} = 0.10$

toward the top of the page.

Once the size parameter transition is reached, a second maximum has become evident in all the cases, testament to the the paired field maxima in a single wavelength, and, interestingly, the enhancement of refraction dramatically reverses its effect and now increases the field density in general and the peak intensity in particular. This is depicted in Figure 3.1.2, which gives the same sequence as before, but now with $\alpha n_{Re} = \pi$; the $n = 1.5 + i4 \times 10^{-6}$ case has been omitted since, just as before, it does not differ appreciably from the $n_{Im} = 0.01$ case. Also, the final case, that of 3.1.2(d), is of still larger refraction this time.

The development of locally high field intensities within the body of the sphere continues, generally, on up into the large size parameters. It is essentially a focusing effect and can result in one or more hot spots of considerable magnitude, usually near the back surface. In the case $\alpha = 35,\ n = 2.5 + i1.5 \times 10^{-3}$ (shown below), for example, the maximum energy density is over 200 times that of the incoming wave. It should be remembered here, however, that this copious energy is only poorly available for thermal conversion due to the small size of n_{Im} [evident from (1.4.10)]. This "backpeak" effect, as well as the wave-type structure of the source function generally, is clearly evident in the plots of Figure 3.1.3, which are for $\alpha n_{Re} = 3\pi$ (The heaviest refraction, Figure 3.1.3(d), it will be noted, shifts the maxima to center stage.).

For comparison, the simulated 3-D plots of the source functions used to

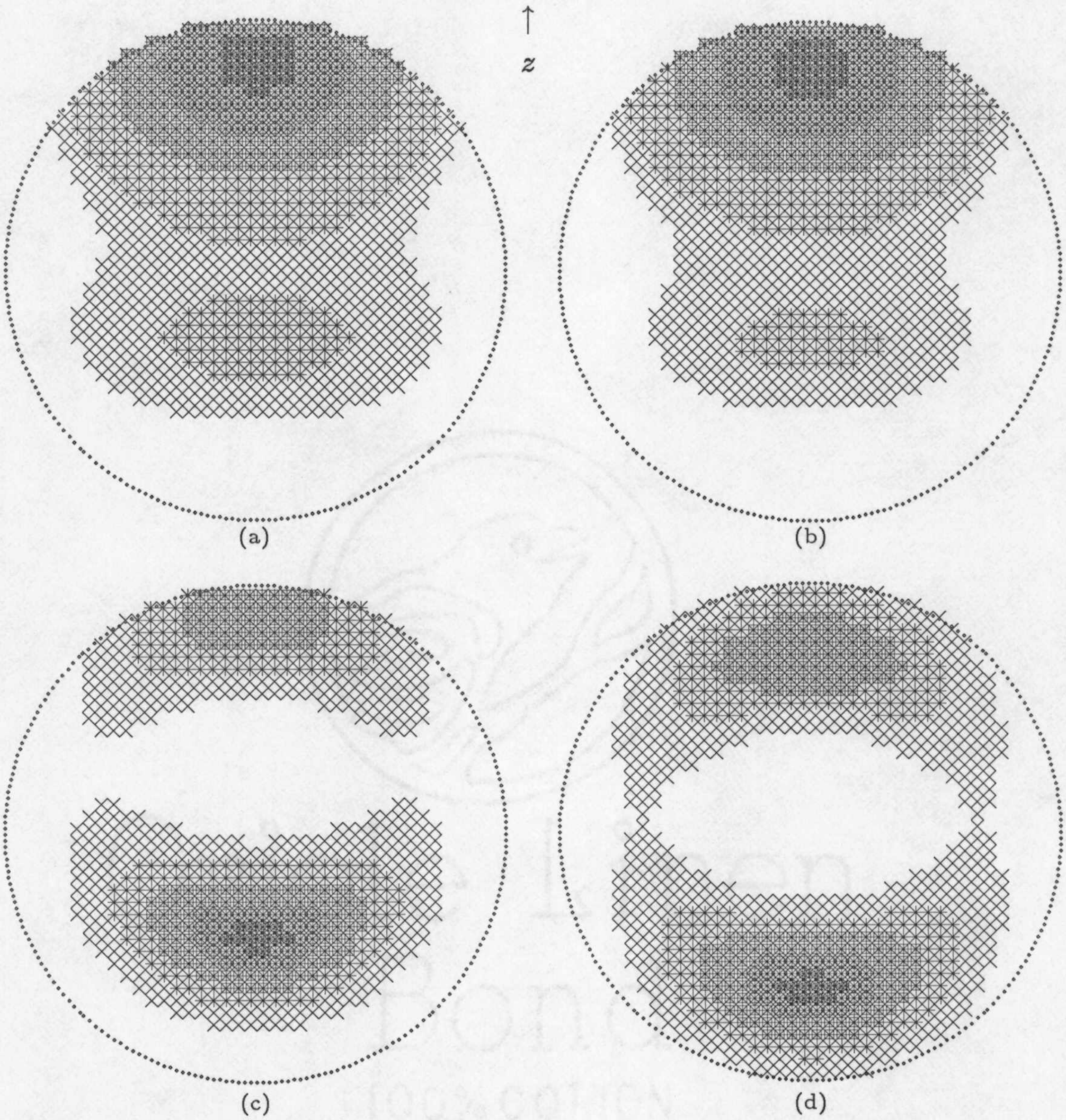

Figure 3.1.2 Low Absorption at the Size Parameter Transition: $\alpha n_{\mathrm{Re}} = \pi$

(a) $\alpha = 2.37$, $\mathrm{n} = 1.327 + i4 \times 10^{-6}$

$\hat{S}_{\mathrm{MAX}} = 2.9$

(b) $\alpha = 2.09$, $\mathrm{n} = 1.5 + i0.01$

$\hat{S}_{\mathrm{MAX}} = 3.1$

(c) $\alpha = 1.26$, $\mathrm{n} = 2.5 + i0.01$

$\hat{S}_{\mathrm{MAX}} = 3.5$

(d) $\alpha = 0.670$, $\mathrm{n} = 4.66 + i0.01$

$\hat{S}_{\mathrm{MAX}} = 12$

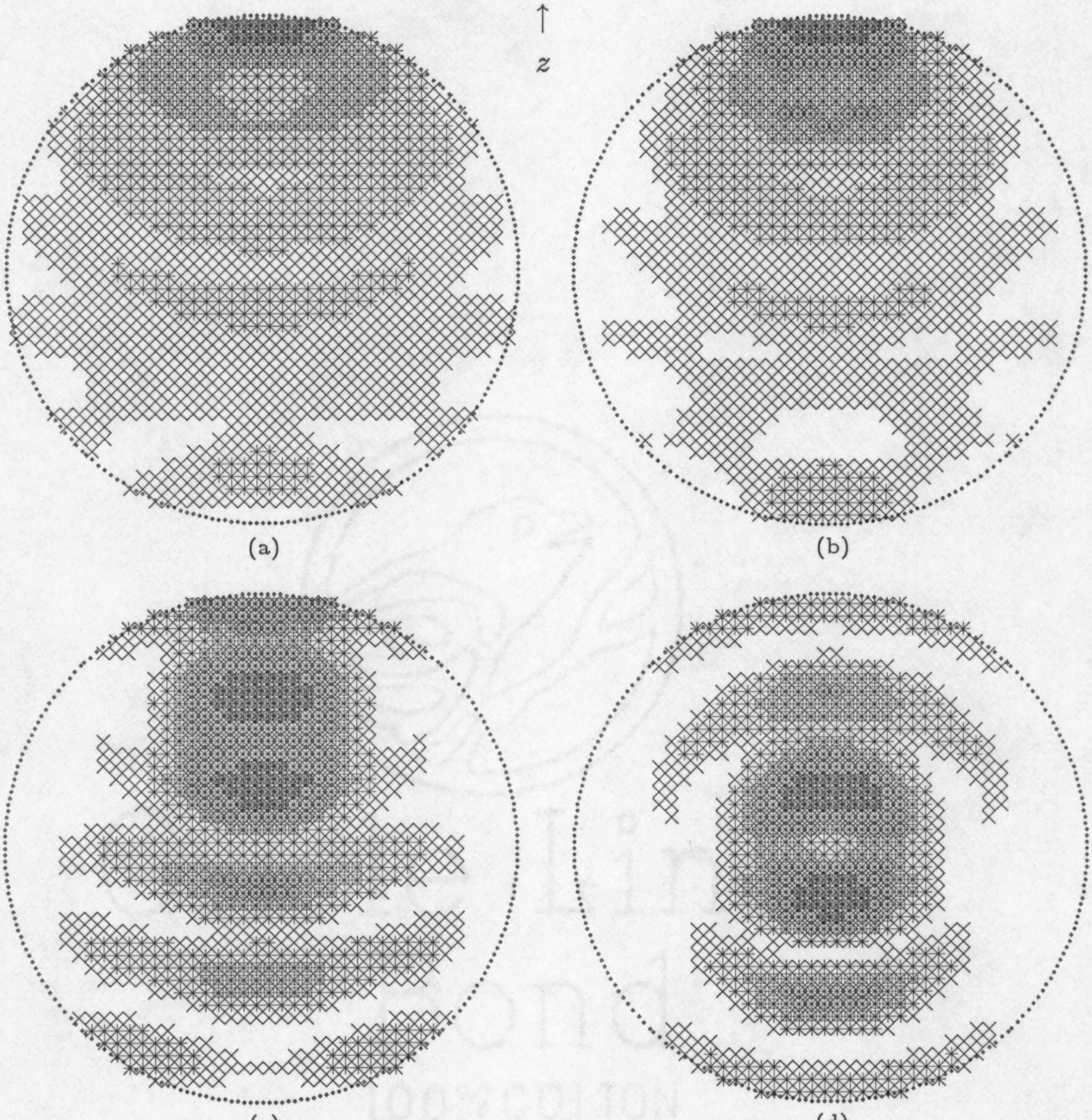

(a)

(b)

(c)

(d)

Figure 3.1.3 Refraction above the Parameter Transition: $\alpha n_{\mathrm{Re}} = 3\pi$

(a) $\alpha = 7.10$, $\mathrm{n} = 1.327 + i4 \times 10^{-6}$
$\hat{S}_{\mathrm{MAX}} = 18$

(b) $\alpha = 6.23$, $\mathrm{n} = 1.5 + i0.01$
$\hat{S}_{\mathrm{MAX}} = 19$

(c) $\alpha = 3.77$, $\mathrm{n} = 2.5 + i0.01$
$\hat{S}_{\mathrm{MAX}} = 10$

(d) $\alpha = 2.02$, $\mathrm{n} = 4.66 + i0.01$
$\hat{S}_{\mathrm{MAX}} = 13$

generate Figures 3.1.2 and 3.1.3 are given in Figures 3.1.4 and 3.1.5. As with all the 3-D plots given here, the positive z direction is to the right.

As the spheres continue to grow larger, there are no significant changes in the general pattern up into size parameters on the order of 10^2. A sample of the increasing intricacy resulting from the inclusion of additional wavelengths involved in this progression is given in Figure 3.1.6.

ABSORPTION

In the region of $n_{\mathrm{Im}} > 0.01$, the development of the internal field patterns with increasing size parameter begins to take on a different character. Below the transition to wavelength-girdling diameters, it is much the same as the small absorption cases, differing chiefly in that the early solo peak tends to drift towards the lit surface as the absorption increases. In the upper regime, front and surface heating progressively dominate the pattern; for heavy absorption, the internal fields are confined to the surface, and, for large spheres generally, to the front hemisphere.

To illustrate the nature of this kind of behavior it may be noted that, since field intensity goes as the square of (the magnitude of) the field itself, the absorption coefficient, a measure of intensity attenuation in traversing the unit distance, is related to n_{Im} by

$$\alpha_{\mathrm{abs}} = \frac{4\pi n_{\mathrm{Im}}}{\lambda} \; ; \tag{3.1.1}$$

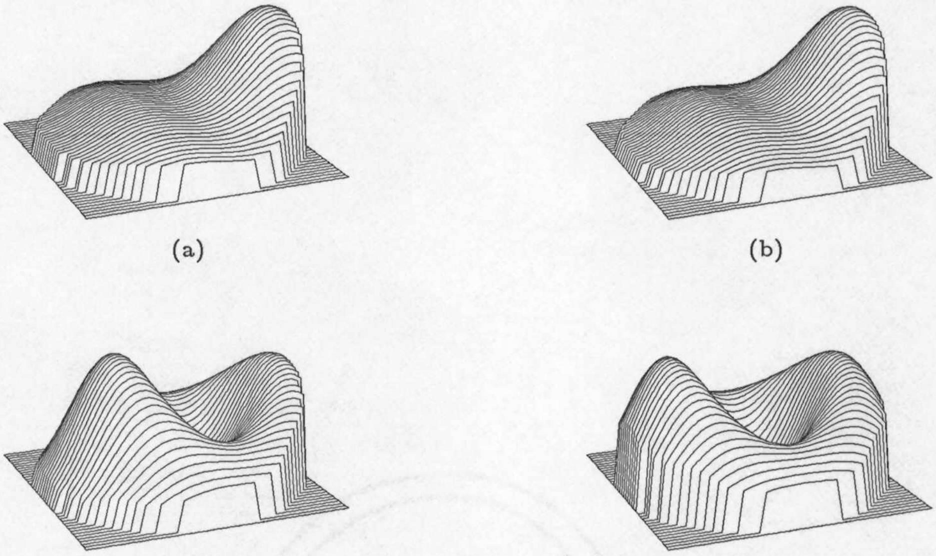

(a) (b)

(c) (d)

Figure 3.1.4 Source Functions for Figure 3.1.2

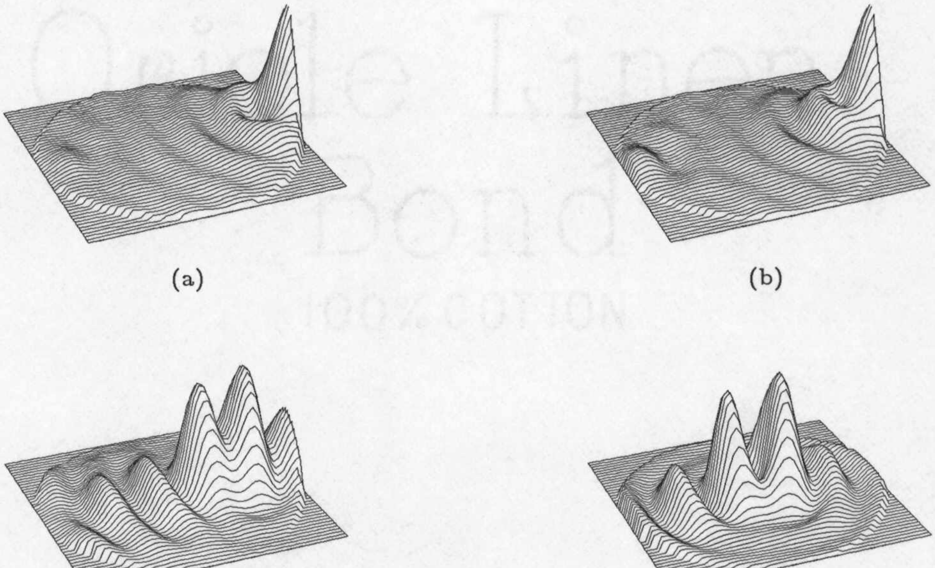

(a) (b)

(c) (d)

Figure 3.1.5 Source Functions for Figure 3.1.3

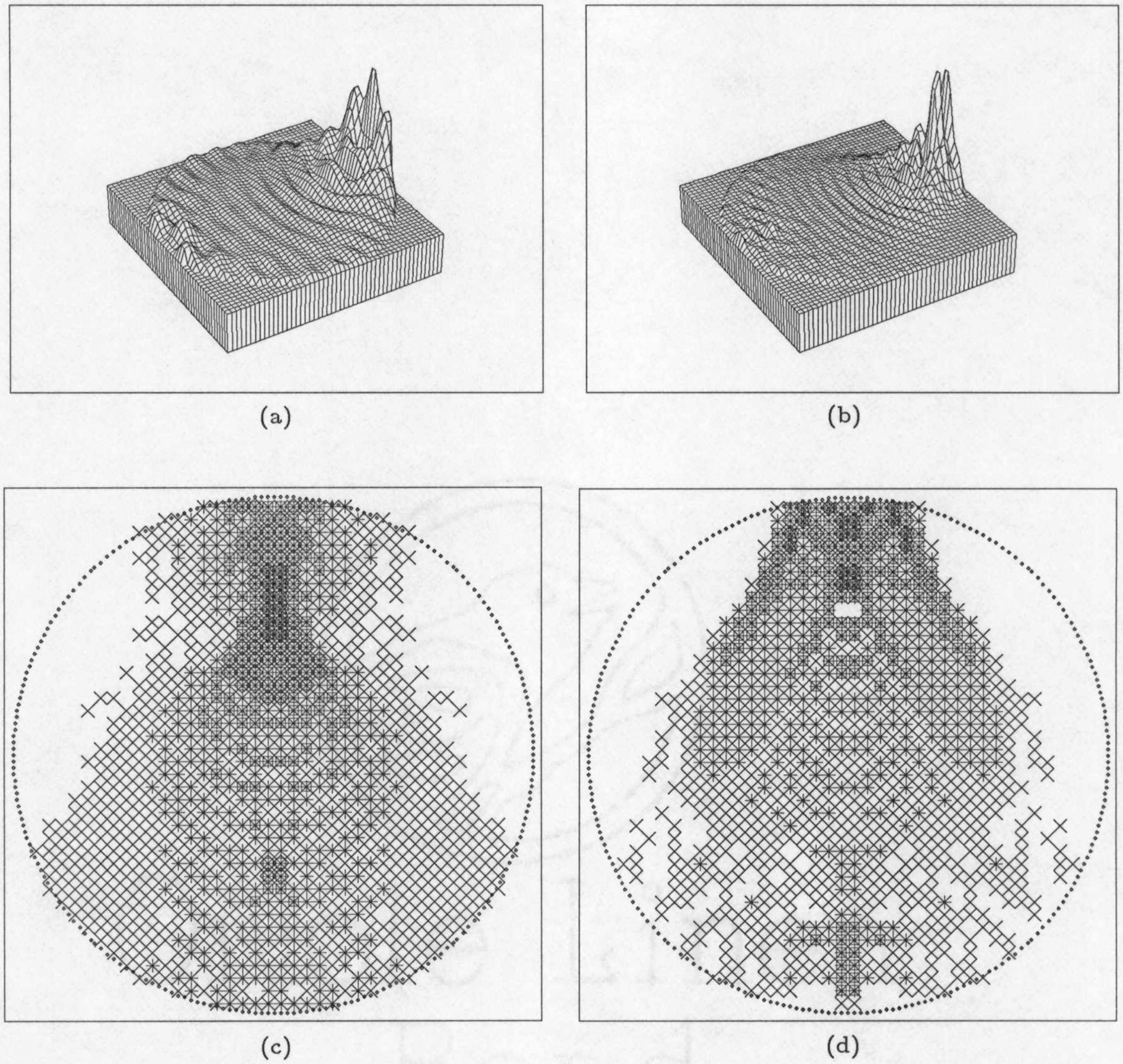

Figure 3.1.6 Large Size Parameters and Low Absorption

(a) $\alpha = 13$, $\mathrm{n} = 1.327 + i4 \times 10^{-6}$

$\hat{S}_{\mathrm{MAX}} = 17$

(b) $\alpha = 18$, $\mathrm{n} = 1.5 + i0.01$

$\hat{S}_{\mathrm{MAX}} = 18$

(c) $\alpha = 35$, $\mathrm{n} = 2.5 + i0.001$

$\hat{S}_{\mathrm{MAX}} > 200$(resolution dependent)

(d) $\alpha = 100$, $\mathrm{n} = 1.5 + i1.5 \times 10^{-4}$

$\hat{S}_{\mathrm{MAX}} = 23$

that is,

$$I(z) \propto \mathbf{E}^{\star} \cdot \mathbf{E} = |e^{ik(n_{Re}+in_{Im})z}|^2 = e^{2i^2 \frac{2\pi}{\lambda} n_{Im} z} \ . \tag{3.1.2}$$

This means that the thickness of material required to reduce the incident energy flux by a factor of I_0/I is given by

$$\Delta = \frac{1}{\alpha_{abs}} \log_e \frac{I_0}{I} \ , \tag{3.1.3}$$

so that, in the case of water at 10.6 microns, for example, where $n_{Im} = 0.071$, the characteristic attenuation length is about equal to a single wavelength. Indeed, for truly heavy absorption ($n_{Im} \geq 10$), the intensity falls precipitously to virtually nothing in a small fraction of the wavelength. This phenomenon is common in good conductors and has been referred to by electrical engineers as the "skin effect" [4,p.614]. (3.1.1) and (3.1.3) also indicate that any definition of "small" n_{Im} must be relative to size parameter: $\alpha n_{Im} \propto a/\Delta$.

It will be convenient to include here, in treating cases of significant absorption, an indication of the effect of plane polarization. All of the plots given thus far in this chapter are in the y-z plane (i.e., $\phi = \frac{\pi}{2}, \frac{3\pi}{2}$), but, as discussed in section 1.4, any (z-axis containing) plane shows the same source distribution, except when the polarization of the incident light is confined to a single direction. For this case, broadly speaking, the contrasts in the source function are heightened for planes whose orientations approach the perpendicular to the polarization direction (taken here to be $+x$), and subdued and shifted for nearly parallel planes, taking on the circular polarization character (intermediate) at $\phi = (2n+1)\frac{\pi}{4}$. This means that maxima in the y-z plane are narrowed and, away from the optical axis, increased as well, and although the effect is typically minor, it can be significant. Examples of such azimuthal variation of the plane polarized source function are given in Figures 3.1.7 and 3.1.8, which are done for the index of water at 10.6 microns, an important laser transition in CO_2. Figure 3.1.7 gives $\hat{S}^{(x)}$ at $\phi = \frac{\pi}{4}$ and $\frac{\pi}{2}$ for $\alpha = 6$, and Figure 3.1.8 shows a variety of planes for $\alpha = 8$. These two cases will be exploited in the the following section to illustrate the results of the heat equation calculations.

Finally, Figure 3.1.9 gives representative cases of strong absorption in large spheres (circular polarization), including two larger size parameters for water in the infrared.

3.2 Heating of Water Drops

Heat diffusion after the initial energy deposit may be unimportant if the material is heated very rapidly. This serves as the basis of the principal utility of the straightforward computations illustrated in the first section of this chapter. If the laser delivers energy more slowly or less copiously, the diffusion of heat acts to reduce temperature extremes, cooling localized hot spots (steep gradient), and may retard the development of explosive vaporization regions.

As indicated in the introduction, liquid water is chosen here to illustrate the mechanisms of the heat equation. The temperature dependences of the refractive index product, $\mathcal{N}(T)$, and the volumetric heat capacity, $\gamma(T)$, are taken from the

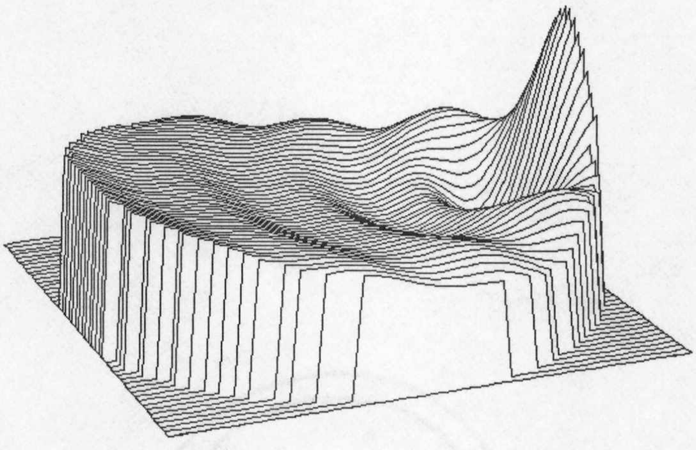

(a) Circularly Polarized Light Case

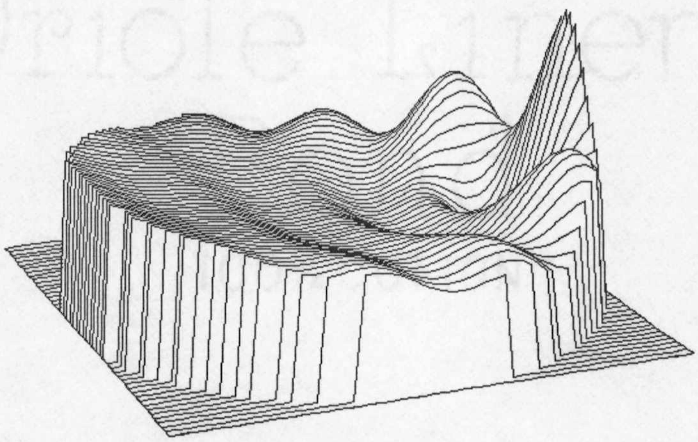

(b) Linearly Polarized Light Case

Figure 3.1.7 Effect of Polarization at $\alpha = 6$ for the Index of Water

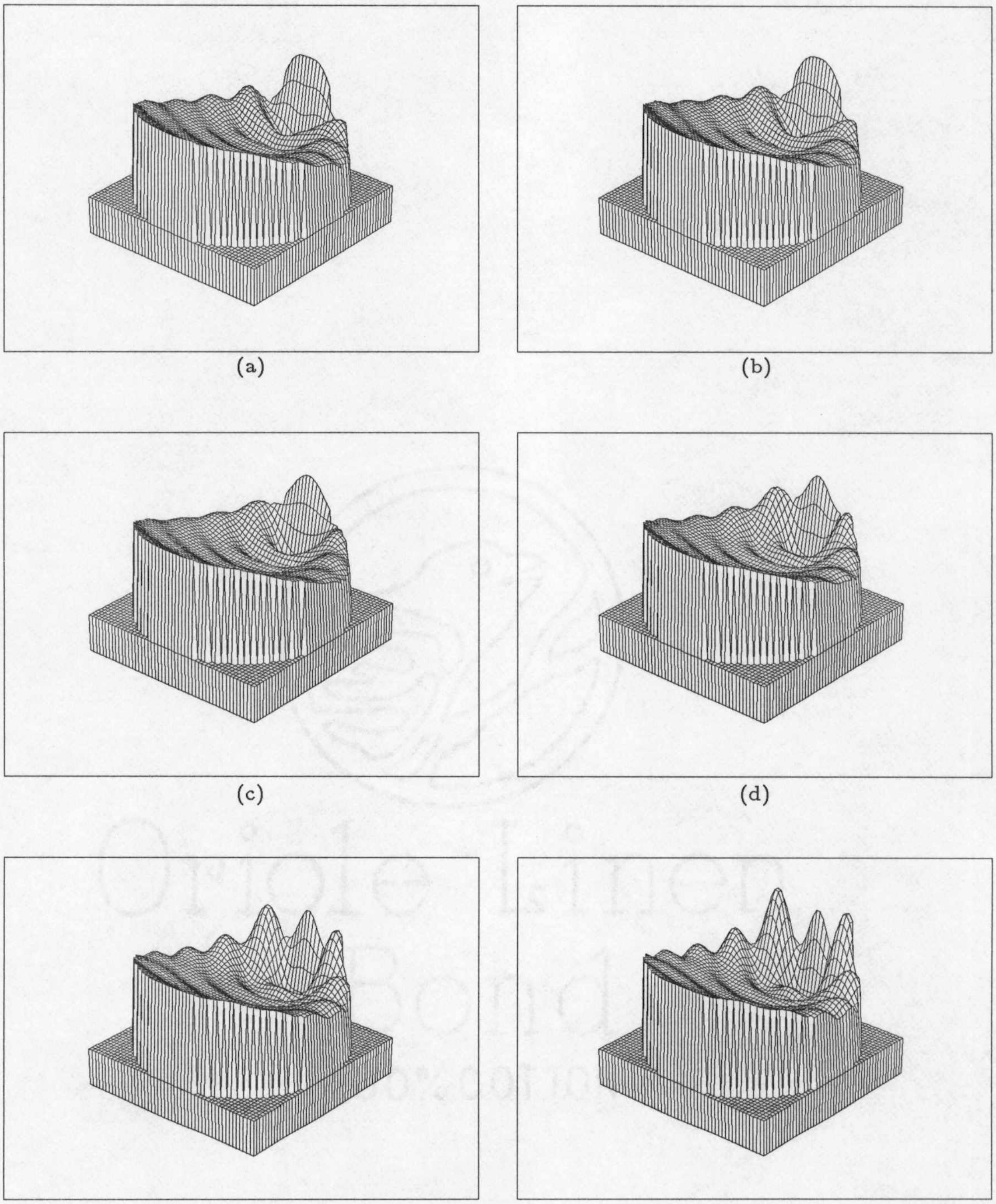

(a) (b) (c) (d) (e) (f)

Figure 3.1.8 Azimuthal Variation of the Source Function

The case is $\alpha = 8$, $\mathrm{n} = 1.179 + i0.071$, and Figures (a)−(f)

give $\hat{S}^{(\mathrm{x})}$ in the planes of $\phi = 0, 15, 30, 45, 60,$ and $90°$, respectively.

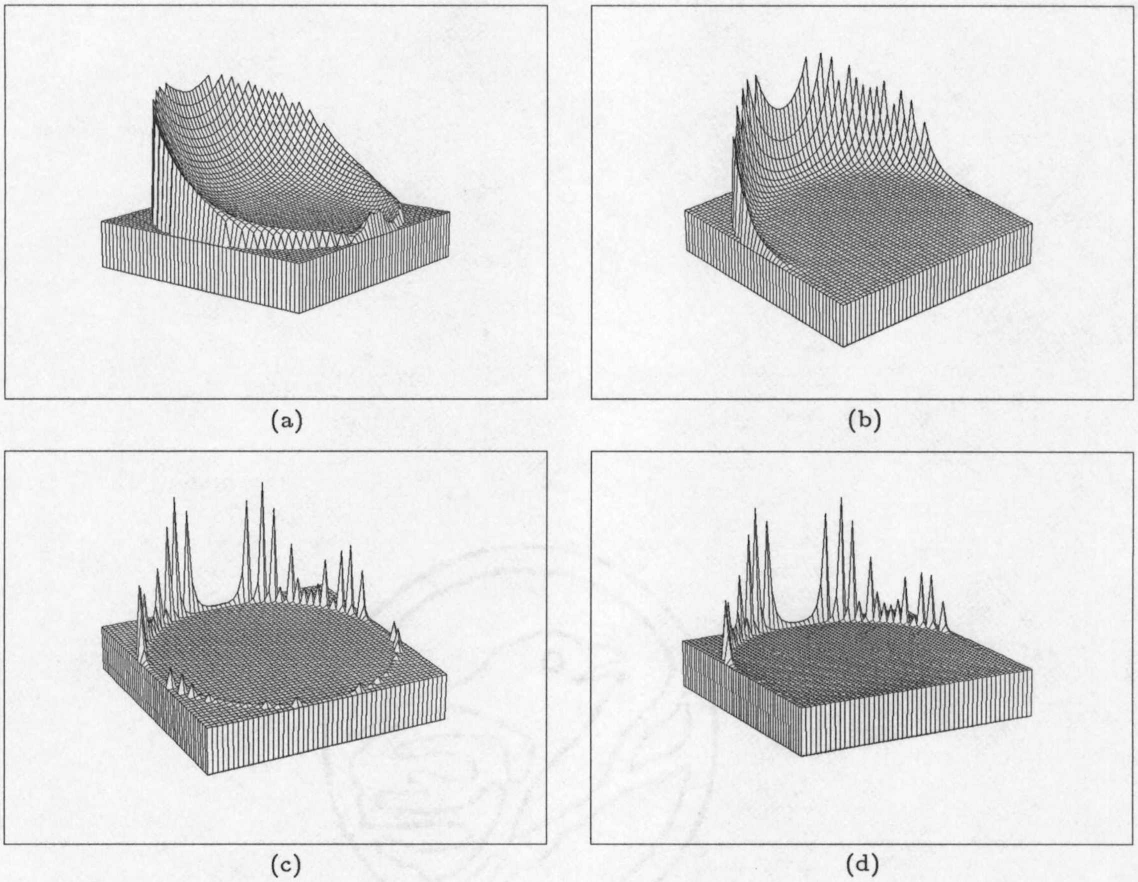

Figure 3.1.9 Heavy Absorption in Large Spheres

(a) $\alpha = 25$, $n = 1.179 + i0.071$ $\quad\hat{S}_{\mathrm{MAX}} = 0.82$

(b) $\alpha = 100$, $n = 1.179 + i0.071$ $\quad\hat{S}_{\mathrm{MAX}} = 0.78$

(c) $\alpha = 12$, $n = 5.0 + i5.0$ $\quad\hat{S}_{\mathrm{MAX}} = 0.042$

(d) $\alpha = 100$, $n = 1.5 + i0.5$ $\quad\hat{S}_{\mathrm{MAX}} = 0.42$

It may be noted that appreciable back heating occurs in cases (a) and (c) even though the internal size parameters are 30 and 60, respectively, and the characteristic attenuation lengths are much less than the spherical diameters. This is an effect of the wave nature of light and disappears in the larger cases.

Pendleton paper [24], as is the value for the superheat temperature: $T_{\mathrm{su}} = 578$ K, and the thermal conductivity, $\mathcal{K}(T)$, is taken from Prishivalko [28]. The size parameter cases examined here are those of Figures 3.1.7 and 3.1.8, which, for the CO_2 laser, correspond to diameters of 20 and 27 microns, respectively. It will be noted that, in what follows, actual breakup is disregarded in the sense that some of the calculations are extended well beyond the threshold temperature, T_{su}; in practice, shattering occurs over microsecond timescales and destroys spherical integrity [2], [17], [18].

There are several calculations available with the numerical solution of the heat equation, (2.3.8). In its simplest form ($\mathcal{K} \longrightarrow 0$), it gives the results of the previous section and could be used, as an extravagant (and inelegant) integration of (2.1.5), to study the effect of the temperature dependence of $\gamma/\mathcal{N}$ in the absence of diffusion. This calculation is the focus of the Pendleton paper cited above; for the observation times relevant to the high intensity pulse used (10^6 to 10^7 watts/cm^2), (2.3.8) gives sensibly the same results [those of (2.1.6)] with or without the inclusion of the spatial derivatives. This is so because, for the relevant size parameters ($\alpha \approx 10$), the characteristic times of (2.2.12) are, for the dominant eigenvalues of (2.2.7e) ($\lambda_{n\ell} \approx 10^5$), orders of magnitude greater than Pendleton's observation times. In order to examine the more general situation, then, the laser pulse plotted by Pendleton (taken from an actual pulse used in experimentation [17]), which is 2.5 μs in duration, has been subdued and lengthened for the calculations here; specifically,

$$I(t) = \chi I_{\mathrm{Pton}}(4t) \ , \tag{3.2.1}$$

where the intensity scale factor, χ is specified below ($\approx \frac{1}{10}$).

If diffusion is included in the numerical calculation, but without variation of the thermal/optical properties, the results are those of the analytic solution, (2.2.11). A comparison of the two equations, (2.2.11) and (2.3.8), for the case of $\alpha = 6$ and $\chi = 0.06$, is presented in Figures 3.2.1 and 3.2.2. The 2-D plots are done at the end of the pulse (10μs) and the cut-off temperatures, except the highest, T_{su}, are in 20 kelvin increments beginning at 490 K. Figure 3.2.1(e) is the case of Figure 3.2.1(f) in the absence of diffusion and was calculated from (2.1.6), and Figure 3.2.2(e) is the same case, but calculated from (2.3.8). It may be noted that Figures 3.2.2(c) and 3.2.2(d) were taken from a substantially coarser grid than that used for the earlier times; this is due to the long run times required for fine resolution of (2.3.8).

To take into account the variability with temperature of the thermal properties of the medium, the numerical solution is required. Figure 3.2.3 gives distributions for $\alpha = 8$, $\chi = 0.085$, for the constant property approximation, as well as the diffusion-free calculation for comparison, and Figure 3.2.4 is the variable property version of 3.2.3. The reference plots, Figures 3.2.3(e) and 3.2.4(e) (no diffusion), are both taken from (2.1.6) in this case. The basic effect of property variability is seen to be, just as in the strong pulse approximation

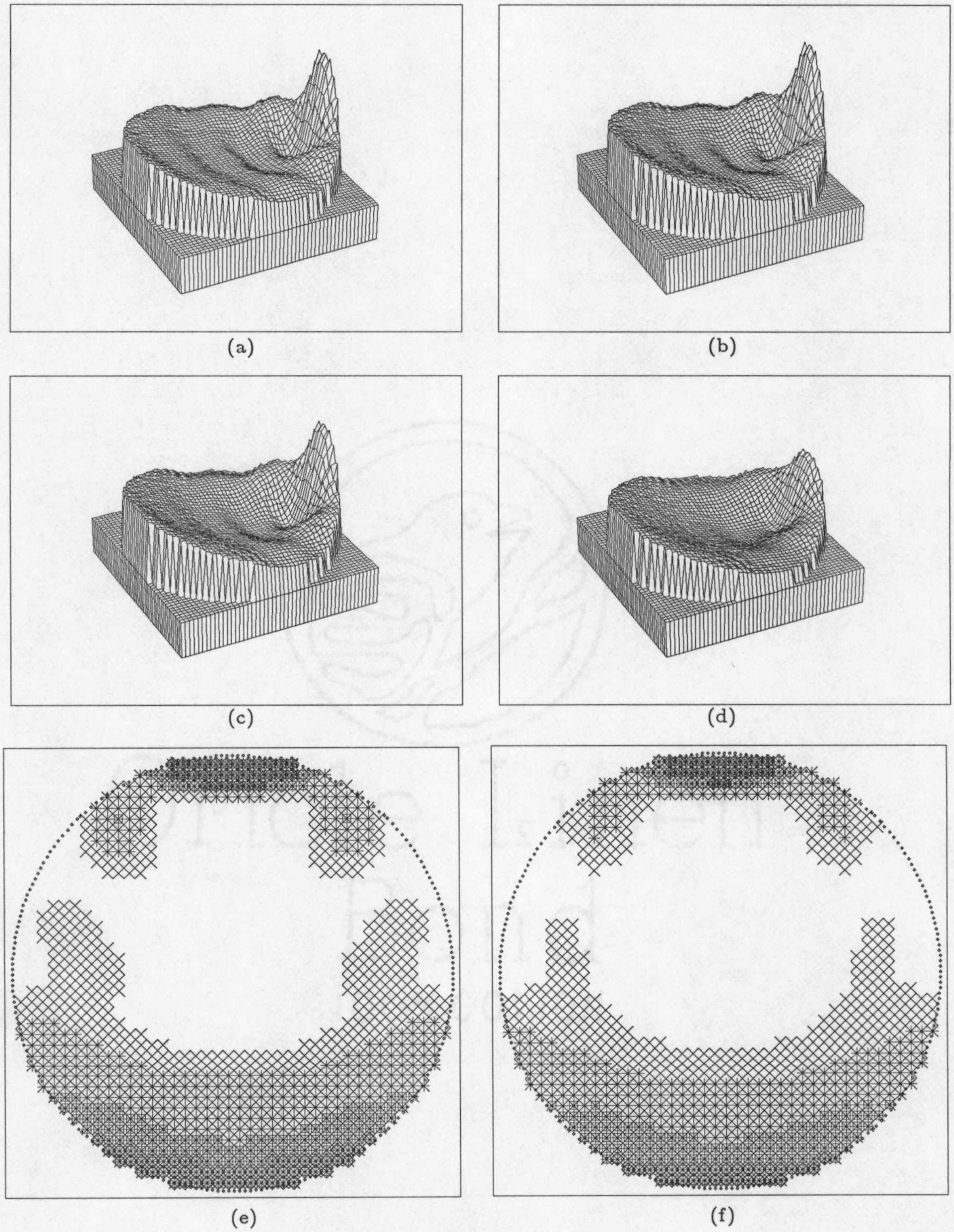

Figure 3.2.1 Analytic Solution: Constant Property Approximation

Figures (a)−(d) give T at 5, 10, 15, and 25 μs, respectively;

Figure (e) gives the case of no diffusion (at 10 μs) and (f) is taken from (b).

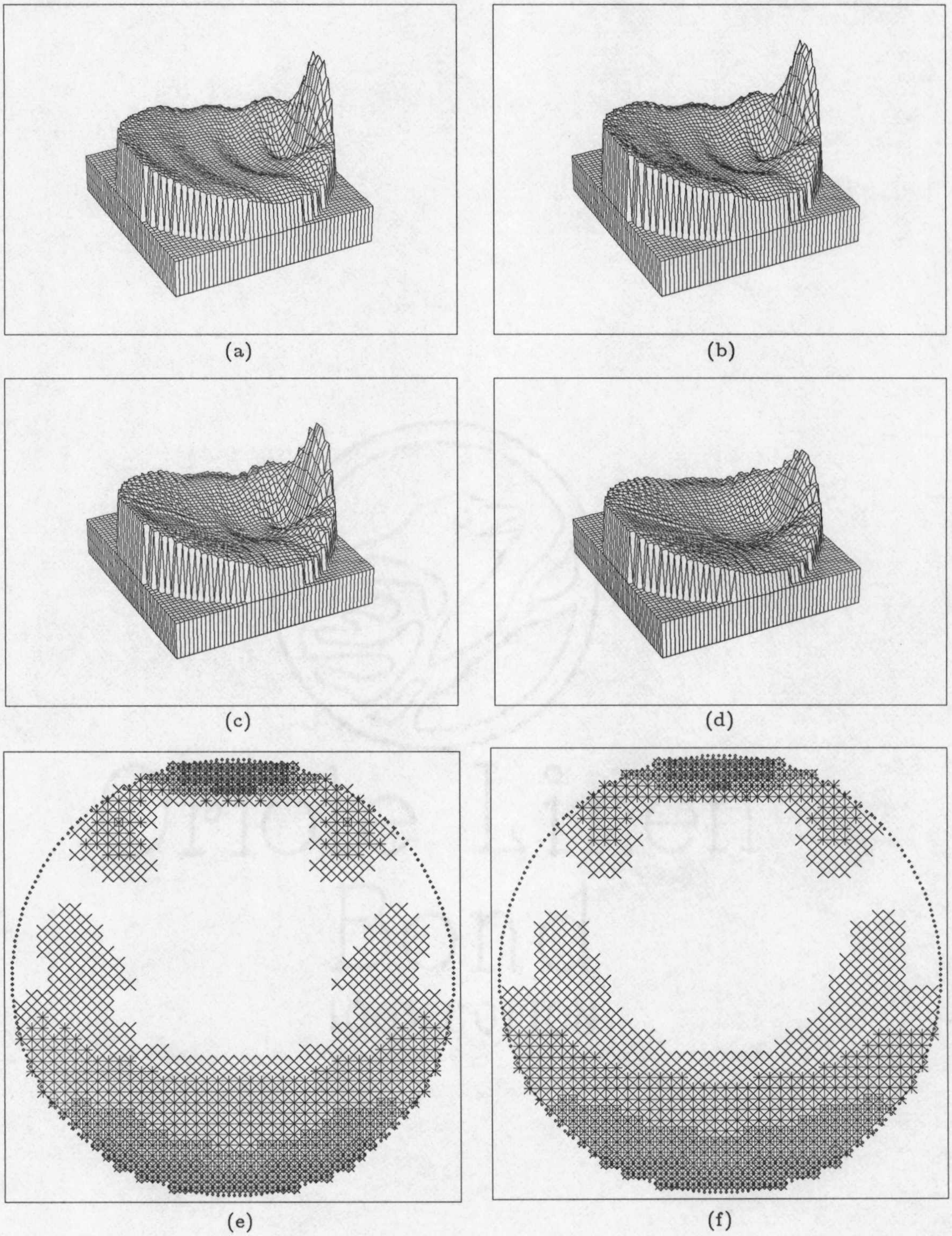

Figure 3.2.2 Numerical Solution: Constant Property Approximation

Figures (a)–(d) give T at 5, 10, 15, and 25 μs, respectively;

Figure (e) gives the case of no diffusion (at 10 μs) and (f) is taken from (b).

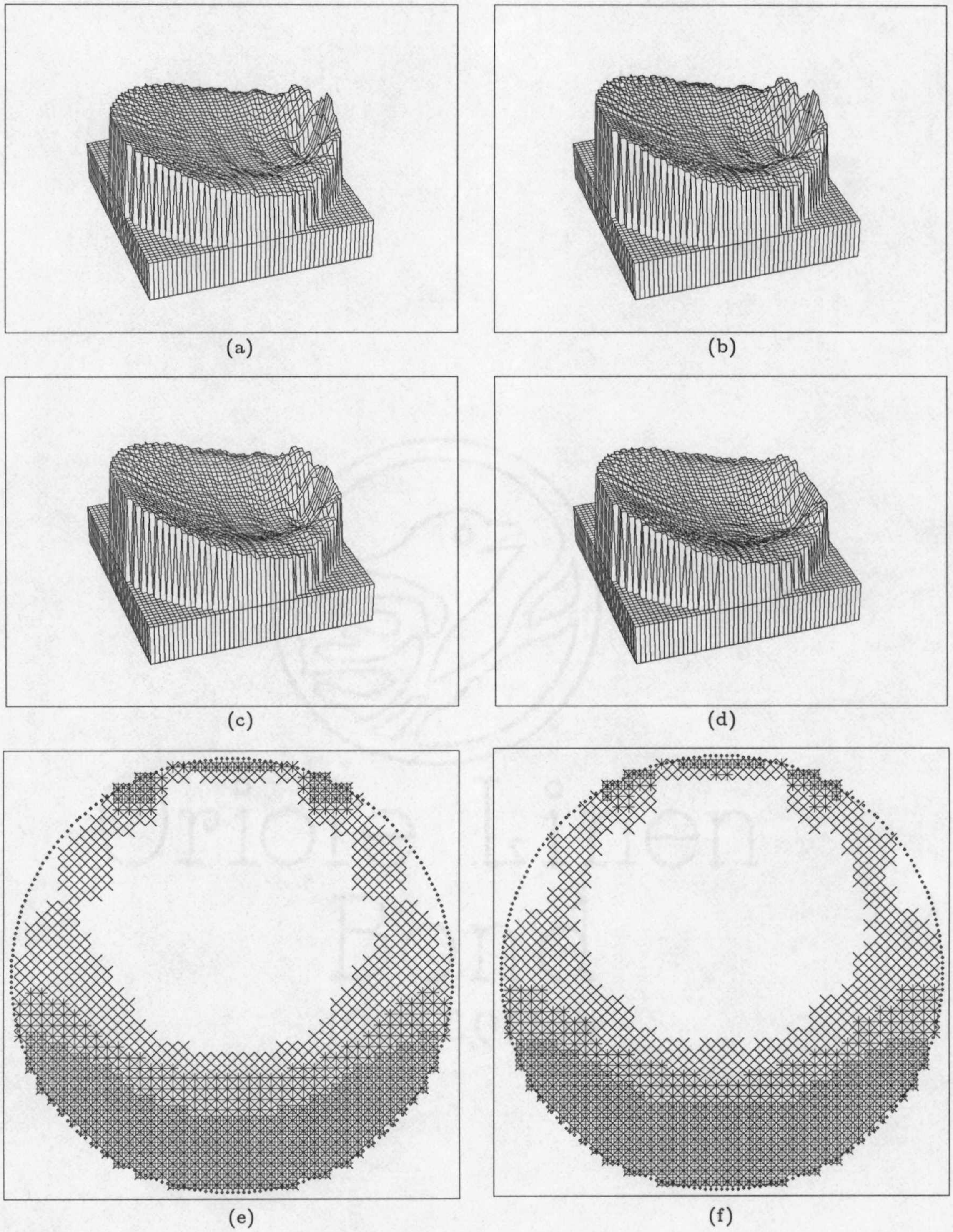

Figure 3.2.3 Explosive Vaporization in the Constant Property Approximation

Figures (a)—(d) give T at 5, 10, 15, and 25 μs, respectively; Figures (e) and (f) (at 10 μs) give $T \geq$ 520, 550, and 578 K, for diffusion off and on, respectively.

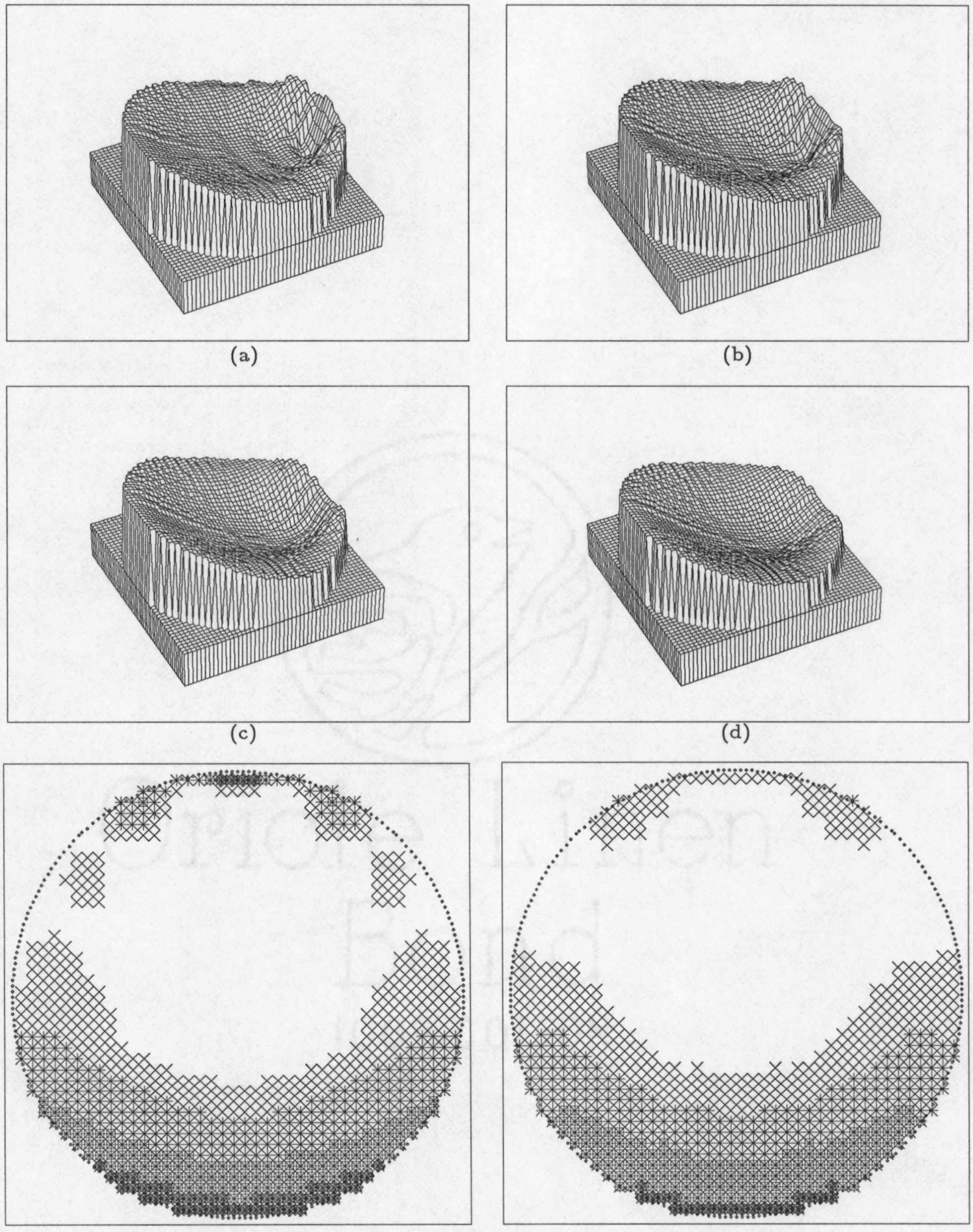

Figure 3.2.4 Variable Property Effect: Retardation of Temperature Growth

Figures (a)−(d) give T at 5, 10, 15, and 25 μs, respectively; Figures (e) and (f) (at 10 μs) give $T \geq$ 495, 520, 550, and 578 K, for diffusion off and on, respectively.

[24], that of curbing temperature growth, which is a consequence of the specific form of $\gamma(T)/\mathcal{N}(T)$ here and not categorical. It is of note that shattering at the back surface in the variable property case, albeit minor in extent, is thwarted by heat diffusion. Although this is contrived in the sense that χ is arbitrary, it indicates possibilities for observational testing of these calculations.

In this spirit, Figure 3.2.5 gives the (constant property) $\alpha = 8$ case with $\chi(= 0.075)$ chosen to exploit the exaggerated maxima of linear polarization, providing a clear case of dependence of the result of irradiation on its polarization. This also affords further comparison of the analytic and numerical solutions, that is, Figures 3.2.3(b) and 3.2.5(a) are nearly identical cases.

As a final example, Figure 3.2.6 gives results for a small sphere ($\alpha = 1$) for $\chi = 0.0585$, in which explosive vaporization is entirely forestalled by heat diffusion. The source function plot of Figure 3.2.6(a) is unique in that the height of the base corresponds to the minimum value in the distribution rather than zero. This is done to resolve the maximum, which otherwise appears flat, and at the cost of concealing the average value of $\hat{S}$. All of the 3-D temperature distributions have been plotted using this method since the fractional spread in temperature is usually much smaller than that of the field density*.

* This accounts for the minor difference in shape between, for example, Figure 3.1.7(a) and 3.2.1(a), where, in the latter, diffusion has been essentially ineffectual, owing to the short time span and the intense heating early in the pulse [24].

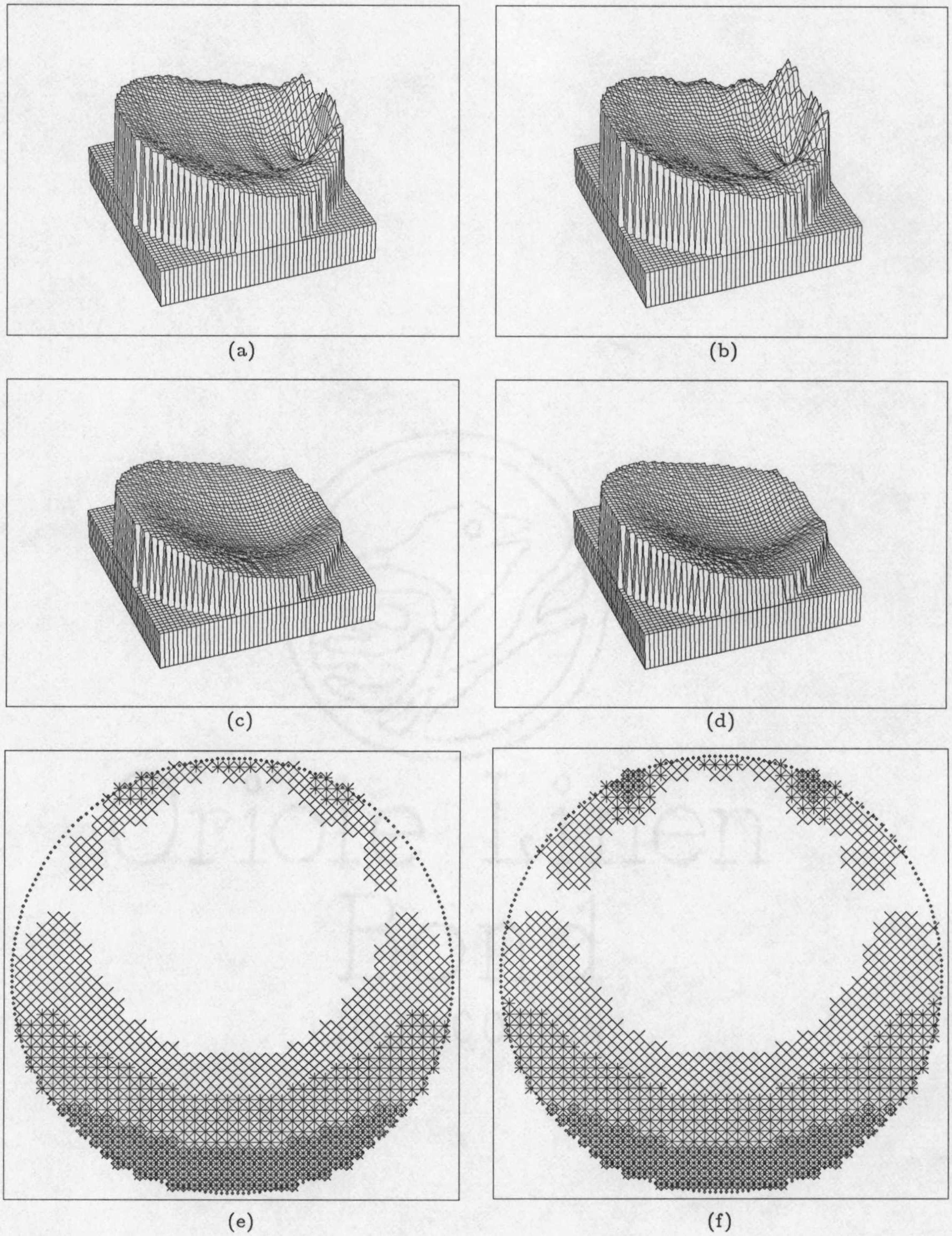

Figure 3.2.5 Effect of Polarization: Back Shattering under Linear Light

Left Side: Circular Light; Right Side: Linear Light. Figures (a) and (b): 10 μs.

Figures (c) and (d): 100 μs. Figures (e) and (f): $T \geq$ 495, 530, and 578 K (10 μs).

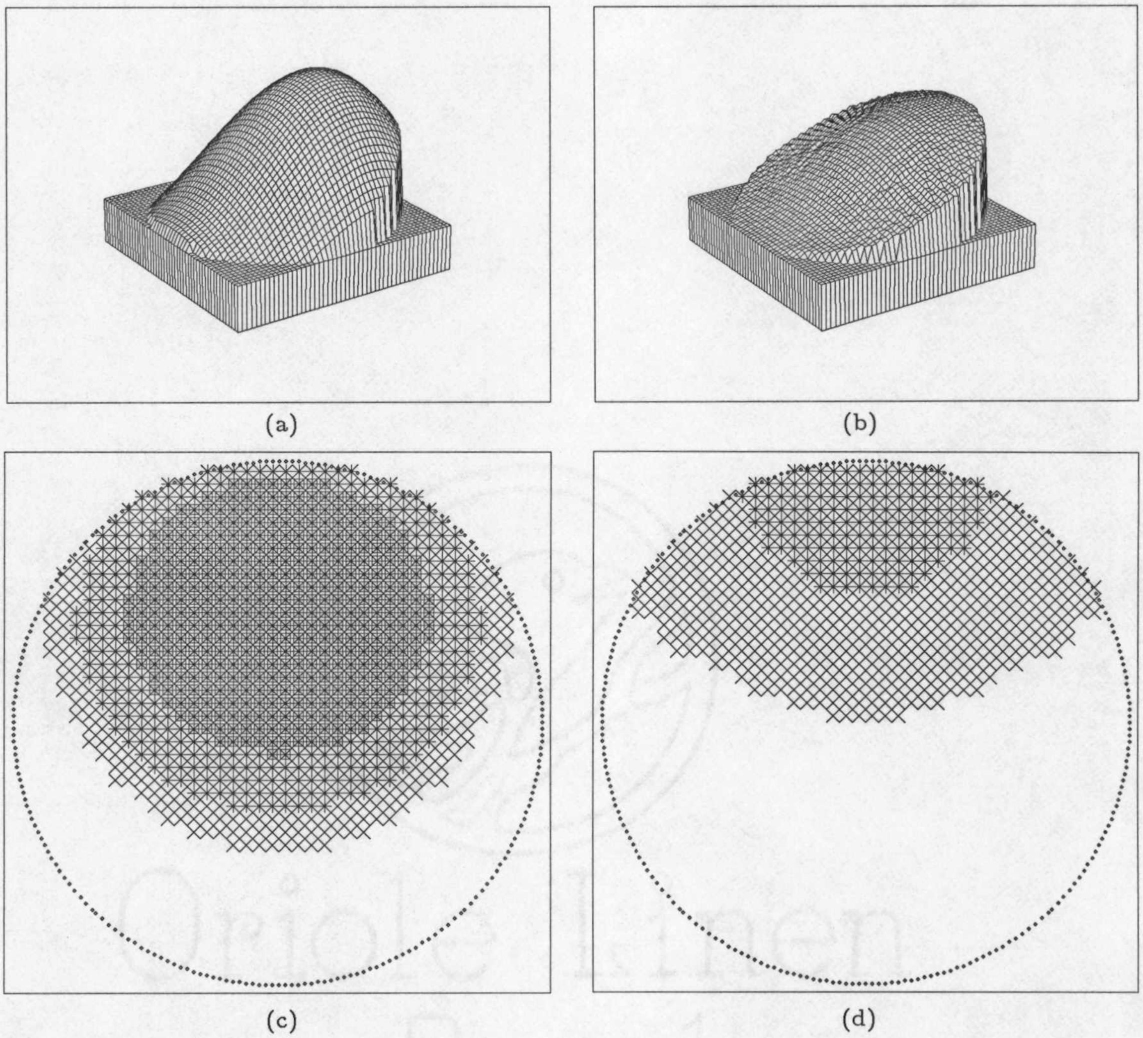

Figure 3.2.6 Diffusive Preclusion of Shattering

(a) $\alpha = 1,\ \mathrm{n} = 1.179 + i0.071$

$\hat{S}_{\mathrm{MAX}} = 0.93$

(b) Constant property heating at $10\mu s$

$T_{\mathrm{MAX}} =$ 571 K

(c) $T \geq$ 565,570, and 578 at 10 μs

Equation 2.1.6

(d) $T \geq$ 565 and 570 at 10 μs

Equation 2.2.11

3.3 Recapitulation and Elaboration

In Chapter 1, the incoming laser beam was modeled as a very long, monochromatic wavetrain of constant amplitude. This is a realistic approximation for the pulses of the previous section, but in other cases, particularly for extremely short pulses, more elaborate description may be warranted. To identify limitations of, and alternatives to this approximation, a brief discussion of laser pulses is included here.

The operation of a laser depends on the coincidence of one or more resonant cavity modes with frequencies lying within the linewidth of the lasing transition. The output will, in general, be a complex distribution of frequencies which may be represented as a continuous superposition of monochromatic waves, that is, an integral over frequency:

$$E(z,t) = \int_{\Delta\nu} A(\nu) e^{i\left[\frac{2\pi}{c}(z-ct)\nu + \delta(\nu)\right]} d\nu \,. \tag{3.3.1}$$

If the integrand in (3.3.1) is confined to a single mode or if it represents a number of modes that are locked in phase, $\delta(\nu)$ is constant and may be disregarded. In this situation, (3.3.1) is integrable analytically if the amplitude function, $A(\nu)$, is specified to the Gaussian form,

$$A(\nu) = e^{-\left[\frac{2}{\nu_e}(\nu-\nu_0)\right]^2} \,, \tag{3.3.2}$$

where ν_e is the characteristic width (at 1/e maximum height), and providing $\Delta\nu \longrightarrow (-\infty, \infty)$:

$$E(z,t) \longrightarrow e^{\left(\frac{2\nu_0}{\nu_e}\right)^2} \int_{-\infty}^{\infty} d\nu \, \exp\left\{ -\frac{4}{{\nu_e}^2}\nu^2 - \left[\frac{2\pi}{c} i(ct-z) - \frac{8\nu_0}{{\nu_e}^2}\right]\nu \right\} =$$

$$\frac{\sqrt{\pi}}{2}\ \nu_e\ e^{\frac{2\pi}{c}i(z-ct)\nu_0}\ e^{-[\frac{\pi\nu_e}{2c}(z-ct)]^2}\ . \qquad (3.3.3)$$

That is, a Gaussian distribution of frequencies corresponds to a Gaussian pulse shape in the time domain, and the characteristic widths of the two are essentially reciprocals of each other ($\frac{4}{\pi} \approx 1$).

In this view, the representation of a single-mode spectrum as a (narrow) Gaussian distribution indicates that (3.3.3) is applicable to the "monochromatic" case as well. Thus, if ν_e is very small, the modulation envelope in (3.3.3) can be set aside until after solution so that the pure sinusoidal form leading to (1.1.5) and (1.2.9) is maintained, and the monochromatic model remains useful. This is the approach in the examples above: an amplitude which varies very gradually along the wavetrain (negligible changes over lengths on the order of particle sizes) is modeled as a wave with an amplitude which is constant along its entire length at any instant, t', but which varies temporally according to $I(t)$.

On the other hand, for large ν_e, the spatial length of the pulse becomes comparable to the dimensions of the sphere and the variation in amplitude over these dimensions is no longer minor. Indeed, in the limit of brevity available from current laser technology ($\frac{1}{\nu_e} \approx 10^{-14}$sec), the entire pulse may not span the spherical diameter. Moreover, (3.3.3) hinges, strictly speaking, on the simple form assumed for $A(\nu)$ [and $\delta(\nu)$], and thus lacks generality. For these reasons, it can prove useful to return to (3.3.1) and resort to numerical evaluation, thus avoiding both the unwanted coordinate dependence, $e^{-(z-ct)^2}$, and the restrictions of analytic integration:

$$E(z,t) \cong \sum_n \mathcal{A}(\nu_n) e^{i(k_n z - \omega_n t)} \ , \quad \mathcal{A}(\nu_n) = W_n(\Delta\nu) A(\nu_n) e^{i\delta(\nu_n)} \ , \qquad (3.3.4)$$

where $W_n(\Delta\nu)$ is the weighting factor for Gaussian quadrature, the form of numerical integration employed in this work.

In short, by remaining in the frequency domain, the Mie theory of Chapter 1 may be extended from the simple case, $A(\nu) = \delta(\nu - \nu_0)$, to general frequency spectra, expressing the resulting internal (or scattered) fields as sums of terms given by (1.4.5,7).

Practical application of (3.3.4) brings into consideration the frequency sensitivity of the source function. The internal fields of (1.4.5,7) derive their frequency dependence entirely from the complex refractive index, n, and the Mie size parameter, α. For changes on the order of a mode width, typically 10^6 Hz, or a span of several modes, about 10^9 Hz (axial mode spacing is $\frac{c}{2L}$), the size parameter varies inappreciably; that is, $\frac{\Delta\alpha}{\alpha} = \frac{\Delta\nu}{\nu}$ and $\nu_{\text{laser}} \gg 10^9$ Hz. Furthermore, although the frequency dependence of n is much more complicated, it, too, is ordinarily negligible for intervals of this size. In the cases examined in the previous section, for example, a gigahertz change in the laser frequency ($\approx 3 \times 10^{13}$Hz) corresponds to fractional changes on the order of 10^{-5} and 10^{-4} for the real and imaginary components, respectively, of n [11], changes seen in section 3.1 to be unimportant. At the other extreme, for very short pulses, with $\Delta\nu$ comparable to ν, both the size parameter and the refractive index can be expected to show substantial variation, and the various plane waves in (3.3.4) give rise to significantly different source functions. To determine the result, the vector components of the internal electric fields of differing frequencies are summed and the source function is computed from the total, composite, E field.

One other consideration which enters the discussion in the regime of picosecond laser pulses is that of coupling mechanisms. The initial field/sphere interaction is that of photon absorption by the atoms or molecules comprising the medium. In atoms, this corresponds to electronic excitation, and, in molecular substances, vibrational and rotational transitions are, in addition, available. The acquired energy eventually appears chiefly as energy of translation and/or vibration of the atoms or molecules, that is, thermal activity. The mechanisms responsible for de-excitation vary depending on the circumstances; it may be noted, however, that radiative de-excitation typically occurs on timescales $\geq 10^{-9}$ seconds and is ordinarily upstaged by faster processes [6].

For the chemical elements, internal non-radiative de-excitation, in the absence of photoionization ($h\nu < I$, the first ionization potential) does not occur, and it is collisions and/or collision-like processes which provide much of the transfer of the energy of atomic excitation to that of thermal motions [6,p.126] (in liquids, collision times are $\leq 10^{-13}$ sec [6,p.132]). In molecular substances, on the other hand, radiationless de-excitation is common and proceeds along avenues such as ionization, dissociation, external influence such as collision

($\sim 10^{-13}$ sec), and internal conversion ($\sim 10^{-12}$ sec), all of which may involve vibrational redistribution and relaxation [6,p.128-135]. Another possible de-excitation mechanism is long-range non-radiative resonance transfer [6,p.140].

The point here is that many complex and incompletely understood processes are at work in the detailed history of the light energy absorbed from the field, and that, since many of these mechanisms operate on picosecond timescales, it becomes relevant to consider them in speaking sensibly about the thermal response of a medium to ultra-short laser pulses.

RESUMÉ

The electromagnetic field patterns within the body of a spherical particle, drop, or bubble are described accurately by the Mie solution, (1.4.5,7). This result is supported by comparison with results given in Born & Wolf [4], Jackson [15], the Pendleton dissertation [23] (and paper [24]), and the paper (cited in the introduction) authored by Düsel, Kerker, and Cooke [8]. It has also been corroborated by numerically performed volume integrations giving absorption cross-sections verified by the Miev0 code from work done at the National Center for Atmospheric Research. Competing phase conventions are treated thoroughly, clarifying and highlighting the mathematical distinctions necessary for consistent solution. Also, the internal fields produced in irradiation by plane light of both circular and linear polarizations are detailed. These equations, (1.4.5,7), have been used in computer simulations to study the shapes and magnitudes of the internal field patterns over a wide range of size parameters and complex refractive indices, revealing systematic evolution of these characteristic structures.

For cases in which it is permissible to ignore convection within the spherical medium, energy transfer subsequent to thermal conversion is governed by conduction. The differential equation of heat conduction with source term, (2.1.2), has been solved numerically and, for the case of constant thermal properties, (2.2.1), analytically as well. These solutions are given by (2.2.11) and (2.3.8) respectively, and have been shown to yield good agreement in several specific cases involving moderate-energy laser pulses acting on spherical water drops.

The model constituted by the solutions to the Mie problem and the heat equation is amenable to elaboration beyond the comparatively simple situations illustrated by the graphics in this chapter. As discussed above, the superposition principle may be employed to calculate the source term for short, polychromatic pulses. Mass loss through steady vaporization or sublimation at the surface can be incorporated by application of (1.4.7,9) to a diminishing sequence of size parameters dictated by a separate surface-loss equation. Similarly, a temporal sequence of "initial" temperature distributions generated interactively from a fluid dynamic model of free convection within the sphere can be used to generalize the heat transport model to cases of slowly heated, low viscosity media [10]. Elaborations of greater complexity include, prominently, the extension to non-sphericity required when the particles either are inherently aspherical, or are deformed by effects such as fluid flow or intense irradiation [2], and calculation of the source function for inhomogeneous refractive index distributions which is, strictly speaking, required for solution of (2.1.1).

LIST OF REFERENCES

LIST OF REFERENCES

1. G. Arfken, **Mathematical Methods for Physicists**, (Academic, New York, 1970).

2. M. Autric, P. Vigliano, E. Mazoyer, D. Dufresne, J. P. Caressa and Ph. Bournot, *Effects of a Pulsed CO_2 Laser Radiation on a Single Water Droplet*, **AIAA-85-1630**, 1985.

3. V. V. Barinov and S. A. Sorokin, *Explosions of Water Drops under the Action of Optical Radiation*, **Soviet Journal of Quantum Electronics**, 3, 89-92 (1974).

4. M. Born and E. Wolf, **Principles of Optics**, (Pergamon, New York, 1975).

5. B. H. Bransden and C. J. Joachin, **Physics of Atoms and Molecules**, (Longman, New York, 1983).

6. L. G. Christophorou, **Atomic and Molecular Radiation Physics**, (Wiley, New York, 1971).

7. E. K. Dabora, *Laser Ignition of Fuel Drops*, **A81-47749 23-25**, 119-133 (AIAA, New York, 1979).

8. P. W. Düsel, M. Kerker, and D. D. Cooke, *Distribution of Absorption Centers within Irradiated Spheres*, **Journal of the Optical Society of America**, 69, 55-59 (1979).

9. A. C. Eckbreth, *Laser Modulated Particulate Incandescence*, **UTRC77-9** (1975).

10. B. P. Gerasimov, V. M. Gordienko, T. G. Elizarova, and A. P. Sukhorukov, *Convective Heat and Mass Transfer Induced by a Laser Beam*, **A79-42886 18-34**, 377-382 (Hemisphere, Washington D. C., 1978).

11. G. M. Hale and M. R. Querry, *Optical Constants of Water in the 200-nm to 200-μm Wavelength Region*, **Applied Optics**, 12, 555-563 (1972).

12. D. Halliday and R. Resnick, **Fundamentals of Physics**, (Wiley, New

York, 1966).

13. **Handbook of Mathematical Functions**, edited by M. Abramowitz and I. A. Stegun, (Dover, New York, 1970).

14. E. Hecht and A. Zająk, **Optics**, (Addison-Wesley, Mass., 1974).

15. J. D. Jackson, **Calssical Electrodynamics**, (Wiley, New York, 1975).

16. Y. Jaluria, **Free Convection, Heat and Mass Transfer**, (Pergamon, New York, 1980).

17. P. Kafalas and A. P. Ferdinand, Jr., *Fog Droplet Vaporization and Fragmentation by a 10.6 μm Laser Pulse*, **Applied Optics**, 12, 29-33 (1973).

18. P. Kafalas and J. Herrmann, *Dynamics and Energetics of the Explosive Vaporization of Fog Droplets by a 10.6-μm Laser Pulse*, **Applied Optics**, 12, 772-775 (1973).

19. M. Kerker, **The Scattering of Light and Other Electromagnetic Radiation**, (Academic, New York, 1969).

20. F. Kreith, **Principles of Heat Transfer**, (International, Pennsylvania, 1966).

21. A. Nussbaum and R. A. Phillips, **Contemporary Optics for Scientists and Engineers**, (Prentice-Hall, New Jersey, 1976).

22. M. N. Özişik, **Heat Conduction**, (Wiley, New York, 1980).

23. J. D. Pendleton, **A Generalized Mie Theory Solution and its Application to Particle Sizing Interferometry**, (University of Tennessee, Knoxville, 1982).

24. J. D. Pendleton, *Water Droplets Irradiated by a Pulsed CO_2 Laser: Comparison of Computed Temperature Contours with Explosive Vaporization Patterns*, **Applied Optics** 24, 1631-7 (1985).

25. L. W. Pinkley, P. P. Sethna, and D. Williams, *Optical Constants of Water in the Infrared: Influence of Temperature*, **Journal of the Optical Society of America**, 67, 494-499 (1977).

26. A. P. Prishivalko, *Heating and Destruction of Water Drops on Exposure to Radiatoin with Inhomogeneous Internal Heat Evolution*, **Izvestiya Vysshykh Uchebnykh Zavedenii**, 2, 46-52 (Plenum, 1983).

27. A. P. Prishivalko, *Influence of Variation of Optical Constants and Drop Material on its Heating, Evaporation, and Rupture under the Action of Radiation*, **Zhurnal Prikladnoi Spektroskopii**, 33, 351-55 (Plenum, 1981).

28. A. P. Prishivalko and S. T. Leiko, *Radiative Heating and Evaporation of Droplets*, **Zhurnal Prikladnoi Spektroskopii**, 33, 727-734 (1979).

29. W. J. Wiscombe, *Mie Scattering Calculations: Advances in Technique and Fast, Vector-Speed Computer Codes*, Technical Note **NCAR/TN-140+STR**, (National Center for Atmospheric Research, Boulder, Colorado, 1979).

APPENDICES

APPENDIX A

THE HELMHOLTZ EIGENFUNCTIONS

The scalar Helmholtz equation is

$$(\nabla^2 + \lambda^2)\psi(\mathbf{r}) = 0 \ . \tag{A.1a}$$

This form is generated from the Maxwell Equations as well as in the constant conductivity heat conduction problem; the two situations differ in that the Classical wave equation is a proportionality between the second space and time derivatives and the heat problem invloves but a single time derivative. Both take their time dependence from the exponential form e^x so that the difference reduces, mathematically, to $x = \pm i\kappa$ on the one hand, and $x = -\beta\lambda^2$ on the other. Of interest, then, is (A.1):

$$\frac{\partial^2\psi}{\partial r^2} + \frac{2}{r}\frac{\partial\psi}{\partial r} + \frac{1}{r^2\sin\theta}\frac{\partial}{\partial\theta}\left(\sin\theta\frac{\partial\psi}{\partial\theta}\right) + \frac{1}{r^2\sin^2\theta}\frac{\partial^2\psi}{\partial\phi^2} + \lambda^2\psi = 0 \tag{A.1b}$$

With the definition $\mu \equiv \cos\theta$, and the substitution,

$$\Psi(r,\mu,\phi,t) = r^{\frac{1}{2}}\psi(r,\mu,\phi,t) \ , \tag{A.2}$$

this is

$$\frac{\partial^2\Psi}{\partial r^2} + \frac{1}{r}\frac{\partial T}{\partial r} - \frac{1}{4}\frac{\Psi}{r^2} + \frac{1}{r^2}\frac{\partial}{\partial\mu}\left[(1-\mu^2)\frac{\partial\Psi}{\partial\mu}\right] + \frac{1}{r^2(1-\mu^2)}\frac{\partial^2\Psi}{\partial\phi^2} = -\lambda^2\Psi \ . \tag{A.3}$$

Provisionally assuming a separable solution of the form

$$\Psi = R(r)M(\mu)Q(\phi) \ , \tag{A.4}$$

and substitution of same in (A.3) leads, after division by Ψ, to

$$\frac{R''}{R} + \frac{R'}{rR} - \frac{1}{4r^2} + \frac{1}{r^2 M}\frac{d}{d\mu}\left[(1-\mu^2)M'\right] + \frac{Q''}{Qr^2(1-\mu^2)} = -\lambda^2 \ . \tag{A.5}$$

The simplest component is the azimuthal function, for which a direct proportionality between the function and its second derivative is productive:

$$Q''(\phi) = -m^2 Q(\phi) \ , \tag{A.6}$$

where the sign is chosen for an oscillatory solution. Multiplying through with r^2 then gives

$$r^2\frac{R''}{R} + r\frac{R'}{R} - \frac{1}{4} + \frac{1}{M}\frac{d}{d\mu}\left[(1-\mu^2)M'\right] - \frac{m^2}{1-\mu^2} = -\lambda^2 r^2 \ , \tag{A.7}$$

which will be satisfied if

$$r^2\frac{R''}{R} + r\frac{R'}{R} - \frac{1}{4} + \lambda^2 r^2 = -\frac{1}{M}\frac{d}{d\mu}\left[(1-\mu^2)M'\right] + \frac{m^2}{1-\mu^2} = \nu \ . \tag{A.8a,b}$$

In order to proceed, the separation constant, ν, is specified to the form $\nu = n(n+1)$, where n is an integer:

$$R''(r) + \frac{1}{r}R'(r) + \left(\lambda^2 - \frac{n^2+n+\frac{1}{4}}{r^2}\right) = 0 \ , \tag{A.9}$$

$$\frac{d}{d\mu}\left[(1-\mu^2)M(\mu)\right] + \left[n(n+1) - \frac{m^2}{1-\mu^2}\right]M(\mu) = 0 \ . \tag{A.10}$$

Equation (A.9) is the Bessel equation for half-integer order functions [13,p.437], and (A.10) is Legendre's associated differential equation [13,p.332]. Together with the obvious exponential solution, (A.6), these give

$$\Psi(r,\mu,\phi) = \sum \gamma_{nm} J_{n+\frac{1}{2}}(\lambda r) P_n^m(\mu) e^{im\phi} \ . \tag{A.11}$$

Finally, from (A.2) and the defining equation for the spherical Bessel function,

$$\psi(r,\theta,\phi) = \sum C_{nm} j_n(\lambda r) Y_{nm}(\theta,\phi) \ , \tag{A.12}$$

where

$$Y_{nm}(\mu,\phi) = \sqrt{\frac{2n+1}{4\pi} \frac{(n-m)!}{(n+m)!}} P_n^m(\mu) e^{im\phi} \tag{A.13}$$

[15,p.99]. If, as in Chapter 2, $\psi(\mathrm{r})$ is confined to a bound region of space, the appropriate form is

$$\psi(r,\theta,\phi) = \sum C_{n\ell m} j_n(\lambda_{n\ell} r) Y_{nm}(\theta,\phi) \ . \tag{A.14}$$

APPENDIX B

CIRCULAR POLARIZATIONS

Plane, monochromatic, light may be considered simply as a fixed, repetitious, field pattern moving (rigidly) through space. If the light is linearly polarized, the electric field vanishes every half-wavelength and is confined to anti-parallel directions. If it is circularly polarized, the field rotates in direction through a full circle every wavelength and does not oscillate in amplitude.

To analyze the case of circular polarization, a coordinate system is defined, fixed in the field pattern, with its positive z axis in the direction of propagation, and two planes, $z = 0, \frac{\lambda}{4}$, are isolated for observation. If the change in the field's direction, between $\frac{\lambda}{4}$ and 0, is a positive(negative) rotation, then the wave is said to have positive(negative) helicity.

Of interest then are the three combinations:

$$\mathbf{E}_{\mathrm{P}}^{(+)}(z) = [\hat{\epsilon}_1 \sin kz + \hat{\epsilon}_2 \cos kz] \tag{B.1}$$

$$\mathbf{E}_{0}^{(+)}(z) = [\hat{\epsilon}_1 \cos kz - \hat{\epsilon}_2 \sin kz] \tag{B.2}$$

$$\mathbf{E}_{\mathrm{M}}^{(+)}(z) = -[\hat{\epsilon}_1 \sin kz + \hat{\epsilon}_2 \cos kz] \ . \tag{B.3}$$

Since

$$\mathbf{E}_{\mathrm{P}}^{(+)}(\tfrac{\lambda}{4}) \times \mathbf{E}_{\mathrm{P}}^{(+)}(0) = \mathbf{E}_{0}^{(+)}(\tfrac{\lambda}{4}) \times \mathbf{E}_{0}^{(+)}(0) = \mathbf{E}_{\mathrm{M}}^{(+)}(\tfrac{\lambda}{4}) \times \mathbf{E}_{\mathrm{M}}^{(+)}(0) =$$

$$\hat{\epsilon}_1 \times \hat{\epsilon}_2 = -\hat{\epsilon}_2 \times \hat{\epsilon}_1 = -\hat{\epsilon}_1 \times -\hat{\epsilon}_2 = \hat{\epsilon}_3 \ , \tag{B.4}$$

these represent positive helicity. Further, the (*positive*) rotation from $\hat{\epsilon}_1$ to $\hat{\epsilon}_2$ begins at $\frac{\lambda}{4}$, 0 and $-\frac{\lambda}{4}$, respectively, for the three cases, so that $\mathbf{E}_{\mathrm{P}}^{(+)}(\mathbf{E}_{\mathrm{M}}^{(+)})$ anticipates(lags behind) $\mathbf{E}_0^{(+)}$ by $\frac{\lambda}{4}$.

If the these fields are altered in that $\hat{\epsilon}_2 \longrightarrow -\hat{\epsilon}_2$,

$$\mathbf{E}_{\mathrm{P}}^{(-)}(z) = [\hat{\epsilon}_1 \sin kz - \hat{\epsilon}_2 \cos kz] \tag{B.5}$$

$$\mathbf{E}_0^{(-)}(z) = [\hat{\epsilon}_1 \cos kz + \hat{\epsilon}_2 \sin kz] \tag{B.6}$$

$$\mathbf{E}_{\mathrm{M}}^{(-)}(z) = -[\hat{\epsilon}_1 \sin kz - \hat{\epsilon}_2 \cos kz] \ , \tag{B.7}$$

the result is

$$\mathbf{E}_{\mathrm{P}}^{(-)}(\tfrac{\lambda}{4}) \times \mathbf{E}_{\mathrm{P}}^{(-)}(0) = \mathbf{E}_0^{(-)}(\tfrac{\lambda}{4}) \times \mathbf{E}_0^{(-)}(0) = \mathbf{E}_{\mathrm{M}}^{(-)}(\tfrac{\lambda}{4}) \times \mathbf{E}_{\mathrm{M}}^{(-)}(0) =$$

$$\hat{\epsilon}_1 \times -\hat{\epsilon}_2 = \hat{\epsilon}_2 \times \hat{\epsilon}_1 = -\hat{\epsilon}_1 \times \hat{\epsilon}_2 = \hat{\epsilon}_3 \ : \tag{B.8}$$

negative helicity. And, again, the (*negative*) rotation from $\hat{\epsilon}_2$ to $\hat{\epsilon}_1$ begins at $\frac{\lambda}{4}$,0 ,and $-\frac{\lambda}{4}$ for the three so that $\mathbf{E}_{\mathrm{P}}^{(-)}$ and $\mathbf{E}_{\mathrm{M}}^{(-)}$ are, again, a quarter-cycle before and behind $\mathbf{E}_0^{(-)}$.

Therefore, since $[\hat{\epsilon}_1 \cos kz \mp \hat{\epsilon}_2 \sin kz] + i[\hat{\epsilon}_1 \sin kz \pm \hat{\epsilon}_2 \cos kz]$ $(= \mathbf{E}_0^{(\pm)} + i\mathbf{E}_{\mathrm{P}}^{(\pm)})$ $= \hat{\epsilon}_1(\cos kz + i\sin kz) \pm \hat{\epsilon}_2(-\sin kz + i\cos kz) = \hat{\epsilon}_1(\cos kz + i\sin kz) \pm$ $\hat{\epsilon}_2[\cos(kz + \frac{\pi}{2}) + i\sin(kz + \frac{\pi}{2})] = (\hat{\epsilon}_1 \pm \hat{\epsilon}_2 e^{i\frac{\pi}{2}})e^{ikz} = (\hat{\epsilon}_1 \pm i\hat{\epsilon}_2)e^{ikz}$,

and $[\hat{\epsilon}_1 \cos kz \mp \hat{\epsilon}_2 \sin kz] - i[\hat{\epsilon}_1 \sin kz \pm \hat{\epsilon}_2 \cos kz]$ $(= \mathbf{E}_0^{(\pm)} + i\mathbf{E}_{\mathrm{M}}^{(\pm)})$ $= \hat{\epsilon}_1(\cos kz - i\sin kz) \mp \hat{\epsilon}_2(\sin kz + i\cos kz) = \hat{\epsilon}_1(\cos kz - i\sin kz) \mp$ $[\cos(kz - \frac{\pi}{2}) - i\sin(kz - \frac{\pi}{2})] = \hat{\epsilon}_1 e^{-ikz} \mp \hat{\epsilon}_2 e^{-i(kz - \frac{\pi}{2})} = (\hat{\epsilon}_1 \mp i\hat{\epsilon}_2)e^{-ikz}$, it is evident that

$$\mathbf{E}^{(\pm)}_{\text{PLUS}} = (\hat{\epsilon}_1 \pm i\hat{\epsilon}_2)\mathrm{e}^{ikz} \tag{B.9}$$

and

$$\mathbf{E}^{(\pm)}_{\text{MINUS}} = (\hat{\epsilon}_1 \pm i^*\hat{\epsilon}_2)\mathrm{e}^{i^*kz} \tag{B.10}$$

represent circularly polarized light in the two conventions, and that the imaginary components are $(kz =)\frac{\pi}{2}$ ahead of(behind) the real in the plus(minus) convention for both helicities. That is, the real part of (B.9) and the real part of (B.10) are the same and are equal to $\mathbf{E}^{(\pm)}_0$, and the imaginary components of the two are equal to $\pm\mathbf{E}^{(\pm)}_{\mathrm{P}}$.

Also of note is that, since $\mathbf{B} = \mathrm{n}\hat{\epsilon}_3 \times \mathbf{E}$ in either convention,

$$\mathbf{B}^{(\pm)}_{\text{PLUS}} = \mathrm{n}\hat{\epsilon}_3 \times (\hat{\epsilon}_1 \pm i\hat{\epsilon}_2)\mathrm{e}^{ikz} = \mathrm{n}[\mp i(\hat{\epsilon}_1 \pm i\hat{\epsilon}_2)\mathrm{e}^{ikz}] = \mp i\mathrm{n}\mathbf{E}^{(\pm)}_{\text{PLUS}} \ ; \tag{B.11}$$

$$\mathbf{B}^{(\pm)}_{\text{MINUS}} = \mathrm{n}\hat{\epsilon}_3 \times (\hat{\epsilon}_1 \mp i\hat{\epsilon}_2)\mathrm{e}^{-ikz} = \mathrm{n}[\pm i(\hat{\epsilon}_1 \mp i\hat{\epsilon}_2)\mathrm{e}^{-ikz}] = \pm i\mathrm{n}\mathbf{E}^{(\pm)}_{\text{MINUS}} \ . \tag{B.12}$$

APPENDIX C

THE VECTOR SPHERICAL HARMONIC

$$\mathbf{X}_{n,\pm1}(\theta,\phi) \equiv \frac{1}{\sqrt{n(n+1)}}\mathbf{L}Y_{n,\pm1}(\theta,\phi) \quad \text{and} \quad \mathbf{L} = \tfrac{1}{i}\mathbf{r}\times\nabla \quad [15].$$

Also, $\nabla \equiv \hat{\mathbf{r}}\partial_r + \hat{\theta}\frac{1}{r}\partial_\theta + \hat{\phi}\frac{1}{rsin\theta}\partial_\phi$, so that $\mathbf{r}\times\nabla =$

$$r\hat{\mathbf{r}}\times(\hat{\mathbf{r}}\partial_r + \hat{\theta}\tfrac{1}{r}\partial_\theta + \hat{\phi}\tfrac{1}{rsin\theta}\partial_\phi) = \hat{\phi}\partial_\theta - \hat{\theta}\tfrac{1}{sin\theta}\partial_\phi \text{ ; then,}$$

$$Y_{n,\pm1}(\theta,\phi) = \left[\tfrac{2n+1}{4\pi}\tfrac{(n\mp1)!}{(n\pm1)!}\right]^{\frac{1}{2}} P_n^{\pm1}(cos\theta)\mathrm{e}^{\pm i\phi} =$$

$$= \left[\tfrac{2n+1}{4\pi}[n(n+1)^{\mp1}]\right]^{\frac{1}{2}} P_n^{\pm1}(cos\theta)\mathrm{e}^{\pm i\phi} ,$$

$$\text{and } P_n^{-1}(cos\theta) = (-1)^1\tfrac{(n-1)!}{(n+1)!}P_n^1(cos\theta) = -\tfrac{P_n^1(cos\theta)}{n(n+1)} \Longrightarrow$$

$$Y_{n,\pm1}(\theta,\phi) = \left[\frac{2n+1}{4\pi}[n(n+1)]^{\mp1}\right]^{\frac{1}{2}}\begin{pmatrix}1\\-[n(n+1)]^{-1}\end{pmatrix}P_n^1(cos\theta)\mathrm{e}^{\pm i\phi}$$

$$= \pm\sqrt{\tfrac{2n+1}{4\pi n(n+1)}}P_n^1(\cos\theta)\mathrm{e}^{\pm i\phi} \Longrightarrow$$

$$\mathbf{X}_{n,\pm1}(\theta,\phi) = \pm\sqrt{\tfrac{2n+1}{4\pi}}\tfrac{1}{n(n+1)}i(\hat{\theta}\tfrac{1}{sin\theta}\partial_\phi - \hat{\phi}\partial_\theta)P_n^1(\cos\theta)\mathrm{e}^{\pm i\phi} \; =$$

$$\mathbf{X}_{n,\pm1}(\theta,\phi) = i\sqrt{\frac{2n+1}{4\pi}}\frac{1}{n(n+1)}\left(\hat{\theta}\frac{i}{sin\theta}\mp\hat{\phi}\frac{d}{d\theta}\right)P_n^1(\cos\theta)\mathrm{e}^{\pm i\phi} . \qquad \text{(C.1)}$$

Therefore

$$\nabla\times f_n(\kappa r)\mathbf{X}_{n,\pm1}(\theta,\phi) = i\sqrt{\tfrac{2n+1}{4\pi}}\tfrac{1}{n(n+1)}\nabla\times f_n(\kappa r)(\hat{\theta}\tfrac{i}{sin\theta}\mp\hat{\phi}\tfrac{d}{d\theta})P_n^1(\cos\theta)\mathrm{e}^{\pm i\phi}$$

$$= i\sqrt{\frac{2n+1}{4\pi}}\frac{1}{n(n+1)}\nabla\times\left\{i\left[f_n(\kappa r)\frac{P_n^1(\cos\theta)}{sin\theta}\mathrm{e}^{\pm i\phi}\right]\hat{\theta} \mp \left[f_n(\kappa r)\frac{dP_n^1(\cos\theta)}{d\theta}\mathrm{e}^{\pm i\phi}\right]\hat{\phi}\right\} .$$

If $F_r = 0,\ \nabla\times\mathbf{F} = \hat{\mathrm{r}}\frac{\partial_\theta(F_\phi sin\theta)-\partial_\phi F_\theta}{rsin\theta} - \hat{\theta}\frac{\partial_r(rF_\phi)}{r} + \hat{\phi}\frac{\partial_r(rF_\theta)}{r}$, which $\Longrightarrow$

$[\nabla\times f_n(\kappa r)\mathbf{X}_{n,\pm 1}(\theta,\phi)]_r =$

$$i\sqrt{\frac{2n+1}{4\pi}}\frac{1}{n(n+1)}\frac{1}{rsin\theta}\left\{\mp\frac{\partial}{\partial\theta}\left[f_n(\kappa r)sin\theta\frac{dP_n^1(\cos\theta)}{d\theta}\mathrm{e}^{\pm i\phi}\right] - i\left[\frac{\partial}{\partial\phi}[f_n(\kappa r)\frac{P_n^1(\cos\theta)}{sin\theta}\mathrm{e}^{\pm i\phi}\right]\right\}$$

$$= \mp i\sqrt{\frac{2n+1}{4\pi}}\frac{1}{n(n+1)}\frac{f_n(\kappa r)\mathrm{e}^{\pm i\phi}}{rsin\theta}\left[\frac{d}{d\theta}(sin\theta\frac{d}{d\theta}P_n^1(\cos\theta)) - \frac{P_n^1(\cos\theta)}{sin\theta}\right] ;$$

since $P_n^1(\cos\theta)$ is a solution of $\left[\frac{1}{sin\theta}\frac{d}{d\theta}(sin\theta\frac{d}{d\theta}) + [n(n+1) - \frac{1}{sin^2\theta}]\right]\psi(\theta) = 0$,

the curl's radial component is $\mp i\sqrt{\frac{2n+1}{4\pi}}\frac{f_n(\kappa r)\mathrm{e}^{\pm i\phi}}{rn(n+1)}[-n(n+1)P_n^1(\cos\theta)] =$

$$\pm i\sqrt{\frac{2n+1}{4\pi}}\frac{f_n(\kappa r)}{r}P_n^1(\cos\theta)\mathrm{e}^{\pm i\phi} .$$

Its theta component is $\pm i\sqrt{\frac{2n+1}{4\pi}}\frac{1}{rn(n+1)}\frac{d}{d\theta}P_n^1(\cos\theta)\frac{d}{dr}[rf_n(\kappa r)]\mathrm{e}^{\pm i\phi}$, and its

azimuthal component is $\sqrt{\frac{2n+1}{4\pi}}\frac{i^2}{rn(n+1)}\frac{P_n^1(\cos\theta)}{sin\theta}\frac{d}{dr}[rf_n(\kappa r)]\mathrm{e}^{\pm i\phi}$:

$$\nabla\times f_n(\kappa r)\mathbf{X}_{n,\pm 1} =$$

$$i\sqrt{\frac{2n+1}{4\pi}}\frac{\mathrm{e}^{\pm i\phi}}{rn(n+1)}\left[\pm\hat{\mathrm{r}}\frac{n(n+1)}{r} + (\hat{\phi}\frac{i}{sin\theta} \pm \hat{\theta}\frac{d}{d\theta})\frac{d}{dr}\right]rf_n(\kappa r)P_n^1(\cos\theta) . \tag{C.2}$$

Also of note:

$$\hat{\mathrm{r}}\times\mathbf{X}_{n,\pm 1} = \frac{\mp 1}{\sqrt{n(n+1)}}\sqrt{\frac{2n+1}{4\pi n(n+1)}}\mathrm{e}^{\pm i\phi}\hat{\mathrm{r}}\times\left[i\hat{\phi}\partial_\theta \pm \hat{\theta}csc\theta\right]P_n^1 =$$

$$\mp\sqrt{\frac{2n+1}{4\pi}}\frac{\mathrm{e}^{\pm i\phi}}{n(n+1)}\left[-\hat{\theta}i\frac{d}{d\theta}P_n^1(\cos\theta) \pm \hat{\phi}csc\theta P_n^1(\cos\theta)\right] \Longrightarrow$$

$$\nabla \times f_n(\kappa r)\mathbf{X}_{n,\pm 1}(\theta,\phi) = \pm i\sqrt{\tfrac{2n+1}{4\pi}}\tfrac{\mathrm{e}^{\pm i\phi}}{r}\hat{\mathbf{r}} f_n(\kappa r) P_n^1(\cos\theta) + \tfrac{1}{r}\tfrac{d[r f_n(\kappa r)]}{dr}\hat{\mathbf{r}} \times \mathbf{X}_{n,\pm 1}(\theta,\phi)$$

$$= i\frac{\sqrt{n(n+1)}}{r}\hat{\mathbf{r}} f_n(\kappa r) Y_{n,\pm 1}(\theta,\phi) + \frac{1}{r}\frac{d[r f_n(\kappa r)]}{dr}\hat{\mathbf{r}} \times \mathbf{X}_{n,\pm 1}(\theta,\phi) \qquad \text{(C.3)} \ ,$$

which agrees with Jackson [15,p.771].

APPENDIX D

THE SOURCE FUNCTION

The rate of reduction of the field energy density of a propagating electromagnetic disturbance, in the absence of field sources, is given by the negative of the real part of the divergence of the complex Poynting vector:

$$\frac{\partial u}{\partial t} = -\Re\left\{\nabla \cdot \left[\frac{c}{8\pi}\mathbf{E} \times \mathbf{H}^\star\right]\right\} \equiv \mathrm{S}(\mathbf{r}) \ , \tag{D.1}$$

from Jackson Eqs. 6.108 and 8.47 [15,pp.237,347].

Pertinent to the simplification of (D.1) are the forms $\mathbf{H}^\star \cdot \mathbf{H}$ and $\epsilon^\star$; from Jackson Eq. 7.73 [15,p.297], the first is

$$\mathbf{H}^\star \cdot \mathbf{H} = \left(\frac{1}{\mu k}\mathrm{n}^\star\mathbf{k} \times \mathbf{E}^\star\right) \cdot \left(\frac{1}{\mu k}\mathrm{n}\mathbf{k} \times \mathbf{E}\right) \ , \tag{D.2}$$

in which, from the vector identities

$$\mathbf{a} \cdot \mathbf{b} \times \mathbf{c} = \mathbf{c} \cdot \mathbf{a} \times \mathbf{b} \ , \ \mathbf{a} \times \mathbf{b} \times \mathbf{c} = (\mathbf{a} \cdot \mathbf{c})\mathbf{b} - (\mathbf{a} \cdot \mathbf{b})\mathbf{c} \ , \tag{D.3a,b}$$

$$(\mathrm{n}^\star\mathbf{k} \times \mathbf{E}^\star) \cdot \mathrm{n}\mathbf{k} \times \mathbf{E} = \mathbf{E} \cdot [(\mathrm{n}^\star\mathbf{k} \times \mathbf{E}^\star) \times \mathrm{n}\mathbf{k}] = \mathbf{E} \cdot (\mathrm{n}^\star\mathbf{k} \cdot \mathrm{n}\mathbf{k})\mathbf{E}^\star - \mathbf{E} \cdot (\mathrm{n}^\star\mathbf{k} \cdot \mathbf{E}^\star)\mathrm{n}\mathbf{k} \ . \tag{D.4}$$

Since the fields are transverse, the complex wave vector, $\mathrm{n}\mathbf{k} \equiv \vec{\kappa}$, has no projection on the E field vector, so that

$$\mathbf{H}^\star \cdot \mathbf{H} = \frac{1}{\mu^2}(\mathrm{n}_{\mathrm{Re}}^2 + \mathrm{n}_{\mathrm{Im}}^2)\mathbf{E}^\star \cdot \mathbf{E} \ . \tag{D.5}$$

Also (taking μ to be real)

$$\epsilon^\star = \frac{1}{\mu}(\sqrt{\epsilon^\star \mu})^2 = \frac{1}{\mu}(\mathrm{n}_{\mathrm{Re}}^2 - \mathrm{n}_{\mathrm{Im}}^2 - 2i\mathrm{n}_{\mathrm{Re}}\mathrm{n}_{\mathrm{Im}}) \ . \tag{D.6}$$

The vector identity,

$$\nabla \cdot (\mathbf{E} \times \mathbf{H}) = \mathbf{H} \cdot (\nabla \times \mathbf{E}) - \mathbf{E} \cdot (\nabla \times \mathbf{H}) \tag{D.7}$$

[15,p.236], in conjunction with (1.1.4,5), implies that the divergence in (D.1) is

$$\nabla \cdot (\mathbf{E} \times \mathbf{H}^\star) = ik(\mu \mathbf{H}^\star \cdot \mathbf{H} - \epsilon^\star \mathbf{E}^\star \cdot \mathbf{E}) \ , \tag{D.8}$$

which, by (D.5,6), is

$$\frac{ik}{\mu}\left[(\mathrm{n}_{\mathrm{Re}}^2 + \mathrm{n}_{\mathrm{Im}}^2)\mathbf{E}^\star \cdot \mathbf{E} - (\mathrm{n}_{\mathrm{Re}}^2 - \mathrm{n}_{\mathrm{Im}}^2 - 2i\mathrm{n}_{\mathrm{Re}}\mathrm{n}_{\mathrm{Im}})\mathbf{E}^\star \cdot \mathbf{E}\right] \ . \tag{D.9}$$

Therefore, from (D.1,9),

$$\mathrm{S}(\mathbf{r}) = \frac{1}{4\pi}\frac{\omega}{\mu_\circ}\mathrm{n}_{\mathrm{Re}}^\circ \mathrm{n}_{\mathrm{Im}}^\circ \mathbf{E}_{\mathrm{INT}}^\star \cdot \mathbf{E}_{\mathrm{INT}} \ , \tag{D.10}$$

in which the case has been specified to the spherical medium of Chapter 1.

The rate of electromagnetic energy transport by a light field is from the complex Poynting vector, itself [15,p.347], which, from Jackson Eq. 6.132 [15,p.242] and relations used above, is seen to be

$$\mathbf{S} = \frac{c}{8\pi}\left[\mathbf{E} \times \left(\frac{1}{\mu k}\mathrm{n}^\star \mathbf{k} \times \mathbf{E}^\star\right)\right] = \hat{\mathbf{k}}\frac{c\mathrm{n}^\star}{8\pi\mu}\mathbf{E}^\star \cdot \mathbf{E} \ . \tag{D.11}$$

For the incident flux of the Mie problem, this gives

$$I = |\Re\{\mathbf{S}\}| = \frac{c\mathrm{n}_{\mathrm{Re}}}{8\pi\mu}\mathbf{E}_{\mathrm{INC}}^\star \cdot \mathbf{E}_{\mathrm{INC}} \ . \tag{D.12}$$

VITA

Christopher Calvin Dobson was born on 19 August, 1955 in Johnson City, Tennessee. He has worked in a variety of occupations, most prominently, as a musician. He received a Bachelor of Science degree in Physics from East Tennessee State University in May 1983, and a Master of Science degree in Physics from the University of Tennessee Space Institute in March 1987.